NASA TECHNICAL
MEMORANDUM

NASA TM X-53768

1968

NASA TM X-53768

CASE FILE COPY

CONTROL SYSTEMS RESEARCH AT MSFC

RESEARCH ACHIEVEMENTS REVIEW

VOLUME III   REPORT NO. 3

GEORGE C. MARSHALL SPACE FLIGHT CENTER

```
ASSISTANT DIRECTOR                    DIRECTOR
FOR SCIENTIFIC &
TECHNICAL ANALYSIS        DEPUTY DIRECTOR,  DEPUTY DIRECTOR,    PUBLIC    CHIEF     PATENT    LABOR
                          TECHNICAL         ADMINISTRATIVE      AFFAIRS   COUNSEL   COUNSEL   RELATIONS

                              EXECUTIVE
                                STAFF

MANAGEMENT   TECHNOLOGY   PURCHASING  TECHNICAL   FINANCIAL    MANPOWER      FACILITIES   NASA        NASA
SERVICES     UTILIZATION  OFFICE      SERVICES    MANAGEMENT   UTILIZATION & & DESIGN     REGIONAL    REGIONAL AUDIT
OFFICE       OFFICE                   OFFICE      OFFICE       ADMINISTRATION OFFICE      INSPECTOR   OFFICE
                                                              OFFICE

        RESEARCH & DEVELOPMENT                              INDUSTRIAL OPERATIONS
             OPERATIONS

ADVANCED    SYSTEMS     EXPERIMENTS  OPERATIONS    CONTRACTS  FACILITIES   PROJECTS    RESOURCES
SYSTEMS     ENGINEERING OFFICE       MANAGEMENT    OFFICE     PROJECTS     LOGISTICS   MANAGEMENT
OFFICE      OFFICE                   OFFICE                   OFFICE       OFFICE      OFFICE

AERO-ASTRO-  ASTRIONICS   COMPUTATION  MANUFACTURING   SATURN I/IB  SATURN V    ENGINE      SATURN-APOLLO
DYNAMICS     LABORATORY   LABORATORY   ENGINEERING     PROGRAM     PROGRAM     PROGRAM     APPLICATIONS
LABORATORY                             LABORATORY      OFFICE      OFFICE      OFFICE      PROGRAM
                                                                                          OFFICE

PROPULSION & QUALITY &    SPACE SCIENCES  TEST         MICHOUD     MISSION     MISSISSIPPI
VEHICLE      RELIABILITY  LABORATORY      LABORATORY   ASSEMBLY    OPERATIONS  TEST
ENGINEERING  ASSURANCE                                 FACILITY    OFFICE      FACILITY
LABORATORY   LABORATORY
```

RESEARCH ACHIEVEMENTS REVIEWS COVER THE FOLLOWING FIELDS OF RESEARCH

- Radiation Physics
- Thermophysics
- Chemical Propulsion
- Cryogenic Technology
- Electronics
- Control Systems
- Materials
- Manufacturing
- Ground Testing
- Quality Assurance and Checkout
- Terrestrial and Space Environment

- Aerodynamics
- Instrumentation
- Power Systems
- Guidance Concepts
- Astrodynamics
- Advanced Tracking Systems
- Communication Systems
- Structures
- Mathematics and Computation
- Advanced Propulsion
- Lunar and Meteoroid Physics

RESEARCH ACHIEVEMENTS REVIEW

VOLUME III   REPORT NO. 3

CONTROL SYSTEMS RESEARCH AT MSFC

1968

PREFACE

In February, 1965, Dr. Ernst Stuhlinger, Director, Research Projects Laboratory (now Space Sciences Laboratory), initiated a series of Research Achievements Reviews which set forth those achievements accomplished by the laboratories of the Marshall Space Flight Center. Each review covered one or two fields of research in a form readily usable by specialists, systems engineers and program managers. The review of February 24, 1966, completed this series. Each review was documented in the "Research Achievements Review Series."

In March, 1966, a second series of Research Achievements Reviews was initiated. This second series emphasized research areas of greatest concentration of effort, of most rapid progress, or of most pertinent interest and was published as "Research Achievements Review Reports, Volume II." Volume II covered the reviews from March, 1966, through February, 1968.

This third series of Research Achievements Reviews was begun in March, 1968, and continues the concept introduced in the second series. Reviews of the third series are designated Volume III and will span the period from March, 1968, through February, 1970.

The papers in this report were presented July 25, 1968

William G. Johnson
Director
Experiments Office

iii

CONTENTS. . .

STATUS OF OPTIMAL CONTROL RESEARCH

By James C. Blair

LIST OF ILLUSTRATIONS

MINIMAX CONTROL

By Jerome R. Redus

CONTENTS (Continued)...

LIST OF ILLUSTRATIONS

DIGITAL THRUST FILTERING

By William H. Walker

LIST OF ILLUSTRATIONS

CONTENTS (Continued) . . .

REDUNDANCY EMPLOYING MAJORITY VOTING FOR
A SATURN SERVOACTUATOR

By Michael A. Kalange, James D. Smith, and Chester W. Martin

LIST OF TABLES

LIST OF FIGURES

INDIVIDUAL ANGULAR MOMENTUM VECTOR DISTRIBUTION AND ROTATION LAWS FOR THREE DOUBLE-GIMBALED CONTROL MOMENT GYROS

By Hans F. Kennel

LIST OF ILLUSTRATIONS

AN OPTIMALLY CONTROLLED MASS DISTRIBUTION GRAVITY GRADIENT SATELLITE CONTROL SCHEME

By George B. Doane III

LIST OF TABLES

LIST OF ILLUSTRATIONS

STATUS OF OPTIMAL CONTROL RESEARCH

By

James C. Blair

SUMMARY

This paper reviews the status of optimal control studies conducted by the Aero-Astrodynamics Laboratory. The general status and applicability of optimal control theory are discussed, along with specific examples of the problem classes considered. Goals and direction of future work are indicated.

INTRODUCTION

The research on control systems done by the Aero-Astrodynamics Laboratory over the past few years has included a significant amount of study of optimal control theory development and application. This review summarizes the status of this research and describes some particular results obtained.

An indication of what is meant by "optimal control" can be obtained by considering Figure 1, a flow chart for a control system design process which proceeds from vehicle and environmental descriptions and a set of control system objectives to the final control system design. This design process can take place by at least the two routes shown on the figure. "Conventional" design, shown on the left, involves hypothesizing a control system design, analyzing the system to see if the objectives have been met, and, if not, making an iteration in which another control system design is guessed and analyzed. This iterative process is repeated until a design is found which, in some sense, meets the control system objectives. The system is then modified to incorporate practical constraints, and finally is simulated to verify the performance of the control system. When an optimal control design procedure is followed, the control system objectives are formulated as a mathematical performance index which is to be minimized or maximized. This mathematical problem is solved analytically or computationally to find the unique control which provides the maximum or minimum. As in conventional design, the proposed optimal control is modified to incorporate practical considerations and finally is simulated to verify performance.

This crude illustration, of course, does not include many complicated facets which are present in either design process. However, it should illustrate the primary difference between the two approaches; that is, conventional design with its iteration to meet the control system goals (sometimes subjectively defined) can yield a number of systems which may meet the goals, whereas optimal control design yields only one control system giving the maximum or minimum value of the performance index which represents the control system objectives.

The remainder of the paper is in three major sections: initially, some comments are made about the general status and applicability of optimal control theory, then Aero-Astrodynamics Laboratory's research into specific areas of optimal control is discussed, and finally, goals and directions for future work are indicated.

GENERAL STATUS OF OPTIMAL CONTROL

Optimal control is a subject that has enjoyed a very great amount of theoretical activity over the past ten years or so. Being a relatively new field, its status is somewhat subject to diverse opinions, ranging from (1) a feeling on the part of some practicing engineers that the theory is of no practical use and is merely a mathematical toy, to another extreme, (2) the feeling on the part of some theoreticians that optimal control is a complete theory and requires no further theoretical development for immediate and complete application to specific problems. Neither of these extremes is entirely correct; there are benefits and there are limitations to optimal control. In its current form, optimal control can be a useful tool for the practical control designer; yet, further theoretical developments could make optimal control more attractive as a design method.

VEHICLE AND ENVIRONMENT DESCRIPTION
CONTROL SYSTEM OBJECTIVES

—————"CONVENTIONAL" DESIGN ————— OPTIMAL CONTROL DESIGN————

HYPOTHESIZE
CONTROL
SYSTEM

ANALYZE

ARE
OBJECTIVES
MET
?

NO

YES

MODIFY FOR
PRACTICAL
CONSIDERATIONS

FORMULATE
PERFORMANCE
INDEX

COMPUTE
OPTIMAL
CONTROL

SIMPLIFY &
SYNTHESIZE
PRACTICAL SYSTEM
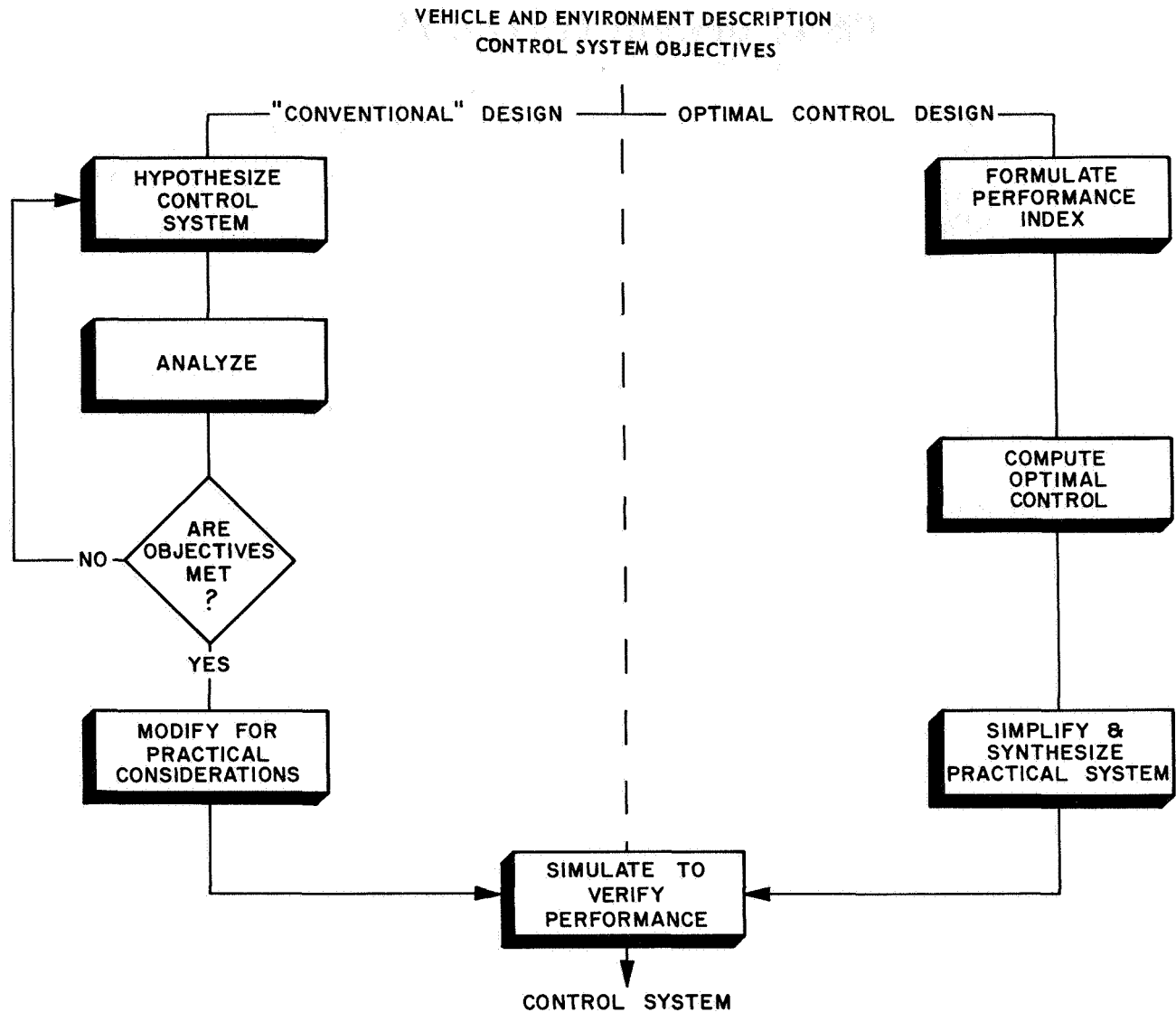
SIMULATE TO
VERIFY
PERFORMANCE

CONTROL SYSTEM

FIGURE 1. COMPARISON OF CONTROL DESIGN METHODS

A number of benefits of optimal control are listed in Figure 2, all of which do not necessarily apply to any given problem. The first benefit listed is the most obvious, in that, for certain complex problems, optimal control theory can be the only direct method for finding a solution which meets the control objectives. This solution maximizes or minimizes the performance index which represents the control objectives. There may be no other way to find that unique control, or else finding it may require an unreasonable amount of computational effort. In another class of problems where the design requirements are less severe and where, for example, a number of conventionally designed control systems could produce adequate results, optimal control theory can lead to a reduction of the total design effort when compared with the iterative design associated with conventional design procedure. This is not to say that optimal control design is completely free from iteration, but the iteration in cases like this is often performed on the values or weighting coefficients within the performance index itself, so that the engineer can apply his judgment at a higher level than would be required in iterations on specific designs for a conventional design process.

A third benefit can be found in using the optimal value of the performance index as a standard against

BENEFITS

1. ONLY DIRECT METHOD FOR OBTAINING BEST SYSTEM

2. REDUCTION OF DESIGN EFFORT

3. ESTABLISHING PERFORMANCE STANDARD

4. PHYSICAL INSIGHT FOR COMPLEX PROBLEMS

FIGURE 2. BENEFITS OF OPTIMAL CONTROL

which suboptimal designs can be compared. This is a situation analogous to the use of optimal trajectories as a performance standard against which implemented guidance schemes can be compared. The fourth benefit listed is probably the least obvious, and yet it is one which some people feel to be the most important. This benefit is the physical insight which can be gained by observing the structure of the optimal control. This insight can augment the engineer's judgment in selecting the proper set of sensors and incorporating the physical constraints which cannot be included in the performance index. For certain complex systems, the insight thus provided may be invaluable.

On the other hand, there are limitations to optimal control which should be as clearly understood as are the advantages. Some of the important limitations are listed in Figure 3. The first item in Figure 3 means that each individual problem solution in optimal control is more complex than a single hypothesis-analysis iteration in conventional design. Storage limitations of available computers often can become a factor in problem formulation. However, when the totality of the iterative effort in conventional design is considered, quite often optimal control can result in a reduction in the total effort (as was mentioned in the discussion of the benefits). Performance index formulation, the second item listed, is a limitation from two standpoints. First, there are factors affecting control design which are difficult to express in a mathematical performance index, for example, cost, confidence level in components, etc. These practical considerations have to be accounted for at a later point in the design process than is the case for conventional design. Second, there are certain physical problems which, when put into optimal control form, yield performance indices which are not amenable to solution. An example of such a performance index which had not yielded a solution until recently is given in the following paper on MINIMAX CONTROL by Mr. Jerome R. Redus.

LIMITATIONS

1. COMPLEXITY OF *INDIVIDUAL* PROBLEM SOLUTION

2. PERFORMANCE INDEX FORMULATION

3. PRACTICAL LIMITATIONS OF CURRENT THEORY

- ANALYTICAL SOLUTIONS GENERALLY UNAVAILABLE
- OPEN-LOOP CONTROL
- SYNTHESIS
- PARAMETER VARIATIONS

FIGURE 3. LIMITATIONS OF OPTIMAL CONTROL

Another area in which there are limitations to the applicability of optimal control is designated "practical limitations of current theory" in Figure 3. Examples of this class of problems are the following: (1) Except for a few restricted classes of problems, analytical or closed-form solutions are generally unavailable, and the solution must be achieved through iteration on split boundary value problems by means of a computer. (2) Optimal control, in general, yields open-loop control; that is, the control is specified as a function of time as opposed to the desired feedback form which would be a function of state. (3) Even for problems where the optimal control yields closed-loop control, optimal control specifies feedback of every dynamical state of the system which, of course, would be impractical. In this case the design engineer must use the specified form of optimal control as a means of augmenting his judgment in selecting realizable or practical sensor complements, filters, etc. (4) There is currently no satisfactory method of including in the initial problem formulation the information that the parameters of the system will not match the deterministic values used in problem formulations; consequently, the control should in some way include a compromise with the optimality of a deterministic system in order to achieve more satisfactory behavior over a wider range of parameter variations.

All of the limitations discussed in the preceding paragraph can be considered to be limitations which are imposed by the current state of the art of implementation as compared with the theory as it stands today. For example, if computer capability is available onboard which is fast enough and reliable enough, the open-loop form of the optimal control could be computed iteratively in fast time to effectively close the loop. Thus, for practical purposes, the limitation indicated here would be resolved.

Similar comments can be made about the state of the art of sensor development and onboard identification as related to the synthesis and parameter variations problem. At the same time, theoretical developments to relieve some of these current restrictions would hasten the broader application of optimally designed controllers.

Lest the limitations be over-emphasized here, it might be well to state that the practicing engineer can obtain a definite benefit from using optimal control despite its limitations and that the use of optimal control theory should be encouraged.

AERO-ASTRODYNAMICS LABORATORY'S RESEARCH IN OPTIMAL CONTROL

Figure 4 is a listing, in roughly chronological order, of some of the areas of optimal control in which research has been conducted by or supported by the Aero-Astrodynamics Laboratory over the past few years. The initial motivation for optimal control research within the Laboratory came from consideration of the launch vehicle control problem [1]. We have carried through this motivation to the present, but we also have expanded our scope of interest to include spacecraft control, as well as other aerospace vehicle control. Initial investigations into optimal control were made on the basis of trying to apply the theory to the launch vehicle control problem. Since optimal control theory was new at that time (in the early 1960's), considerable effort was spent in trying to "warp" the launch vehicle control problem into a form which would produce a readily solvable optimal control problem such as time-optimal control. Other than providing some background and experience, there was little direct benefit from this work. Another optimal control problem which yields a direct solution is deterministic linear optimal control where the performance index is a quadratic function of state and control, yielding linear state feedback. While the direct application of a quadratic performance index does not directly reflect most of our control system objectives, linear optimal control does not fall completely into this class of nonapplicable problems, because linear optimum control has proven to be useful as a tool in reducing the total design effort. As mentioned earlier, the design engineer can iterate on the parameters of the performance index, as opposed to iterating on the specific proposed design, and can thereby exercise a more powerful control over the system design than is possible with conventional design [2].

TIME – OPTIMAL   CONTROL

LINEAR   OPTIMAL   CONTROL

MINIMAX

- ● WORST   DISTURBANCE

- ● MINIMUM   PEAK

SYNTHESIS   PROBLEMS

PARAMETER   SENSITIVITY

STATISTICAL   OPTIMAL   CONTROL

PARAMETER   OPTIMIZATION

FIGURE 4. AERO-ASTRODYNAMICS RESEARCH

From this initial period of seeking easily solvable optimal control problems and attempting to force the launch vehicle control problems to fit these forms, the character of optimal control research within the Aero-Astrodynamics Laboratory evolved further. We began to ask the questions, "What is the nature of launch vehicle control objectives, and can these control objectives be fitted into an optimization problem?" This viewpoint resulted in what we call "minimax" control, which is concerned with control for worst disturbances and/or minimization of response peak values. A brief discussion of the early work with references may be found in Reference 3. The most recent minimax research efforts are discussed in the next paper in this review.

Further evolution of the problem formulation resulted in development of some of the other study areas listed in Figure 4, particularly statistical optimal control. Meanwhile, work was continued on the problem of synthesizing a practical closed-loop system with realizable filters once the optimization problem had been solved. Also, a continuing effort has been concerned with solving the parameter variation problem mentioned in the discussion of limitations. The remaining portion of this paper will be devoted to a more detailed discussion of two remaining areas: statistical optimal control and parameter optimization as applied to spacecraft control problems.

STATISTICAL OPTIMAL CONTROL

The original work in statistical optimal control in the Aero-Astrodynamics Laboratory was motivated by launch vehicle control but has since expanded to include other applications in different aerospace vehicles. The statistical formulation arose from the consideration that the wind (which is the primary influence on flight control design for a launch vehicle) is a statistical rather than a deterministic quantity, and thus a stochastic formulation of the control problem would seem very reasonable. However, it has been only recently that new techniques of wind measurement have allowed the collection of sufficiently complete wind data to permit confidence in a design achieved on a statistical basis. While there have been some earlier, simplified versions of dynamic statistical models for wind representation, the body of wind statistics information has been growing. A current contract with Hayes International Corporation has the purpose of developing an up-to-date model of the wind statistics to be used in control studies. Under the reasonable assumption that the wind is a Gaussian, Markovian process, a set of linear differential equations can be constructed such that, when the equation solutions are forced by white noise and summed with the mean value of the wind, the resultant output quantity has the same statistics as the wind statistics used to generate the time-varying differential equations. As indicated in Figure 5, this representation of the wind can be adjoined to a representation of the vehicle and control system dynamics. Under the assumption that the vehicle dynamics can be represented by linear variational equations about the nominal trajectory and linear control, this total model can be driven by white noise, and the statistics of any given responses of the vehicle can be computed in a fairly straightforward manner. Such a simulation could be used to evaluate a given proposed control system design or could be used as part of an iterative design process.

Thus far, nothing has been said about optimization. It is likewise reasonable to form the launch vehicle control problem in the presence of a stochastic wind disturbance as a problem in statistical optimal control. Stating the control objectives directly would yield a performance index which would be the probability of failure of the vehicle during its flight, where failure of the vehicle can be considered to be an exceedance of any given constraint, such as structural strength limits or angle of attack and rate limits at the end of first stage flight, which affect the success of separation of the second stage. Ideally, we would then like to make use of this performance index in an optimal control problem so that the theory would yield a control system which would produce the minimum probability of failure. Unfortunately, this is not possible. It is not currently possible to compute the value of the probability of failure under the assumptions stated, much less find a control which minimizes that quantity. However, a significant contribution toward an approximation to this idealized problem has been made by Honeywell, Inc., under contract to the Aero-Astrodynamics Laboratory [4,5]. In Figure 6, the idealized performance index, which is the probability of failure, is represented by J. In the research work by Honeywell, Inc., a new quantity represented by J^* is shown to be an upper bound to J, and J^* is a quantity which is computable. Therefore, if we can find the control which minimizes J^* and if the resultant value of J^* is small enough, we can achieve a satisfactorily small probability of failure, J. The theory goes one step further and develops a third performance index, J^{**}, which is a quadratic form which will yield linear feedback control as described earlier in the discussion of linear optimal control. The parameters of J^{**} are adjusted so that the performance measure has the same first variation in control as does J^*, and thus the control system which minimizes J^{**} will also minimize J^*. Since J^{**} is quadratic, the resultant problem is able to make use of the powerful linear control system theory which has been developed in obtaining a usable solution.

In addition to the advantage of linearity as listed on Figure 7, the statistical optimal control approach yields physical insight into determining which quantities should be sensed and fed back, and aids the design engineer in arriving at a simplified design which will approximate the optimal system. At the same time, some questions can be raised. First is the question concerning the approximate nature of the problem, that is, do we find the control that truly minimizes J? Of course, the answer is "not necessarily." However, in the applications to date, minimizing J^* has produced a low enough value of J^* that the assurance that J is lower than J^* yields an adequate result. A second problem is that there is no systematic, analytical means of proceeding from the complete state feedback that

5

ASSUMPTIONS

GAUSSIAN WIND

VARIATIONAL EQUATIONS FOR THE VEHICLE

LINEAR CONTROL

MODEL
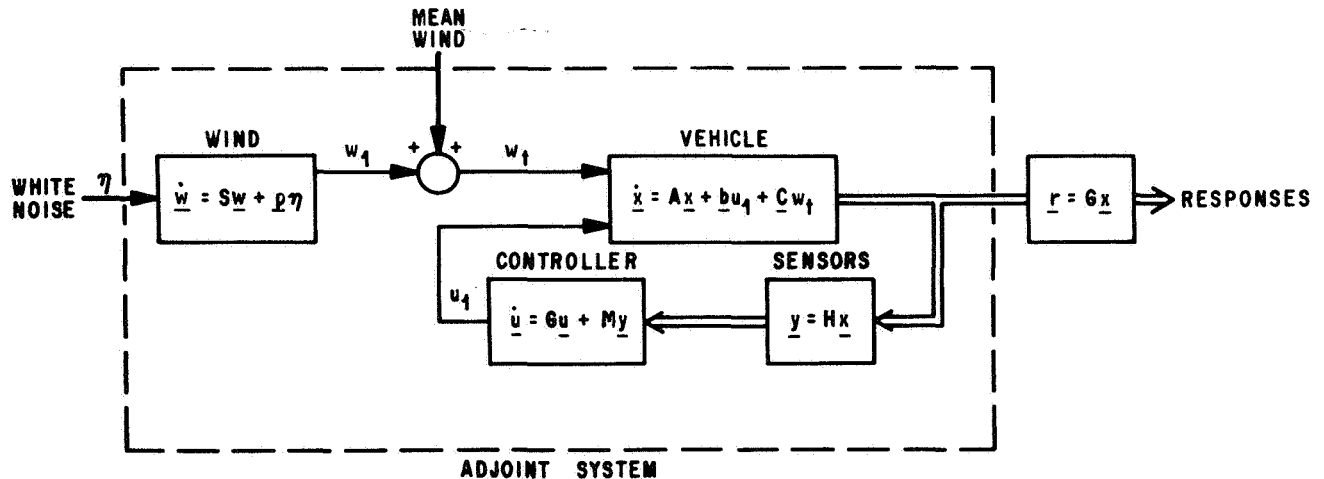
FIGURE 5. STOCHASTIC MODEL

PERFORMANCE MEASURES

J   = PROBABILITY OF FAILURE

J* = SUM OF EXPECTATIONS OF EXCEEDING CONSTRAINTS ≥ J

J** = WEIGHTED QUADRATIC FORM IN MEANS AND COVARIANCES

APPROACH

1. FIND WEIGHTS FOR J** SO THAT IT HAS THE SAME FIRST VARIATION IN CONTROL AS J*

2. MINIMIZE J**

FIGURE 6. STATISTICAL OPTIMAL CONTROL – LINEARIZED SYSTEM

is specified by the theory to a practically implementable system with a reasonable number of sensors and feedbacks. Again, this is an area where the engineer's judgment must be used. Despite the problems, it should be emphasized

ADVANTAGES

1. J MEANINGFUL

2. RESULTS IN LINEAR CONTROL

3. YIELDS PHYSICAL INSIGHT INTO THE PROBLEM

PROBLEMS

1. IS J MINIMIZED ?

2. ANALYTIC TECHNIQUES NOT AVAILABLE FOR SIMPLIFYING OPTIMAL CONTROL

FIGURE 7. STATISTICAL OPTIMAL CONTROL – ADVANTAGES AND DISADVANTAGES

that this particular statistical optimal control approach is a very powerful design tool and has been shown to

be applicable to various problems, for example, the launch vehicle application described earlier, as well as a gust alleviation control system for the B-52 airplane which is currently undergoing flight tests. It would also be applicable to a spacecraft control problem where there is a dominant disturbance which is described by an additive Gaussian process, and the control objective can be expressed as a set of constraints which are not to be violated.

PARAMETER OPTIMIZATION OF SPACECRAFT CONTROL

Another area of optimal control that has been receiving recent attention is the application of optimization theory to spacecraft control system problems, particularly for the Apollo Telescope Mount (ATM) system. Figure 8 is a rough block diagram of the ATM system, which can be seen to be quite complex by realizing that the heavy blocks are complete control subsystems. The ATM system makes use of control moment gyros as a means of producing attitude control torques. The momentum management subsystem is the subject of a later paper in this review. The application of optimization theory has been investigated in two portions

of this total system. First, in the area of momentum dumping, the problem of preventing control moment gyro momentum saturation is being formulated as an optimal control problem, under the constraint that gravity gradient torques be used as a means of dumping the momentum.

An application which is further advanced at this point is the use of parameter optimization to study the combination of the control-moment-gyro control law and the telescope mount fine-pointing control system. A proposed design, which was arrived at by heuristic methods, serves as a basis or a nominal around which perturbations can be investigated. The use of this method of parameter optimization insures that the resultant system will be a feedback control system, a condition which would not be guaranteed if the total nonlinear problem were formulated. The objective of the study is either to verify that the existing system is truly the best system or to arrive at configurations which improve on the current system. The ATM control problem is a very complex one which includes many conflicting constraints so that it will be necessary to form a number of candidate performance indices, determine the optimum control for each of these, and investigate the trade-offs involved.
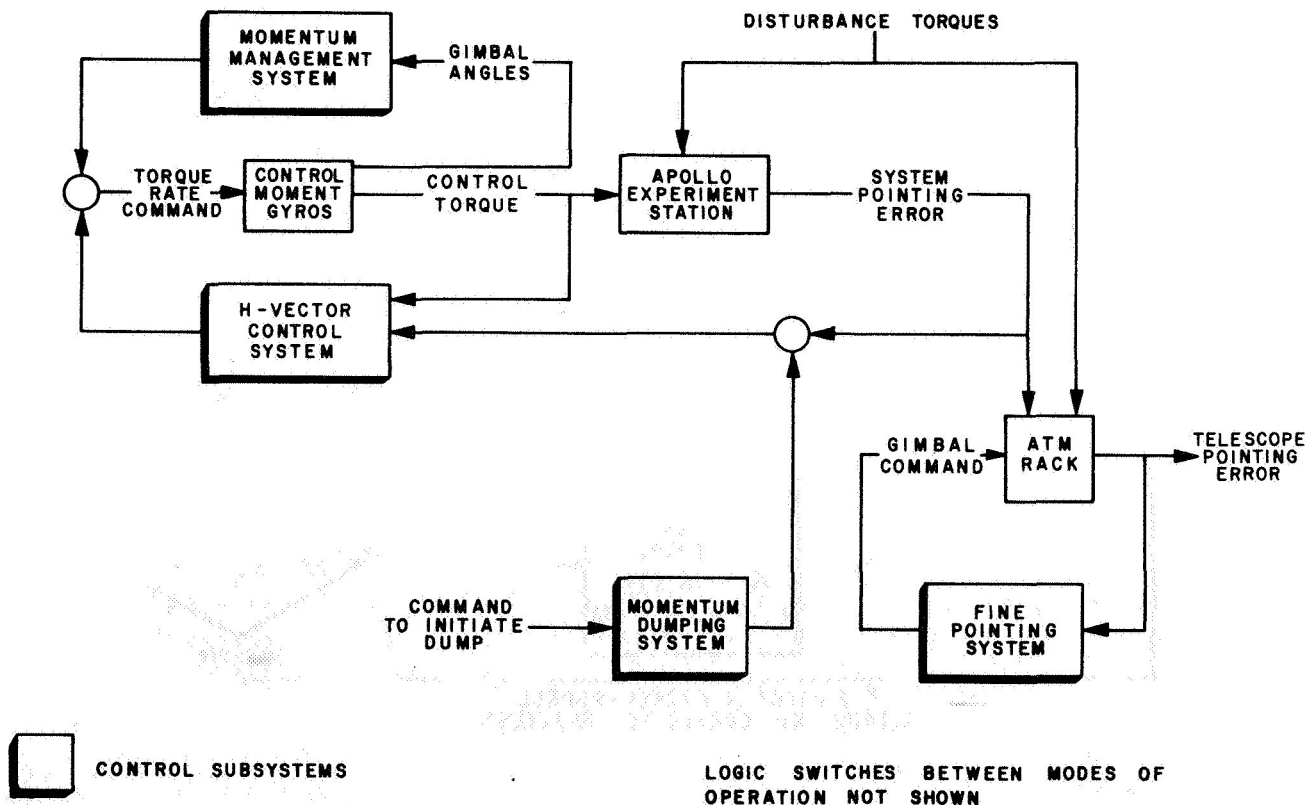

FIGURE 8. APOLLO TELESCOPE MOUNT CONTROL SYSTEM

Under a support contract, Lockheed Missiles and Space Company, Huntsville, Alabama, is developing a hybrid computer simulation which will make use of the parameter optimization method to study this problem. As shown in Figure 9, the dynamics of the vehicle and control system and the performance measure evaluation are done on the analog portion of the computer and the optimization technique is accomplished on the digital portion. The optimization technique being used here is a second order gradient technique. The hybrid computer seems especially well suited for this type of problem, and a secondary objective of the study is to prove the usefulness of the hybrid simulation technique for complex optimization problems of this nature.

CONCLUSIONS AND FUTURE DIRECTION

In summary, optimal control is currently a very beneficial design tool which can augment, rather than replace, the engineer's judgment, and its usefulness is more likely to increase than to decrease as further developments in the state of the art of hardware implementation occur. In the Aero-Astrodynamics Laboratory, an evolution in our optimal control research parallels the changes in the general field of optimal control, in that emphasis has been shifted from problems more directly solvable in closed form to those which either better
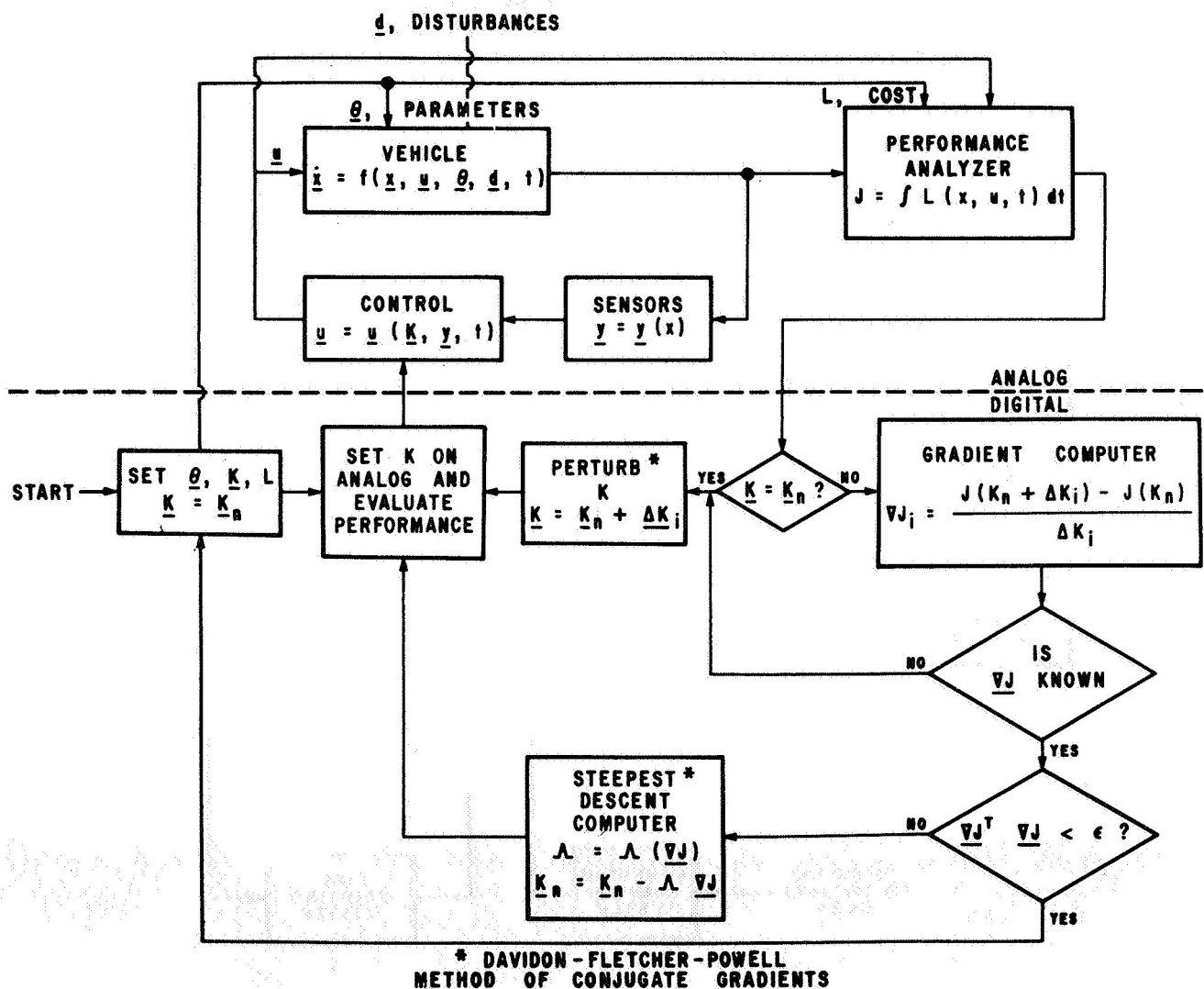

FIGURE 9. HYBRID SIMULATION OF PARAMETER OPTIMIZATION

reflect the control design objectives and constraints or provide more general solutions, even though more computation is required. We expect this maturing process to continue. In our future research, we intend to continue to apply optimal control theory to specific vehicle problems and to encourage such applications of the theory. We also expect to continue the theoretical developments indicated in Figure 10, both in the extension of theory to include other performance measures of practical interest and in the area described earlier as "practical limitations of current theory" in which we will seek systematic means of incorporating practical constraints and arriving at systems which are implementable while using optimal control theory as a basis for design. Finally, a future goal is to seek ways of including information concerning vehicle parameter variations into the initial design of the control system so that the optimal control is optimal in the sense that it accounts for the range

of expected parameter values and does not ignore this significant piece of information.

FUTURE GOALS

APPLICATION TO SPECIFIC PROBLEMS

EXTENSION TO OTHER PERFORMANCE INDICES

INCORPORATION OF PRACTICAL CONSTRAINTS

SYNTHESIS METHODS

PARAMETER VARIATIONS

FIGURE 10. FUTURE GOALS OF AERO-ASTRODYNAMICS LABORATORY'S RESEARCH

REFERENCES

1. Lovingood, J. A.: Launch Vehicle Control Systems Research. Research Achievements Review Series No. 6, NASA TM X-53374, 1965.

2. Rynaski, E. G.; Whitbeck, R. F.; and Wierwille, W. W.: Optimal Control of a Flexible Launch Vehicle. Cornell Aeronautical Laboratory Report IH 2089-F-1, July, 1966.

3. Blair, J. C.; Lovingood, J. A.; and Geissler, E. D.: Advanced Control Systems for Launch Vehicles. Astronautics and Aeronautics, August, 1966.

4. Edinger, L. D., et. al.: Design of a Load-Relief Control System. NASA CR-61169, April, 1967.

5. Harvey, C. A.: Application of Optimal Control Theory to Launch Vehicles. Honeywell Report 12073-FRI, July, 1968.

MINIMAX CONTROL

By

Jerome R. Redus

SUMMARY

A basic optimization technique has been developed for a class of optimization problems not previously amenable to solution. The technique minimizes the peak value of a function of the current state of the system, no matter when that peak occurs. The method of solution is outlined in this paper and areas of current research are noted.

INTRODUCTION

In an optimal control problem, we are given a description of the motion of the plant or object being controlled,

$$\dot{x} = \frac{d}{dt} x = f(x, t, u),$$

where x is the state of the plant and t the time; the initial conditions of the plant, (x_0, t_0); a set of acceptable final conditions (x_T, T) described by the terminal manifold, $\mathcal{T}(x_T, T) = 0$; and a set of admissible control functions $u \in U$.

It is assumed that there are several controls $u(t)$ or $u(x, t) \in U$ which are satisfactory in the sense that they all can transfer the plant from its initial conditions (x_0, t_0) to acceptable final conditions $(x_T, T) \in \mathcal{T}(x_T, T)$, and we are asked to find, from among the set of satisfactory controls, that control which also minimizes some scalar function of the plant motion, or trajectory, in going from (x_0, t_0) to some $(x_T, T) \in \mathcal{T}(x_T, T)$. The function to be minimized, $J(x_0, t_0; u)$, depends on the control and initial conditions, since these determine the trajectory.

Most optimization problems considered in the past have been of either the Mayer type where the function to be minimized is evaluated only at the final time,

$$J(x_0, t_0; u) = M(x_T, T) \quad ;$$

of the Lagrange type where the function is an integral over the entire trajectory,

$$J(x_0, t_0; u) = \int_{t_0}^{T} L(x, t, u) \, dt \quad ;$$

or of the Bolza type, a combination of the above two. These three problems can be shown to be equivalent and can, at least conceptually, be solved by any one of a number of means. A key feature is that the function needs to be evaluated only at the final time T, by virtue of their equivalence, and we know ahead of time at which time the function needs to be minimized.

In opposition to this, the problem which is being considered here is that of minimizing the peak value of a function of the current state of the system, no matter when that peak occurs,

$$J(x_0, t_0; u) = \max_{t_0 \leq t \leq T} C(x, t) \quad . \quad \textbf{1}$$

The problem is to find the control $u_0 \in U$ minimizing the peak value (maximum value) of $C(x, t)$ in going from (x_0, t_0) to (x_T, T),

$$u_0 = \text{Arg} \min_{u \in U} \max_{t_0 \leq t \leq T} C(x, t) \quad .$$

---

1. Since the peak value can occur anywhere, it takes some extremely artificial mathematics to convert this to a problem of minimizing the final value of a function. The artifices that could be employed would upset the use of the usual optimization procedures for this problem.

Hence, the name <u>minimax control</u>. To differentiate between peak-value minimization and some game theory optimization problems, *this problem is called a C-Minimax optimization problem.*

The need to minimize the peak value of some function of the state of the system can arise in a number of physical situations, for example, minimizing the peak bending moment over the trajectory at a critical point on a launch vehicle, minimizing the peak pointing error of a photographic satellite, etc. The need for a theory to handle this class of problems was recognized by personnel at MSFC and the basic optimization procedure was developed by Dr. C. D. Johnson of the University of Alabama in Huntsville. The theory is treated rigorously in Reference 1; this paper presents a simplified explanation of how the optimization procedure works and indicates the direction of future research.

BASIC NOTIONS

Since

$$J(x_0, t_0; u) = \max_{t_0 \leq t \leq T} C(x, t) \quad,$$

it is clear that

$$J(x_0, t_0; u) \geq C(x_0, t_0) \quad.$$

Assume that the initial conditions are such that there are several satisfactory controls which have the property that

$$\dot{C} = \frac{d}{dt} C \leq 0$$

everywhere along the trajectory from (x_0, t_0) to (x_T, T). For each of these controls, $\max_{t_0 \leq t \leq T} C(x, t)$, the peak value of C, occurs at the initial conditions and

$$J(x_0, t_0; u) = C(x_0, t_0) \quad,$$

which is the best that we can hope to do. Clearly, each one of these controllers is an equally optimum controller, and not only are there several satisfactory controls in the sense defined previously, <u>the optimum control is not unique for this set of initial conditions.</u>[2] If, for another set of initial conditions, every satisfactory controller performs such that $J(x_0, t_0; u) > C(x_0, t_0)$, (that is, the peak value occurs <u>after</u> the initial time), then we would appear to have a unique optimization problem, at least until the time that the peak has occurred. Although these are heuristic notions, they are important, because they form the basis on which C-Minimax theory works, as will become clear in the next section.

SOLUTION TO C-MINIMAX PROBLEMS

We are given the usual equations of motion, initial, and final conditions. The control u is contained in a set U of bounded, sequentially compact, piecewise continuous controls.[3] The task is to minimize

$$J(x_0, t_0; u) = \max_{t_0 \leq t \leq T} C(x, t) \geq C(x_0, t_0) \quad.$$

Based on what was said in the last section, we divide the state space into two classes of regions:

R_0: (x_0, t_0) is such that there exists one or more satisfactory controls such that
$$J(x_0, t_0; u) = C(x_0, t_0) \quad.$$

R_m: (x_0, t_0) is such that, for all satisfactory controls,
$$J(x_0, t_0; u) > C(x_0, t_0) \quad.$$

In the process of conceptually building up these regions, we obtain the solution to the peak minimization problem.

---

2. It is this non-uniqueness that causes difficulties in directly applying the usual optimization procedures, which work well with Mayer and equivalent problems, to this problem.

3. Boundedness is obviously required physically. It also keeps the control from always exerting enough effort to make $J(x_0, t_0, u) = C(x_0, t_0)$ for all initial conditions (i. e., boundedness makes the problem interesting). The other requirements are physically reasonable and convenient.

Consider first a subspace of the R_0 space, denoted R_0^1. R_0^1 is such that for every point in R_0^1 there exists at least one control leading to the terminal manifold such that $\dot{C} \leq 0$ all the way to the terminal manifold (like the example under BASIC NOTIONS). Typical time histories of C versus t are shown in Figure 1, along with the properties of the region R_0^1. Formally, the terminal manifold may be considered to be in or on the boundary of $R_0^{\,1}$. Hence, any trajectory going to the terminal manifold must pass through the boundary of R_0^1, denoted ∂R_0^1. Suitable controls in the R_0^1 region may be found by any one of several means, including backward time flooding, as discussed in Reference 2.

$$R_0^1$$

$\dot{C}(x, t) \leq 0$ EVERYWHERE ALONG THE TRAJECTORY

NO INTERIOR MAXIMA
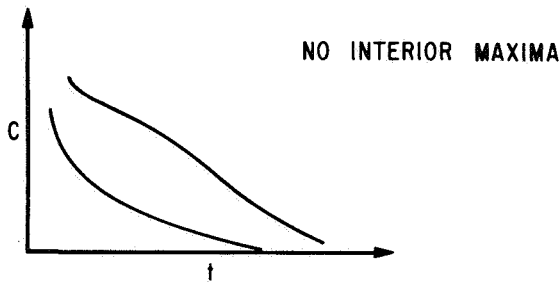
∂R_0^1: THE BOUNDARY OF R_0^1

$\mathcal{J}(x_T, T) \subset R_0^1$

ANY TRAJECTORY MUST PASS THROUGH R_0^1

FIGURE 1. PROPERTIES OF THE R_0^1 REGION

Consider now a point outside of R_0^1 in an R_m region but sufficiently close to R_0^1 that $\dot{C} > 0$ for all points between (x_0, t_0) and ∂R_0^1 for all controls

$u \in U$ leading to $\mathcal{J}(x_T, T)$.[4] For all trajectories emanating from that point and passing through the boundary of R_0^1 (to reach the terminal manifold), $\dot{C} > 0$ all the way to ∂R_0^1 and it is known that one can find controls such that $\dot{C} \leq 0$ from the boundary on in. Hence, the peak value occurs on the boundary of R_0^1, ∂R_0^1, and we can introduce an auxiliary optimization problem — one of minimizing the "final value" of $C(x, t)$ in transferring the state (x_0, t_0) to the "terminal manifold," ∂R_0^1. This subsidiary problem is exactly a Mayer-type problem for which optimization techniques are well known.

These points, being in an R_m region, are such that $J(x_0, t_0; u) > C(x_0, t_0)$. They have one interior maximum on a plot of C versus t and are thus said to belong to an $R_m^{\,1}$ region. Although it is difficult to set forth, a little consideration on the reader's part will allow him to recognize that for any initial point in the $R_m^{\,1}$ region,

$$\max_{t_0 \leq t \leq T} C(x, t) = C(\partial R_0)$$

for optimal control, and the optimum control is found by solving the Mayer problem in going to ∂R_0^1. The boundary of $R_m^{\,1}$, $\partial R_m^{\,1}$, is characterized by $C(\partial R_m^{\,1})$ $= C(\partial R_0^1)$ with optimal control. These arguments and typical plots of C versus t for trajectories starting in the $R_m^{\,1}$ region are summarized in Figure 2.

Consider next a point outside of $R_m^{\,1}$ and R_0^1. Assume initially that it is close to the boundary of $R_m^{\,1}$ and further assume that it is in an R_0 region. Since it is in an R_0 region, there must be controls such that $\dot{C} \geq 0$ at least initially. However, since it is not in R_0^1, $\dot{C}$ is not nonpositive all the way to the terminal manifold, and there must be at least one interior relative maximum in a plot of C versus t. We conclude that it must pass through an R_m region. A suitable control policy is to choose any control which will take the trajectory to $\partial R_m^{\,1}$ such that $\dot{C} \leq 0$ all the way to the boundary of $R_m^{\,1}$, follow

---

4. For points infinitesimally outside the boundary of R_0^1 and in an R_m region, it must be true that at those points $\dot{C} > 0 \; \forall \; u \in U$ leading to the terminal manifold or else the points would be on the boundary or interior to R_0^1.

$$R^1_m$$

1. ASSUME $(x_0, t_0) \notin R^1_0$, SUFFICIENTLY CLOSE TO ∂R^1_0 THAT $\dot{C} > 0 \; \forall \; u \in U$

MUST GO UPHILL ALL THE WAY UNTIL REACH ∂R^1_0; C_{max} OCCURS ON ∂R^1_0

**OPTIMIZATION PROBLEM:
MAYER TYPE –**

    MINIMIZE "FINAL VALUE" OF C IN TRANSFERRING TO "TERMINAL MANIFOLD" ∂R^1_0

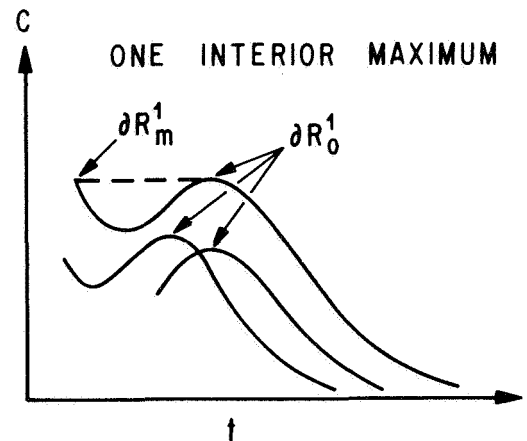**2. EXTEND REGION R^1_m UNTIL $C(x_0, t_0) = C(\partial R^1_0)$**

C

ONE INTERIOR MAXIMUM

∂R^1_m ∂R^1_0

t

FIGURE 2. CONSTRUCTION OF THE $R_m^{\ 1}$ REGION

the optimal control policy for that point on $\partial R_m^{\ 1}$ across $R_m^{\ 1}$ so that

$$C(\partial R^1_0) = C(\partial R_m^{\ 1}) \leq C(x_0, t_0) \quad ,$$

and follow any suitable control policy in R^1_0. The boundary of R^2_0 is analogous in its properties to the boundary of R^1_0.

If we are outside of R^1_0, $R_m^{\ 1}$, R^2_0, and close to the boundary of R^2_0, we can again argue that we are in an R_m region and we have a Mayer problem in

going to ∂R^2_0, the boundary of R^2_0. Abbreviated discussions of these regions and plots of C versus t are shown in Figure 3.

The whole process can be continued until the state space of interest has been covered and all of the regions occurring for the given problem have been identified. It is interesting to note that, for the R_m type regions, the peak value of C (x, t) always occurs at the <u>first</u> passage of the trajectory into an R_0 region.

In the example problem shown in Figure 4, tne plant is a so-called "double integrator," the control is bounded by unity, and the terminal manifold is $x_1 = x_2 = 0$. The optimization problem is to minimize the peak value of x_1^2. [5] The R^1_0, R^2_0, and $R_m^{\ 1}$ regions

<hr>

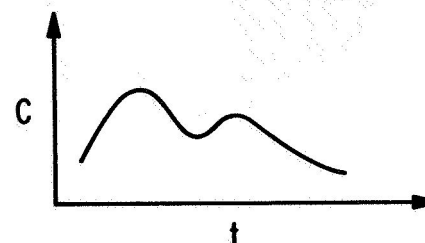[5] or equivalently, minimize the peak value of $C(x) = |x_1|$, or in general $C(x) = |x_1|^\nu$, $\nu \geq 1$.

14

$$R_0^2$$

R_0^2: $\dot{C} \leq 0$ EVERYWHERE TO

       BOUNDARY ∂R_m^1
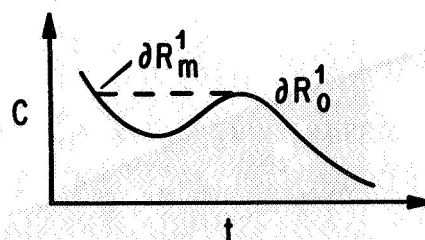
$$R_m^2$$

R_m^2:   MAYER PROBLEM TO ∂R_0^2

AND SO FORTH

FIGURE 3. PROPERTIES OF THE REGIONS OF HIGHER RANK

are shown, as are curves of constant cost, where

$$V(x) = J(x_0, u_0) .$$

One possible realization of the control is

$$u_0 = -\text{sgn} \left[x_1 + \tfrac{1}{4} |x_2| x_2 \right]$$

as shown on the illustration. Another is

$$u_0 = -\text{sgn} \left[x_1 + \tfrac{1}{2} |x_2| x_2 \right] .$$

A trajectory for the latter law is shown in the illustration starting at point $(-3.75, 3.4)$. [6]

Two other examples are treated in Reference 3. For those examples, the optimum control and

---

6. In the oral presentation, some time was spent on physical arguments as to why the R_0^1 and R_m regions occur where they do. The same physical reasoning can be extended to solving the whole problem with pencil and paper and without recourse to formal optimization procedures. This will lead to an initial postulated control law of

$$u_0 = -\text{sgn} \left[x_1 + \tfrac{1}{2} |x_2| x_2 \right] \text{ in } R_0^1$$

$$= -\text{sgn } x_2 \qquad \text{ in } R_m, R_0^2$$

which is equally optimum to the two given above, again demonstrating the non-uniqueness of the control.

EXAMPLE

$$\dot{x}_1 = x_2$$

$$\dot{x}_2 = u$$

$$|u| \leq 1$$

$$C(x) = x_1^2$$
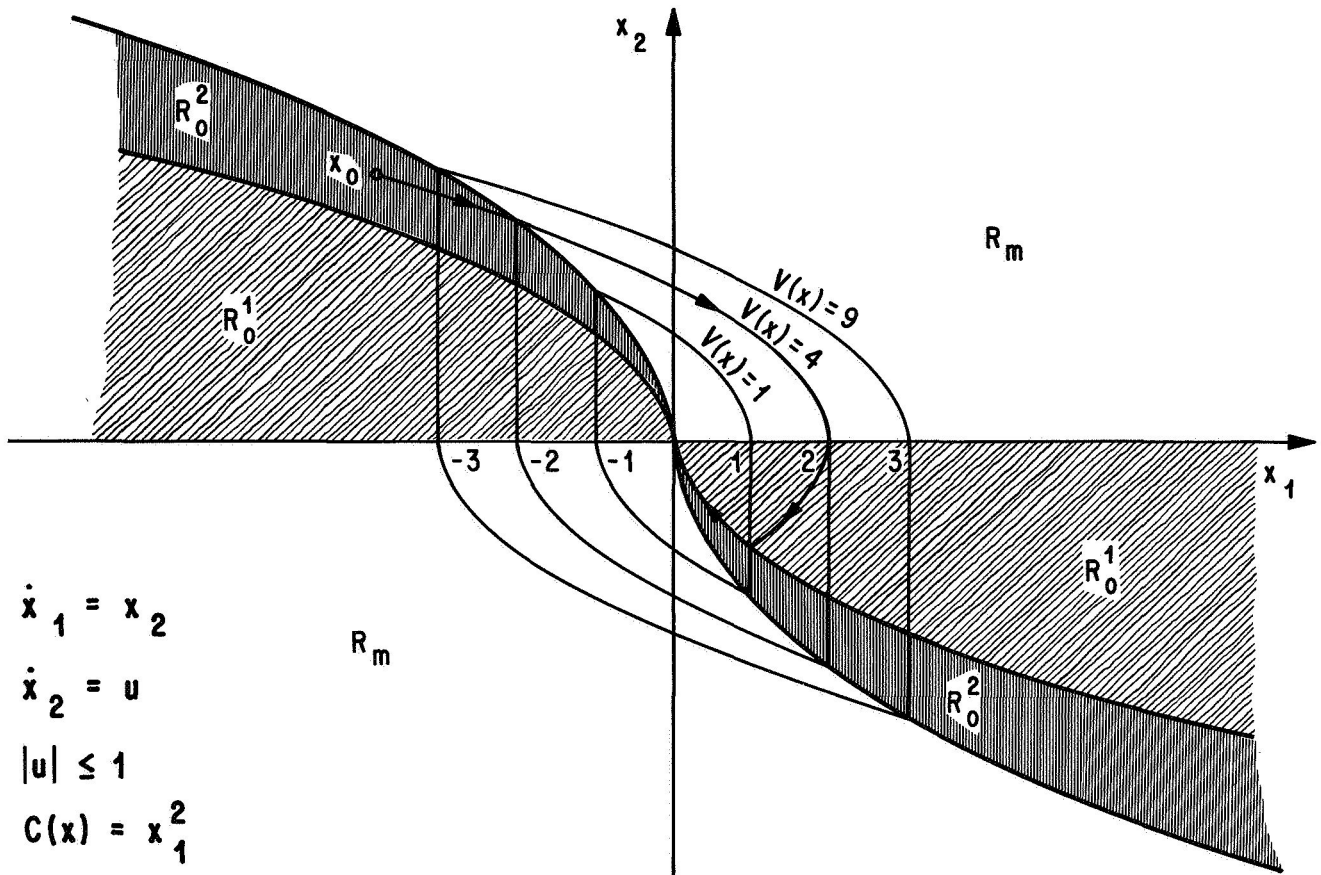
$$u_0 = -sgn \left[x_1 + \frac{1}{4} |x_2| \, x_2 \right]$$

FIGURE 4. EXAMPLE PROBLEM

performance are demonstrated and the results are compared with the performance of suboptimal control systems designed by other methods.

A general computer algorithm has been devised which identifies the various regions of state space for a given problem and simultaneously solves for the optimum control where the optimum control is unique, i.e., in the R_m regions. The algorithm is described in Reference 2.

A basic feature of the algorithm is that it floods the state space in backward time in order to identify the various regions. This feature is quite analogous to the direct application of Bellman's Principle of Optimality and suffers from an analogous "curse of dimensionality." This feature is not necessarily

bad if we are trying to flood the state space to compare the optimum solution with candidate suboptimal controllers for several initial conditions. Also, the "curse" is not as severe as for some applications of Bellman's Principle, as the algorithm proceeds straightforwardly in backward time without any iteration on a given trajectory. Nevertheless, we still have some visualization and flooding difficulties in high-dimension space.

FUTURE RESEARCH

Because the current computational methods are not without drawbacks, planned research is directed towards obtaining analytic solutions for common general classes of problems, for example, those

problems for which the plant is adequately described by a set of deterministic linear autonomous differential equations.

Research is also being conducted on finding alternate means of solution for problems where there is only one set of initial conditions of interest, and the backward time flooding would desirably be eliminated.

Another problem currently being considered is that of minimax control in the presence of incompletely specified disturbances. Two approaches are being considered, a stochastic formulation and a formulation in which the disturbance is of a specified functional form with specified bounds on the functional parameters.

REFERENCES

1. Johnson, C. D.: Optimal Control with Chebyshev Minimax Performance Index. ASME Transactions, Journal of Basic Engineering, vol. 89, Series D, No. 2, June 1967, pp. 251-262.

2. Johnson, C. D.: A Study of Minimax Solutions for Saturn Control Problems. Report GDC DDF 67-003, Convair Division, General Dynamics Corporation, May 1967.

3. Johnson, C. D.; and Redus, J. R.: Application of C-Minimax Optimal Control Theory to Flight Control Problems. Presented at the AIAA Guidance, Control, and Flight Dynamics Conference, Pasadena, California, Aug. 12-14, 1968. AIAA Preprint no. 68-871.

DIGITAL THRUST FILTERING

By

William H. Walker

SUMMARY

Saturn launch vehicle guidance requires that measured thrust data be processed on a real time basis during flight. A digital filter is used to smooth the raw thrust data before they are used by the guidance system. Conventional digital filter designs do not provide satisfactory responses to steps in the input signal that may be caused by engine mixture ratio shifts or engine malfunctions. A new type of digital filter has been designed for this service. The new filter design is largely the result of heuristic and experimental work and exploits both the logical and arithmetic capabilities of digital computers. This filter uses a simple statistical scheme to detect step changes in the input signal level which will trigger the logical modification of the filter algorithm permitting the filter to respond very rapidly to input steps.

DIGITAL THRUST FILTER

Saturn launch vehicle guidance requires that measured thrust data be processed as a real-time input. Digital thrust data are derived from sampled accelerometer outputs by digital computation. The raw digital thrust data are noisy and must be filtered before use by the guidance system. A simplified schematic of the thrust data system is shown in Figure 1. This paper is concerned with the digital filter which is implemented as a stored program in the launch vehicle digital computer. This digital filter must, of course, operate in real time.
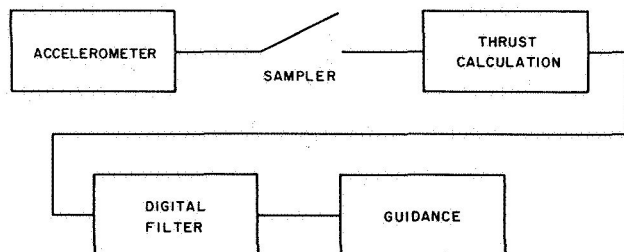

FIGURE 1. SYSTEM SCHEMATIC

The data sampling rate is rather low with the sampling interval being on the order of two seconds. The digital filter input has the following characteristics:

1. It is essentially a constant level signal with additive Gaussian noise.

2. The signal may change level in a steplike manner as a result of engine mixture ratio shifts or engine malfunctions.

Qualitative digital filter performance requirements are:

1. The filter must provide good noise suppression during constant signal level operation.

2. The filter must respond rapidly to steps in the input signal level.

3. The filter must be suitable for programming on the launch vehicle digital computer.

FILTER DESIGN

The filter performance requirements for good noise suppression and fast step response are difficult to meet using conventional linear filters. Digital simulations using several conventional and Kalman filter designs led to the conclusion that simple linear filters were satisfactory for constant signal level operation, but a new development was needed to give the desired step response. Further appraisal of the filter performance requirements suggested the possibility of using some programmed logic to switch in a special filter during input signal level steps. The critical problem in this approach is the detection of a step in the input signal.

STEP DETECTION

The detection of a step in the input signal can be considered to be a problem in pattern recognition. A frequent approach in developing computer pattern recognition programs is to try to determine how a

human would perform the pattern recognition task and then attempt to program this procedure. Small scale paper-and-pencil experiments indicated that this approach had some interesting possibilities. A data generator computer program was written to provide a ready supply of unbiased data for pattern recognition experiments. The data were produced in graphical form by using a line printer as a plotter. Figure 2 is part of a typical synthetic data record. The data points, plotted with asterisks, have been manually connected with straight lines for illustrative purposes. The background grid of plus signs is printed to provide a reference framework.

Step detection experiments were conducted by masking off the data record from the right and letting the person acting as the experimental subject view only the historical data. At each simulated sample

time, the mask was moved to the right, exposing one new data point. At each sample time, the experimental subject would express an opinion as to the presence or absence of a step in the input signal level.

A few step detection experiments indicated that experimental subjects armed with at least an elementary background in statistics would tend to set up a tolerance band about the estimated mean value of the signal and declare a step present whenever a raw data point fell outside the tolerance band. With the tolerance band set at the mean plus-and-minus-three noise standard deviations, this scheme is similar to the commonly used quality control chart. An estimated mean signal level and the tolerance limits are shown in Figure 2 near the start of the downward step. This step detection procedure suffers from a defect in that wild data samples will often be misinterpreted
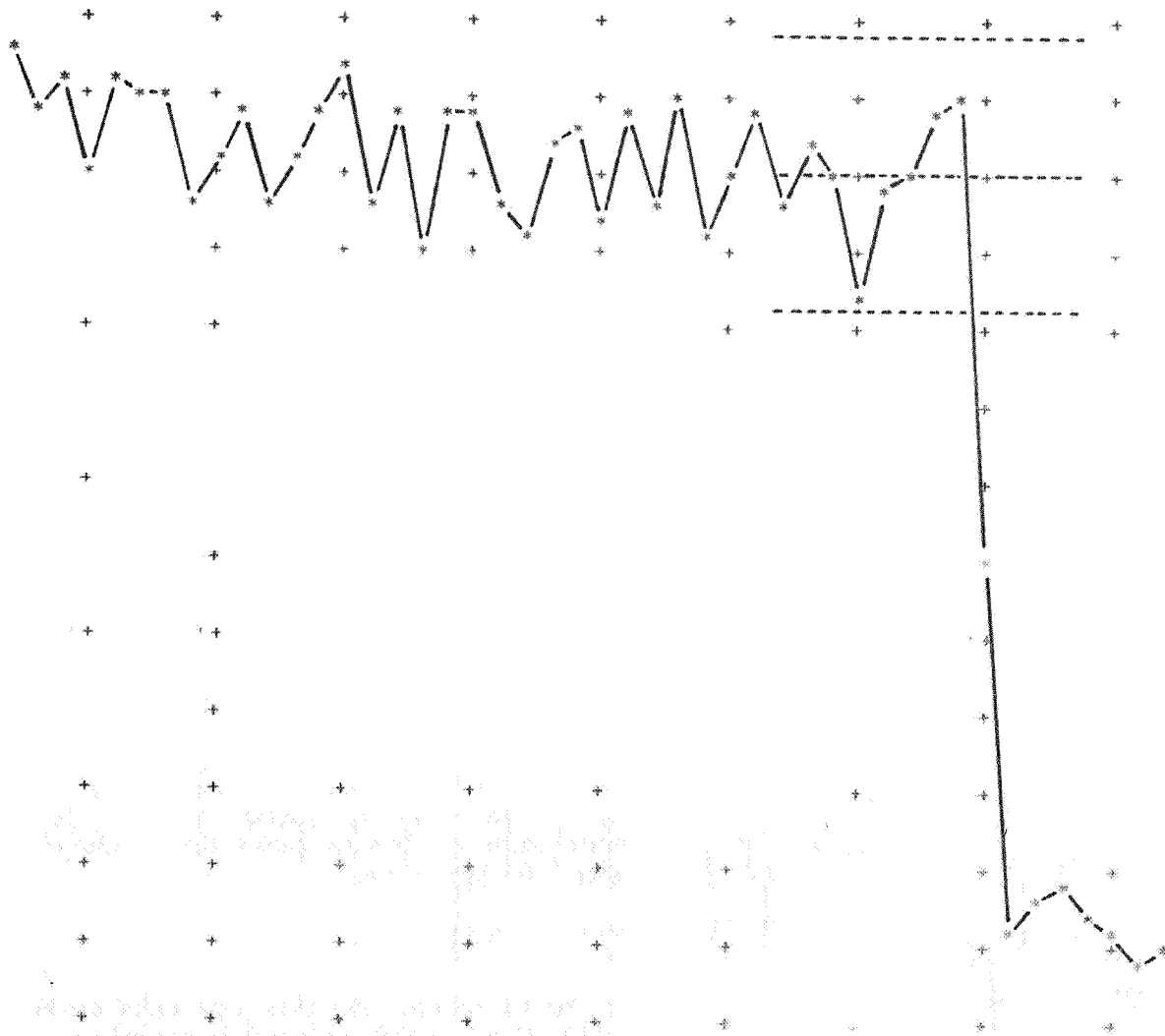

FIGURE 2.   SYNTHETIC DATA RECORD

as the start of a step. False alarm protection can be purchased by delaying the decision on a step at least one more sample time. A simple decision rule, such as requiring two consecutive raw data samples to fall outside the tolerance band, proved to be quite effective in discriminating between true signal steps and wild data points.

STEP DECISION RULE

The step detection decision rule actually adopted is slightly more complicated. This rule uses two tolerance bands centered about the estimated signal mean value as shown in Figure 3. The inner tolerance band is set at plus-and-minus-two noise standard deviations and the outer tolerance band is set at plus-and-minus-four noise standard deviations. A cumulative tolerance exceedance count is kept and is incremented by the values shown in Figure 3. The cumulative exceedance count and the exceedance count increments are signed numbers with the sign indicating the polarity of the exceedance. The cumulative exceedance count is reset to zero whenever a raw data sample falls inside the inner tolerance band or whenever the sign of the exceedance count differs from the sign of a nonzero exceedance increment. This procedure means that, when consecutive exceedances of alternating polarity occur, only the most recent exceedance will be remembered. The step detection decision rule is as follows: A step is declared to be present whenever the magnitude of the cumulative exceedance count is three or more. Note that the cumulative exceedance count is not reset when a step is detected and the filter may therefore be in the "step present" mode for several consecutive sample times.
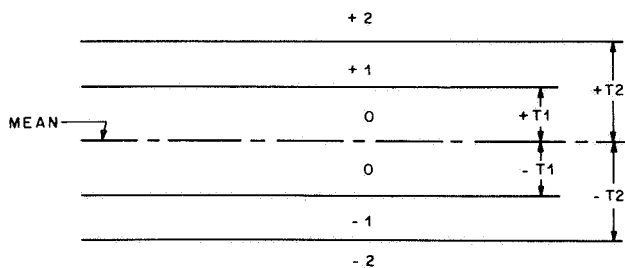

FIGURE 3. PAIR OF TOLERANCE BANDS

EXPONENTIAL FILTER

The experiments, using human subjects for the digital filter, indicated that there is a natural tendency for humans to weight the most recent data more heavily than older data when estimating the mean signal level. This sort of unequal weighting allows the filter to track a signal that has minor variations in signal level so that the level variations are not large enough to be considered as step changes. The well-known exponential digital filter provides a convenient mathematical formulation for digital filtering with the most recent data receiving more weight than older data. The computational equation for the exponential filter is

$$S_N = \alpha \cdot R_N + (1 - \alpha) \cdot S_{N-1} \quad ,$$

where S_N is the Nth smoothed data sample, R_N is the Nth raw data sample, S_{N-1} is the $N-1^{st}$ smoothed data sample, and α is a positive constant less than one. The constant, α, establishes the filter performance with the usual values of α falling in the approximate range 0.3 to 0.01. Small values of α give good noise suppression for constant level signals and slow step response. Larger values of α give faster step response and less noise suppression for constant level signals. The exponential filter is very convenient from a digital computer programming point of view because the required computation per data sample is merely two multiplications and one addition. The only data storage requirement is that the smoothed data sample from the preceding sample time must be saved. The exponential filter computational equation is a recursive relation that makes some special procedure necessary at start-up time. A common practice is to preload the S_{N-1} data storage location with an estimated value of the signal level.

Additional insight into the operation of the exponential filter may be gained by expanding the recursive computational equation in terms of the raw data samples. The expansion is

$$S_N = \alpha \cdot \sum_{K=0}^{N-1} (1 - \alpha)^K \cdot R_{N-K} + (1 - \alpha)^N \cdot R_O \quad ,$$

where R_O is the preloaded initial condition. This equation shows that the Nth smoothed data sample is a linear weighted combination of all preceding raw data samples with the weights decreasing with raw data sample age. The name of the exponential filter is derived from the exponential term under the summation sign. Notice in particular that the exponential filter effectively remembers something about all of the raw data samples that have been processed.

The exponential filter appears to be satisfactory for use in the thrust filtering problem during periods of constant signal level operation. The exponential filter constant, α, can be adjusted to provide satisfactory noise suppression, and the light computational and data storage requirements are ideal for real-time use. Re-examination of the typical synthetic signal in Figure 4 indicates that the filter operational mode may be broken down into phases as shown. The exponential filter provides a satisfactory technique for the constant signal level phases, but it is difficult to use during the initialization and step phases.

During the step phase, it is desired that the filter track the step rapidly and also provide some low pass filtering action. It is also desirable for the filter to discard all knowledge of the signal level before the start of the step. A very simple scheme that meets both of these objectives is to have the filter output consist of just the simple average of the last two raw data samples during the step phase. This procedure will provide fast step tracking with some low pass filtering action and also effectively discard knowledge of the signal level that existed before the step.

VARIABLE EXPONENTIAL FILTER

Modifying the exponential filter to allow the filter parameter α to be a function of time will provide a
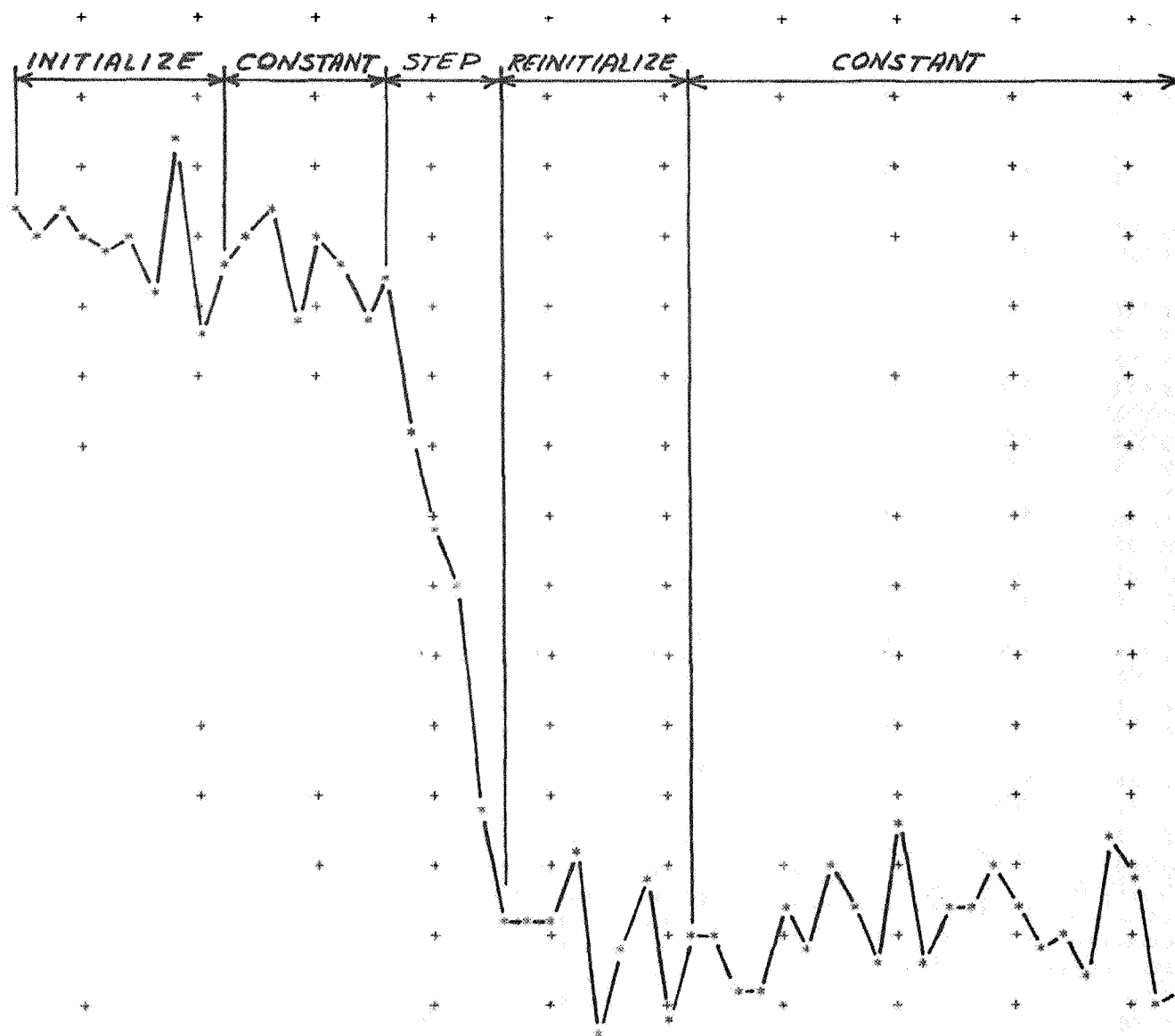

FIGURE 4. FILTER OPERATING MODES

workable scheme for filter initialization. The modified exponential filter equation is

$$S_N = \alpha(t) \cdot R_N + \left(1 - \alpha(t)\right) \cdot S_{N-1} \; .$$

The rule for the variation of $\alpha(t)$ should be chosen so that the numerical values smoothly decrease with time while the filter is in the initialization phase. Following initialization phase, $\alpha(t)$ should have a constant value for constant signal level operation. A simple functional form for $\alpha(t)$ is

$$\alpha(t) = 1/M \; ,$$

where M is an integer defined by

$$M = N - N_X + 2$$

with the condition

$$2 \le M \le M_{MAX} \; .$$

In these expressions, N is the current data sample serial number, N_X is the data sample serial number of the last sample for which the filter was in an input signal step mode and M_{MAX} is a constant that sets the value of α for constant signal level operation. This time variation of α will provide rapid convergence of the filter output to a good estimate of the signal level following a step and during initial start-up.

FILTER ALGORITHM

The necessary components for constructing a filter algorithm have been discussed. The flow chart of the filter algorithm in Figure 5 is intended to illustrate the mathematics and logic involved rather than an actual computer program. The chart is complete except for the details of preloading and original start-up of the filter. Since these details are best discussed in terms of an actual computer program, they will not receive further consideration here.

A detailed description of each numbered box in the flow chart is given below:

Box 1. The "error" signal, E, is calculated from the current raw data sample, R_N, and the best available estimate of the true signal level given by the smoothed data sample from the preceding sample time, S_{N-1}.

Box 2. An integer called L1 is calculated from the sign of the cumulative tolerance exceedance count, Q, and the sign of E. Integer arithmetic is used. If the signs of Q and E are opposite, L1 will have the value zero; if they are the same, L1 will have the value one.

Box 3. An integer called L2 is calculated from E and the tolerances T1 and T2. Integer arithmetic is used. The minimum functions limit the value of L2 to zero, one, or two. L2 is the magnitude of the tolerance exceedance incremental value for the current raw data sample. If the raw data sample falls inside the inner tolerance band, L2 will be zero. If the raw data sample falls between the two tolerance bands, L2 will be one; if it falls outside the outer tolerance band, L2 will be two.

Box 4. The cumulative exceedance count, Q, is incremented. The first term on the right effectively retains or discards the previous value of Q since L1 only takes on the values of zero or one. The second term on the right attaches the proper sign to the magnitude of the tolerance exceedance increment, L2.

Box 5. The value of the tolerance exceedance increment, L2, is tested and then the program flow branches. If L2 is zero, the raw data sample fell within the inner tolerance band and the flow goes to box 6; otherwise, the flow goes to box 7.

Box 6. The raw data sample is within the inner tolerance band. The cumulative tolerance exceedance count, Q, is set to zero, and the flow goes to box 10.

Box 7. The raw data sample is not within the inner tolerance band. The magnitude of the cumulative tolerance exceedance count, Q, is tested. If the magnitude of Q is less than two, it means that the current raw data sample fell between the tolerance bands, and the preceding raw data sample was either in tolerance or had a tolerance exceedance of opposite polarity. In the case at hand, the tolerance exceedance is merely noted, and the flow goes to box 10. If the magnitude of Q is equal to two, the situation is that either (1) the last two consecutive data samples have fallen between the tolerance bands, or (2) the last data sample fell outside the outer tolerance band and the previous data sample was either in tolerance or the exceedance was of opposite
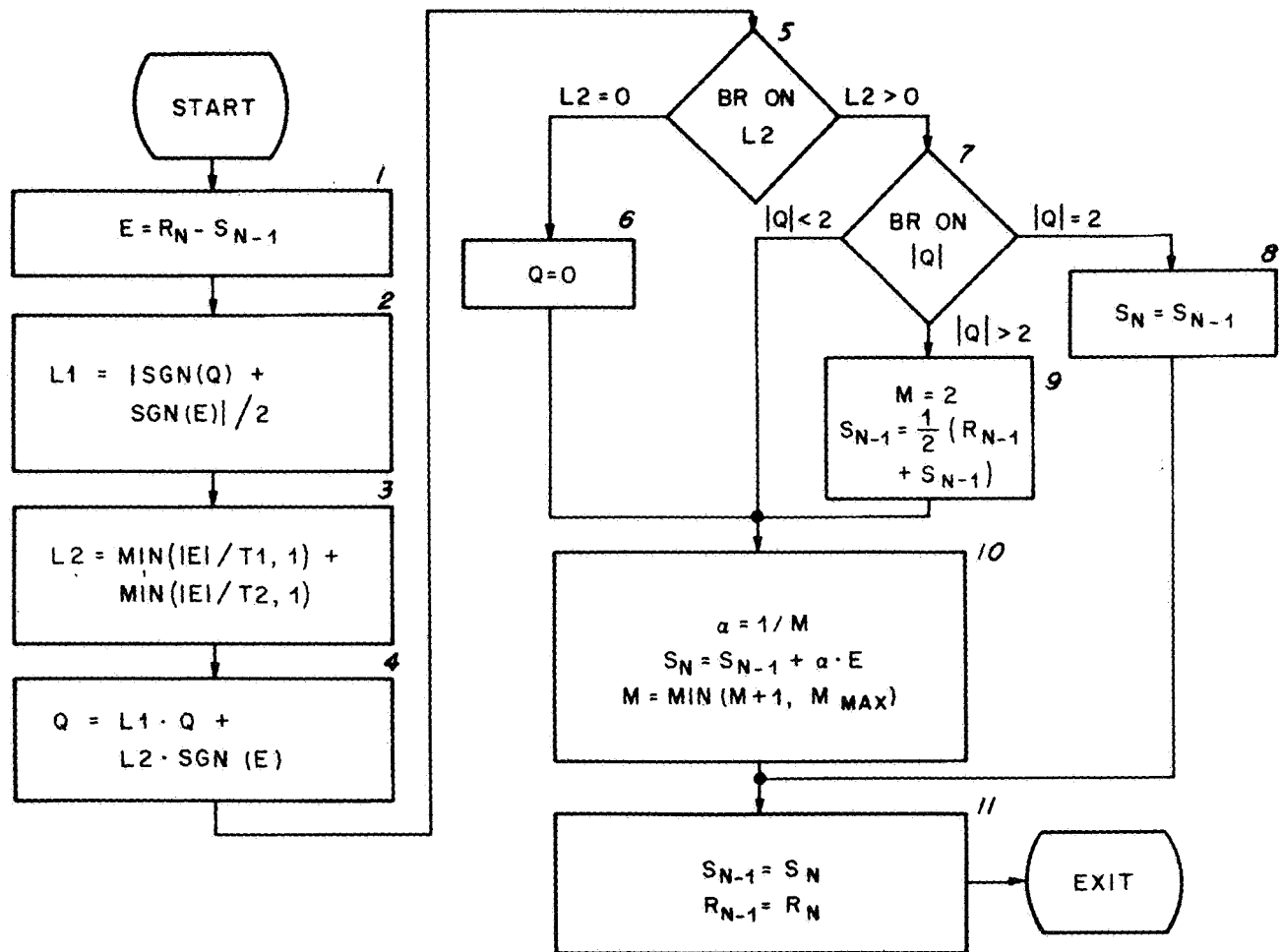
FIGURE 5. FILTER ALGORITHM

polarity. This is the possible wild data point condition with the flow going to box 8. If the magnitude of Q is greater than 2, the decision rule declares that a step in the input signal is present. This condition may be caused by three or more consecutive raw data samples falling between tolerance bands all with the same polarity, or two or more consecutive raw data samples falling outside the outer tolerance all with the same polarity, or some combination of consecutive raw data samples having tolerance exceedances split between the two tolerance bands with all exceedances of the same polarity. The flow goes to box 9.

Box 8. A possible wild data sample or start of a step condition exists. The decision rule requires that action be delayed until the next sample time and the best available estimate of the signal level, which is the output data sample from the preceding sample time, be used for the filter output. The flow bypasses the main smoothing computation and goes to box 11.

Box 9. A step in the input signal level is present. The output data sample will be forced to be the simple average of the last two raw data samples. The procedure is to set the filter coefficient control parameter, M, to two and to make the substitution shown for the value of the output data sample at the preceding sample time. This substitution is necessary because the main smoothing computation uses the value of E calculated in box 1.

Box 10. This is the main smoothing computation. The variable filter coefficient is calculated by the first line. The second line is the actual smoothing computation using the value of E calculated in box 1. The third line increments M by one

and limits M to be less than or equal to the constant M_{MAX}. This computation, together with that in box 9, provides for the time-varying coefficient operation during initialization and re-initialization following a step. The limiting provides for constant coefficient operation during periods of constant signal level.

Box 11. The necessary data exchanges required to set the filter for processing the next raw data sample are made in this box.

FILTER PERFORMANCE

Examples of filter performance are shown in Figures 6, 7, and 8, which are computer-printer plots with the filter input and output superimposed.

The filter input data are plotted with R's, and the output data are plotted with S's. Points where the input and output data points coincide are plotted with * 's. When the filter is in the input signal step mode, the output data are plotted with $'s. The raw data points were manually connected with dashed lines, and the smoothed data points were connected with solid lines for ease of interpretation. The background grid of plus signs was printed to provide a reference framework. These examples will be individually discussed. The value of M_{MAX} was set at 10 for all of these examples.

The input data in Figure 6 include a rather steep step. The filter detected the step and tracked it downward stabilizing at the new input signal level. The filter was in the step mode for two consecutive sample times with the step mode output plotted with
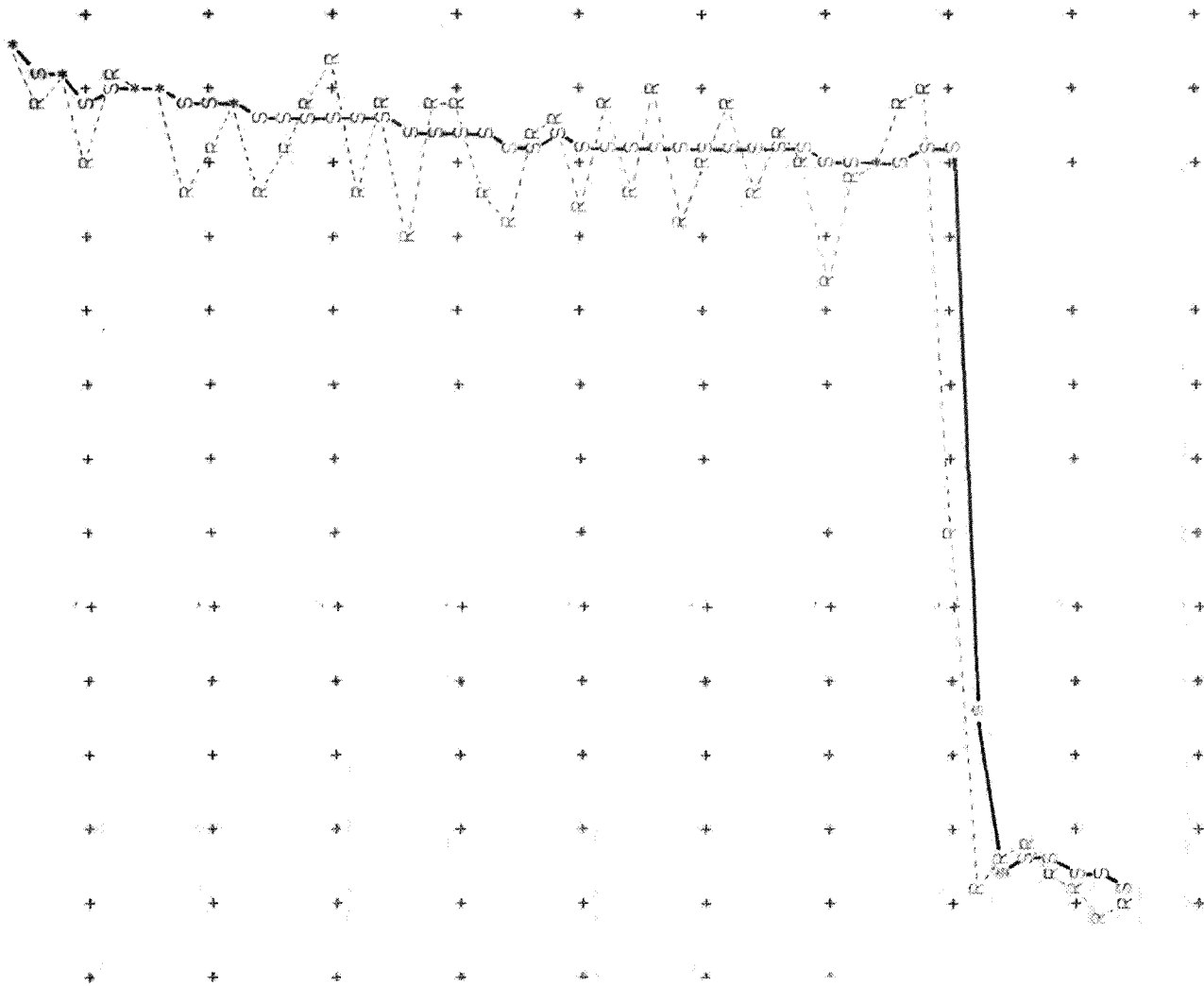
FIGURE 6. FILTER PERFORMANCE
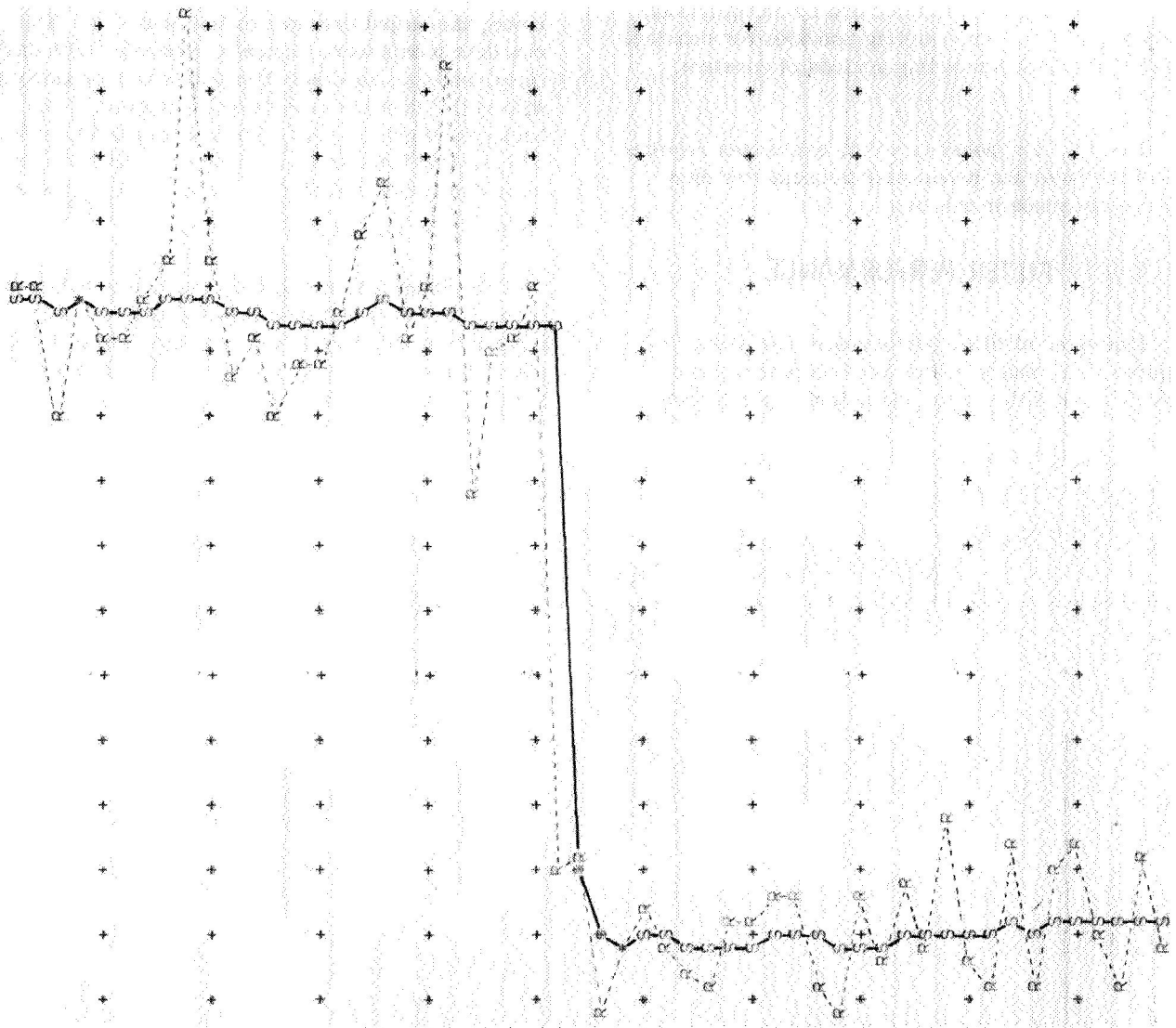
FIGURE 7. FILTER PERFORMANCE

$'s. While in the step mode, the output data is just the simple average of the last two input data samples.

The input data in Figure 7 include two wild data points with both wild point excursions being in the same direction. The filter recognized these points as being wild data, discarded them, tracked the step downward, and then stabilized at the new input signal level.

The input step in Figure 8 is smeared out over several data samples. The raw data in the step region are such that they appeared to be stabilizing at a new level about half-way down the step. This conclusion was false, and the filter corrected and tracked the step downward to the true signal level.
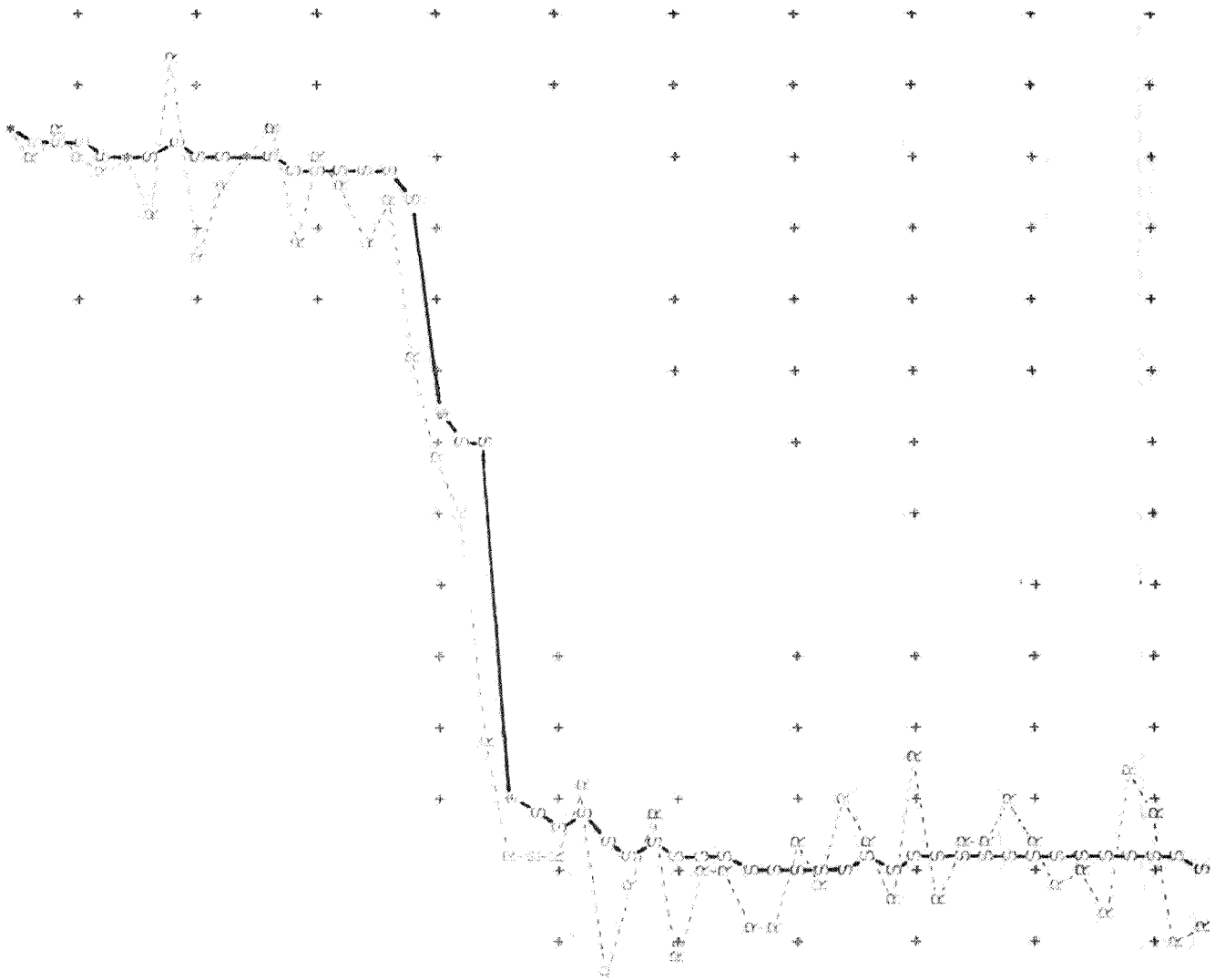
FIGURE 8. FILTER PERFORMANCE

CONCLUSIONS

The digital filter discussed in this paper has demonstrated that good filter performance in a difficult signal environment may be obtained by using a combination of a constant coefficient linear filter, a variable coefficient linear filter, and programmed logic. The greater utilization of the logical capabilities of digital computers in real-time signal processing is a fertile field for further research. This filter design illustrates the use of heuristic and experimental methods in achieving a practical solution to a technical problem.

BIBLIOGRAPHY

. R. G.: Smoothing Forecasting and Prediction of Discrete Time Series. Englewood Cliffs, N. J., ce-Hall, 1963.

2. ckman, R. B.: Data Smoothing and Prediction. Reading, Mass., Addison-Wesley, 1965.

REDUNDANCY EMPLOYING MAJORITY VOTING
FOR A SATURN SERVOACTUATOR

By

Michael A. Kalange, James D. Smith, and Chester W. Martin

SUMMARY

The servoactuator was developed to improve the reliability of the Saturn S-IVB thrust vector control system by insuring continued system operation if single point failures occur.

The selection of the majority voting technique is discussed. Its simplicity is cited along with the advantages of minimum weight, size, and power consumption, and compatibility with existing control electronics.

Operational features, design mechanization, and the analysis of test results are covered.

INTRODUCTION

A redundant, majority voting servoactuator has been developed for the attitude control system of the Saturn S-IVB stage (Fig. 1), the stage that provides the velocity increment to place the Apollo spacecraft into a trajectory to the moon. During powered flight, the Saturn vehicle attitude control is obtained by gimbaling the main propulsion engines of each respective stage. The engines are gimbaled by hydraulic actuation systems where servoactuators convert electrical command signals and hydraulic power into mechanical output which controls the vehicle thrust vector.

The Saturn booster lower stages (Fig. 2) have a clustered, multiengine arrangement which provides a redundancy effect for not only the propulsion system but also the thrust vectoring system. With this arrangement, satisfactory vehicle control can be maintained even with a failure of one engine (two at some times of flight). Other methods of enhancing the reliability of the single engine S-IVB stages were necessary. The complex mission requirements of this stage as a part of both the uprated Saturn and Saturn V launch vehicles dictate maximum reliability of all flight critical systems to insure mission success. The original, non-redundant S-IVB thrust vector control servoactuators
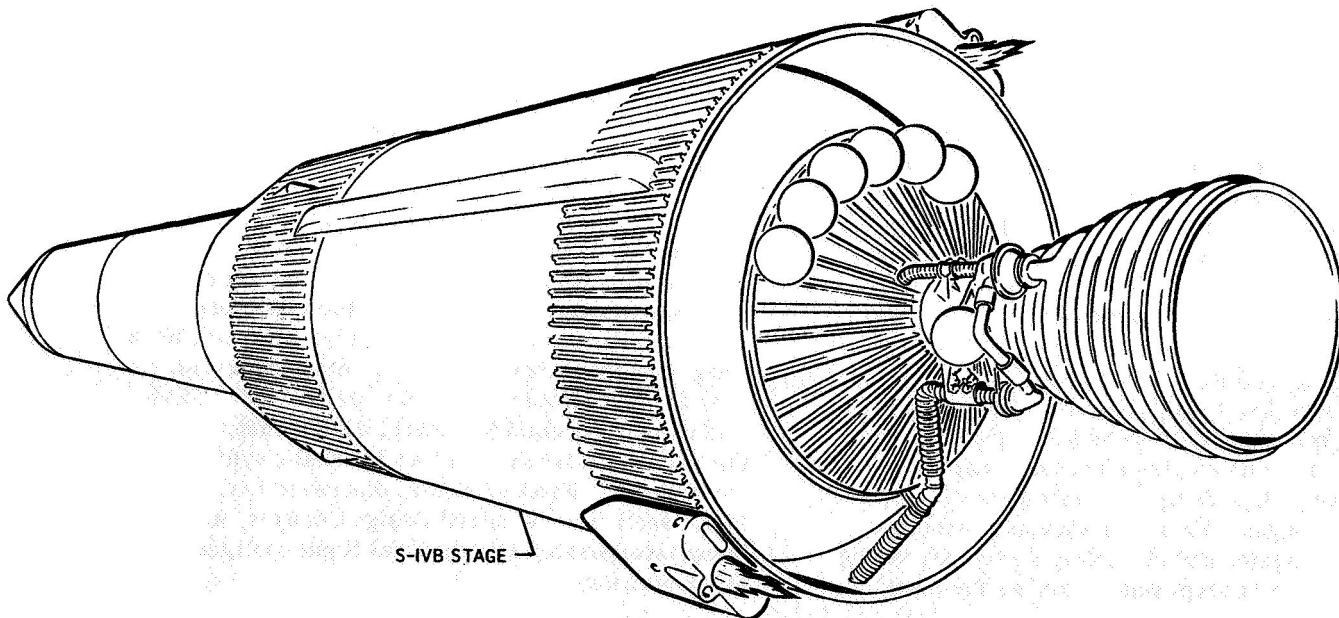

FIGURE 1. SATURN S-IVB STAGE

APOLLO
SPACECRAFT

INSTRUMENT UNIT

THIRD STAGE
(S-IVB)

111 m

SECOND STAGE
(S-II)

FIRST STAGE
(S-IC)

APOLLO
SPACECRAFT

INSTRUMENT UNIT

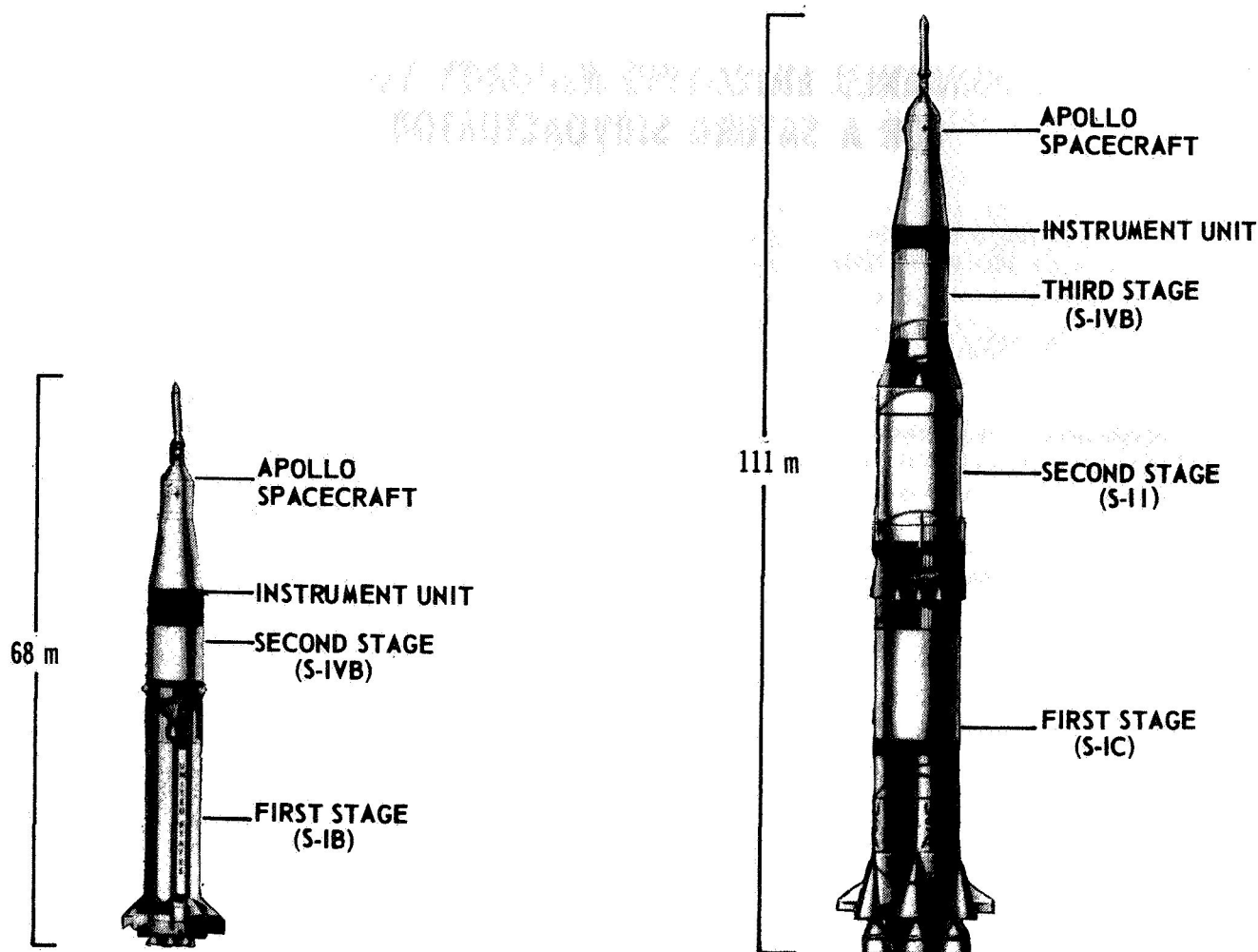SECOND STAGE
(S-IVB)

68 m

FIRST STAGE
(S-IB)

FIGURE 2. SATURN LAUNCH VEHICLES

are adequate in all operational performance aspects, but they are also a single point failure source. The need to eliminate single point failure possibilities in the thrust vectoring system resulted in a program to study various reliability improvement techniques. The already stringent quality control, inspection, and acceptance test procedures being employed were considered adequate. The only alternative was to consider a redundancy concept as the most likely reliability improvement approach.

Under the constraints of a requirement that any redundant servoactuator would have to be mechanically and electrically interchangeable with the existing stage design, a preliminary feasibility study was begun. Various redundancy schemes were investigated and ultimately a majority voting servoactuator concept was chosen as the most

feasible method to employ in reducing single point failures. Majority voting provided redundancy of the most critical servoactuator components without imposing weight and power consumption penalties on the system.

Two majority voting servoactuators were designed, fabricated, and subjected to extensive development testing. Actuator operating characteristics with various failures in the redundancy scheme were studied. The prototype actuators were integrated into a breadboard type stage hydraulic system, and further testing was performed. These initial tests resulted in several design changes to the servoactuator and to other hydraulic system components. These changes, discussed in detail in the section on Required Design Changes, are being incorporated into the final flight configuration servoactuators.

FEASIBILITY STUDIES AND RELIABILITY CONSIDERATIONS

Feasibility studies were initiated to investigate the S-IVB thrust vectoring system requirements and the existing hardware design to determine if any system changes could be made to improve the overall system reliability and performance. A study program of hydraulic control system optimization techniques indicated that from an overall mission requirements standpoint, no changes in the S-IVB stage control system were required. Reliability considerations, however, made it highly desirable that single point failure sources be reduced.

Studies which considered overall stage requirements including the gimbaling system indicated that some redundancy scheme could best satisfy the increased reliability requirements. The study of any redundancy concept involves considerable judgment in deciding between the actual gains made by going redundant against the losses from the added complexity of a redundant system. It is possible that in incorporating redundant components, failure detection devices, and switching devices, a decrease in reliability may result. Such an approach also leads to greater system weight and volume and to higher power consumption.

Since the S-IVB stage was already designed and flight qualified, it became necessary to consider parameters other than just the servoactuator. Any change in the actuator would have to be compatible with the existing control requirements, mechanical envelope dimensions, and control electronics. To keep the actuation system as simple as possible, the selected redundancy scheme should incorporate only those features necessary to eliminate possible single point failures. Dual hydraulic cylinders, pumps, accumulators, etc., would not increase the overall system reliability enough to compensate for the penalties imposed by greater system weight, power requirements, and cost.

The most critical component of any hydraulic servoactuator is the servovalve. Typical high performance servovalves require extremely close fitting spools and sleeves and small orifices in the nozzle-flapper area. This makes the servovalve susceptible to contamination present in the operating fluid. In addition, the servovalve first stage has an electrical torque motor which is susceptible to open or short circuits. A system that would provide

redundancy of these components would offer significant gains in system reliability without undue penalties of overall system complexity.

The original nonredundant S-IVB stage servoactuator has a position mechanical feedback arrangement whereby the need for an electrical feedback transducer is eliminated. Mechanical feedback was a significant advancement in hydraulic servoactuator technology because it eliminated the requirement for the electrical feedback transducer (an inherently failure-prone component), the electrical power supply, and associated wiring. Mechanical feedback also eliminated the need for a feedback amplifier and summing network in the control electronics system. Because of the improvements resulting from a mechanical feedback actuator, this design feature was retained in the redundant majority voting servoactuator configuration.

SERVOACTUATOR OPERATION AND DESIGN

The majority voting actuator uses three active torque motors driven by three separate amplifiers as shown in Figure 3. Voting is performed in the servoactuator only. The torque motors receive feedback from the valve spool and actuator piston. The output pressures of the three torque motor-driven hydraulic amplifiers are summed at the end of the valve spool. The actuator piston behaves as the majority of the hydraulic amplifiers dictate. A majority decision exists when two hydraulic amplifiers are in agreement.

Each of the three hydraulic amplifier assemblies is as nearly alike as possible (Fig. 4) to minimize the differences of each assembly in overall performance characteristics. Each torque motor has a balanced T-shaped armature-flapper mounted for pivotal motion on a flexure tube. A polarizing magnetic flux circuit is formed by upper and lower pole pieces supported by two permanent magnets. The motor armature is positioned in the magnetic flux circuit by the flexure tube. The flexure tube also acts as a seal between the electrical and hydraulic sections of the servovalve. For increased reliability, two torque motor coils are wired in parallel and positioned about the armature. Majority operation is possible because the mechanical feedback torque motor armatures are essentially free beams sensitive to force balance. A failure of any redundant element (loss of input, loss of feedback,
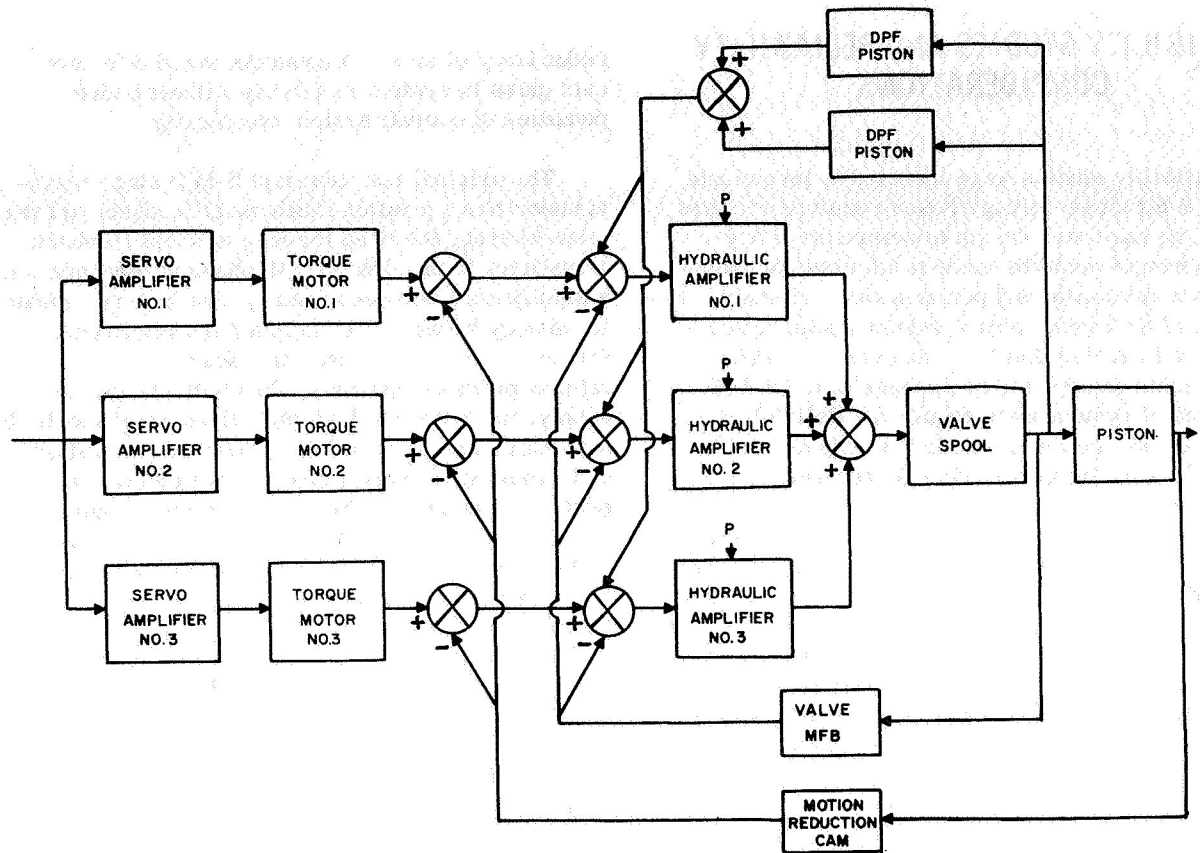
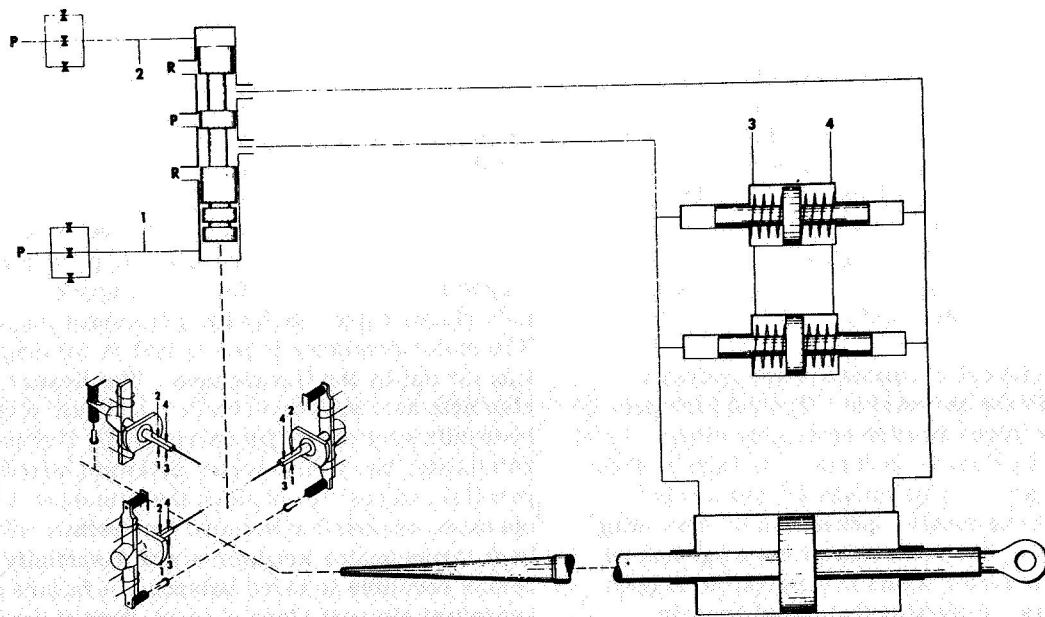FIGURE 3. BLOCK DIAGRAM OF MAJORITY VOTING CONCEPT

FIGURE 4. SCHEMATIC OF MAJORITY VOTING SERVOACTUATOR

hardover armature-flapper, change of forward-loop gain, etc.) would result in a change in the output of that respective hydraulic amplifier and result in a change in spool end pressure and a change in valve spool position. The change in spool position is fed back to the torque motor flappers and in turn the two properly functioning hydraulic amplifiers equalize the spool end pressure generated by the faulty hydraulic amplifiers. The feedback and hydraulic amplifier gains were made high enough so only a very small spool displacement is required to correct the effect of the failure.

In accordance with the specific and performance criteria for the S-IVB stage, two prototype servoactuators (Fig. 5) were fabricated and subjected to an extensive development test program.

servoactuator incorporated the following features, whose functions are described.

SERVOVALVE

The three torque motor mechanical feedback majority voting servovalve (Fig. 6) is the key element of the selected redundancy concept. The three first stage assemblies consist of a dual coil d.c. torque motor, flexure mounted flapper, first stage nozzles, filter orifice assembly, feedback cantilever spring, load damping nozzles, and load damping nozzle filters. The first stage assemblies control fluid flow to the servovalve, actuator, piston, and cylinder. The load damping, or dynamic pressure feedback (DPF), is a method of damping resonant loads to minimize their effect on control system

Original Nonredundant Concept
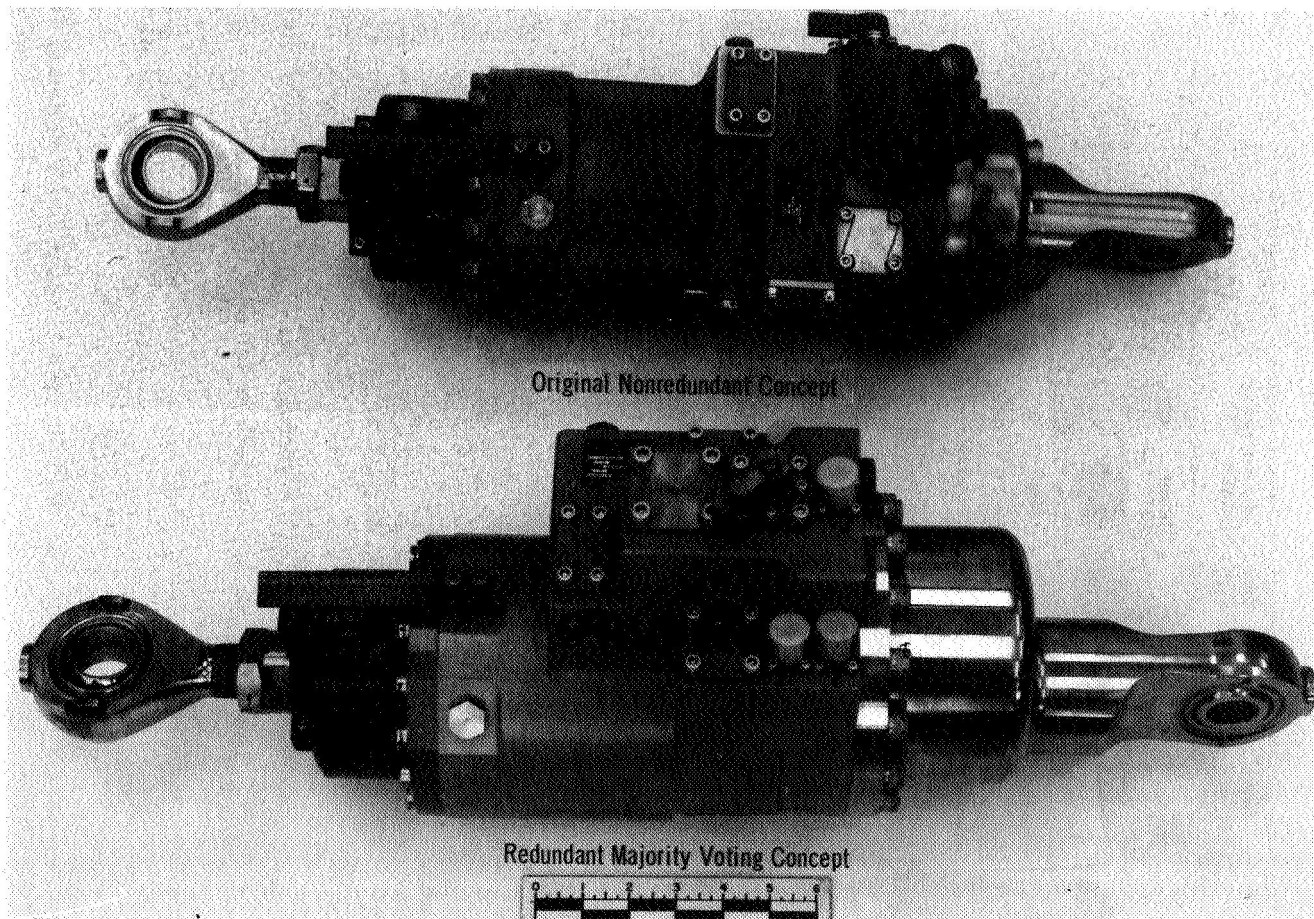
Redundant Majority Voting Concept

FIGURE 5. MAJORITY VOTING SERVOACTUATOR

The test program included hardware evaluation at both a component and system level. A schematic of the redundant actuator is shown in Figure 6. Each

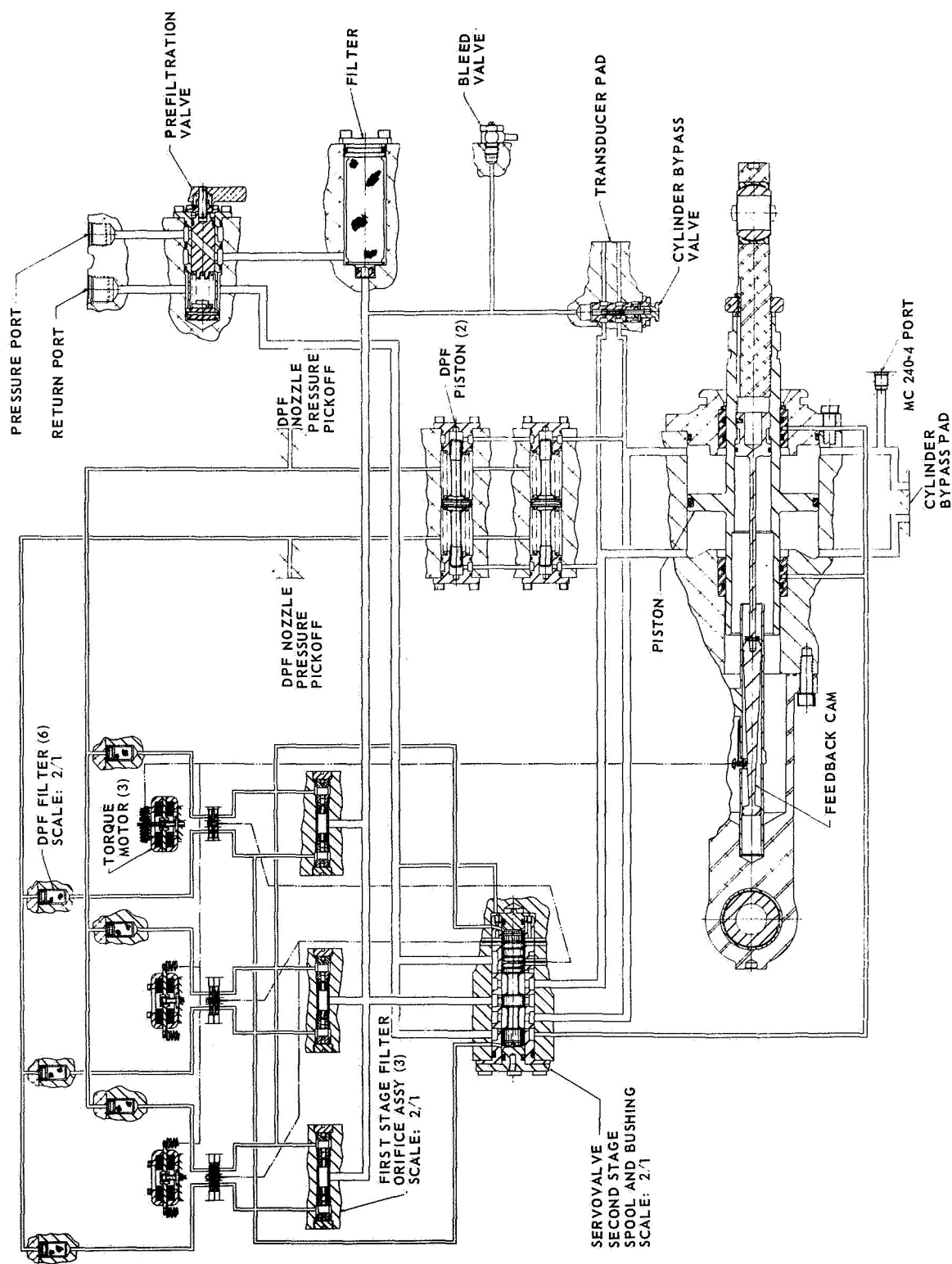performance. This will be discussed in more detail later.

FIGURE 6. SCHEMATIC OF REDUNDANT SERVOACTUATOR

Of the three first stage hydraulic amplifiers, two used a balance armature feedback concept. For these two assemblies, springs are located at each end of the motor armature where the ends protrude through the air gaps. One spring is preadjusted to a fixed position between the armature and servovalve body. The other spring is fitted between the armature and the position feedback cam by a cantilever beam cam follower assembly. The third hydraulic amplifier differs in that it uses a flapper extension to hold the flapper and armature assembly in a balanced position. This design arrangement provides a simpler design of the mechanical feedback mechanism. The flapper of each first stage amplifier is rigidly attached to the midpoint of the armature. Each flapper extends through a flexure tube and passes between two first stage nozzles and two dynamic pressure feedback (DPF) nozzles to provide two sets of variable orifices between the nozzle tips and the flapper. The amplifier passages from the first stage nozzles terminate in common chambers at the ends of the second stage spool. The DPF nozzle passages are joined in a common bushing groove and are ported through the servovalve body by the DPF pistons. Each torque motor is linked mechanically to the feedback wire to provide mechanical feedback force during servovalve operation.

SECOND STAGE BUSHING AND SPOOL ASSEMBLY

The second stage bushing and spool is physically larger than a normal electro-hydraulic servovalve. This large physical size provides comparatively high spool driving forces and thereby reduces the valve's susceptibility to contamination. The bushing itself is a flange-mounted laminar fit into a dead end bore.

POSITION FEEDBACK MECHANISM

The actuator position feedback mechanism consists of a tapered cylindrical cam, three cam follower assemblies, and three position feedback springs. The cam is attached to the servoactuator piston rod and any movement of the rod is transmitted through a cantilever beam cam follower assembly and position feedback wire back to the first stage hydraulic amplifier assembly. Restraining devices are used to minimize deadband in the moving mechanical joints. This position feedback mechanism provides triple mechanical feedback redundancy of servoactuator piston position.

DYNAMIC PRESSURE FEEDBACK (DPF) NETWORK

The servovalve incorporates a DPF network using two nozzles and two spring-centered capacitance pistons to provide damping of resonant loads. A pair of DPF nozzles are located directly above each pair of first stage nozzles and are hydraulically connected to opposite sides of the spring-centered pistons. These pistons provide redundant operation and are located in the servoactuator body. The piston stubs are exposed to the cylinder pressure lines and are hydraulically coupled to the DPF nozzles to form the frequency sensitive DPF network.

The DPF arrangement is identical to that used on the original S-IVB stage servoactuator. Balancing the spool end pressures, nozzle flow, and torques throughout the servovalve accomplishes load damping. Two spring-centered capacitance pistons provide redundant operation in the event one DPF piston fails. The system is designed to dampen resonant loads well below the resonant frequency.

ELECTRICAL POSITION TRANSDUCER

The S-IVB stage majority voting actuator utilizes a strain gage position indicating transducer. The strain gages are mounted on the cam follower cantilever beams of the mechanical feedback mechanism. The free end of the cantilever beam, in moving, is stressed linearly and in turn is read as strain by the wire type strain gage. Signal conditioning equipment is provided to amplify the output up to a level compatible with existing measuring and telemetry equipment. The strain gages also eliminate the use of the potentiometer shaft as a feedback cam driving mechanism.

ACCESSORY COMPONENTS

In addition to the major subcomponents of the majority voting servoactuator, other items are provided to protect the assembly during operation or to facilitate actuator and stage checkout. Briefly, these items are:

1. Hydraulic Fluid Filter. A non-bypass type filter is located in the main actuator housing. It is rated at 505 cm^3/s (8 gpm) with a 17 N/cm^2 (25 psi) pressure drop. It is a 5 micron nominal,

15 micron absolute filter fabricated from a stainless steel wire cloth material. In addition, smaller wire mesh type filter orifices are provided for the servo-valve first stage hydraulic amplifier assemblies and for the DPF network.

2. Prefiltration Bypass Valve. The prefiltration valve assembly allows fluid circulation through the actuator inlet port and directly through to the outlet to facilitate complete hydraulic system flushing.

3. Cylinder Bypass Valve. The cylinder bypass valve, when operated, allows manual movement of the piston rod by interconnecting both sides of the cylinder. The bypass valve also connects the cylinder lines to a transducer pad that is equipped with a differential pressure transducer to monitor actuator cylinder line pressure.

4. Midstroke Lock. A simple, removable midstroke lock is provided to mechanically lock the actuator piston rod at a mechanical null position. The lock is designed to withstand full actuator force output without damage to either the lock or actuator.

5. Piston Position Indicator. A mechanical indicating device is included to aid in actuator calibration and checkout at field sites. The indicator is calibrated in degrees of engine displacement and, when used with the vernier provided, is capable of 0.04 degree readout accuracy.

6. Bleed Ports, etc. Various bleed ports, test ports, and oil sample ports are located to provide proper bleeding of the actuator and to allow easy installation of measuring transducers for checkout and flight telemetry.

TEST PROGRAM DETAILS

Initial testing of the S-IVB majority voting actuator consisted of performing acceptance tests on each unit to the current S-IVB stage servoactuator acceptance test criteria. Additional tests were derived to properly test the majority voting portion of the servoactuators. Both prototype actuators were operated in a normal mode with all three torque motors active. All performance parameters were within the S-IVB stage actuator requirements with the exception of total internal leakage and mechanical stroke.

To meet the external envelope dimensions of the S-IVB stage, the actuator stroke was reduced. The higher internal leakage resulted from having three hydraulic amplifier assemblies instead of one as in the nonredundant actuators. These differences did not represent design or performance discrepancies; only required deviations to fabricate the two prototype actuators are represented. The effect of the deviations will be discussed in the section on Required Design Changes.

Additional testing was performed to illustrate operation of the actuator with various failures induced in the actuator. Examples of these failures include plugged nozzles, plugged inlets, broken flexure sleeve, broken DPF springs, electrical opens, hardovers, and null offsets. This test program was designed to provide meaningful data on overall actual differences in actuator performance with various failure modes. The test series provided data on the servovalve, the actuator, and the two subassemblies together under both loaded and no-load conditions. A summation of the testing performed and the results on servoactuator performance is shown in Table I.

To further demonstrate the overall performance and reliability gains of the majority voting actuator, high temperature and vibration environmental tests were performed. Again, no major design discrepancies were detected. The servovalve did show sensitivity to certain sinusoidal vibration inputs; however, this can be corrected by minor redesign of the servovalve first stage. This vibration sensitivity has been experienced on other actuator designs and has been corrected with very minor changes such as mechanical stops to limit flapper travel and variation of the support spring rates.

One known characteristic of the majority voting configuration was accurately demonstrated by the test program. The majority voting actuator operating in a normal mode essentially duplicates the nonredundant actuator in performance. Certain failure modes such as one open torque motor or one hardover torque motor will affect performance. With one motor hardover there will be approximately a two percent shift in the normal output position and the normal gain position will be reduced by one-third. Although overall actuator performance is affected by a torque motor failure, the system will compensate and will still provide adequate control forces to complete a flight mission. A torque motor

TABLE I. PERFORMANCE CHARACTERISTICS
SINGLE POINT FAILURE vs. ALL ACTIVE MODE CONFIGURATION

CHARACTERISTIC	PLUGGED NOZZLE FIRST STAGE	PLUGGED NOZZLE DPF	PLUGGED INLET	BROKEN FLEXURE SLEEVE	HARDOVER ONE CHANNEL	OPEN ONE CHANNEL	DRIFT ONE CHANNEL	JAMMED DPF PISTON	BROKEN SPRING DPF PISTON	FAILED SEAL DPF PISTON	ALL ACTIVE MODE	REMARKS	PRESENT ACTUATOR (REF.)
ACTUATOR SENSITIVITY	NO CHANGE	NO CHANGE	NO CHANGE	NO CHANGE	NO CHANGE	NO CHANGE	NO CHANGE	NO CHANGE	NO CHANGE	NO CHANGE	NOMINAL	WITH AN OPEN CHANNEL, A LOW SENSITIVITY (2/3 NORMAL) EXISTS NEAR ACTUATOR NULL. A DRIFT INPUT FOLLOWED BY OPEN, CAUSES THE 2/3 AREA TO SHIFT A LIKE AMOUNT.	NOMINAL
ACTUATOR NULL BIAS	≅ 2%	NO CHANGE	≅ 1%	≅ 1%	< 2%	NO CHANGE	< 2%	NO CHANGE	NO CHANGE	NO CHANGE	0%		0%
ACTUATOR THRESHOLD	NO CHANGE	NO CHANGE	NO CHANGE	NO CHANGE	NO CHANGE	NO CHANGE	NO CHANGE	NO CHANGE	NO CHANGE	NO CHANGE	0.5% OF RATED		< 0.5% OF RATED
ACTUATOR HYSTERESIS	NO CHANGE	NO CHANGE	NO CHANGE	NO CHANGE	NO CHANGE	NO CHANGE	NO CHANGE	NO CHANGE	NO CHANGE	NO CHANGE	3.0% OF RATED		< 3.0% OF RATED
SIMULATOR DYNAMICS	IN SPEC.	IN SPEC.	IN SPEC.	IN SPEC.	IN SPEC.	IN SPEC.	IN SPEC.	IN SPEC.	IN SPEC.	IN SPEC.	IN SPEC.		IN SPEC.
VALVE'S INCREMENTAL SPOOL DRIVING FORCE	55.5 N (12.5 lb) / 1% OF RATED	NO CHANGE	NO CHANGE	NOT MEASURED	53.5 N (12 lb)/1%	46.7 N (10.5 lb)/1%	46.7 N (10.5 lb)/1%	NO CHANGE	NO CHANGE	NO CHANGE	66.7 N (15 lb)/1% OF RATED		≅ 1/2, ie. 334 N (75 lb)/1% RATED
ULTIMATE SPOOL DRIVING FORCE	712 N (160 lb)	NO CHANGE	NO CHANGE	NOT MEASURED	267 N (60 lb)	334 N (75 lb)	245 N (55 lb)	NO CHANGE	NO CHANGE	NO CHANGE	845 N (190 lb)	IN ALL CASES, VALUES LISTED ARE THE LOWEST OBTAINED WHEN EXAMINING BOTH POLARITIES OF INPUT SIGNAL.	≅ 1/2, ie 423 N (95 lb)
VALVE FLOW GAIN	NO CHANGE	NO CHANGE	NO CHANGE	NOT MEASURED	NO CHANGE	SEE REMARKS	SEE REMARKS	NO CHANGE	NO CHANGE	NO CHANGE	NOMINAL	WITH AN OPEN CHANNEL, A 2/3 GAIN AREA WILL EXIST NEAR NULL. A DRIFT INPUT CAUSES THE 2/3 GAIN TO SHIFT A LIKE AMOUNT.	NOMINAL
VALVE NULL BIAS	≅ 2% OF RATED	NO CHANGE	≅ 1%	NOT MEASURED	<2.0%	CHANGE	<2.0%	NO CHANGE	NO CHANGE	NO CHANGE	0%		0%
DPF CORNER FREQUENCY & DAMPING SLOPE	NO CHANGE	0.87 Hz 0.302 cc/s N/cm² (0.0127 cis/psi)	1.32 Hz 0.321 cc/s N/cm² (0.0135 cis/psi)	NOT MEASURED	1.30 Hz 0.366 cc/s N/cm² (0.0154 cis/psi)	1.0 Hz 0.397 cc/s N/cm² (0.0167 cis/psi)	≅1.2 Hz 0.357 cc/s N/cm² (0.015 cis/psi)	3.25 Hz 0.324 cc/s N/cm² (0.0136 cis/psi)	0.87 Hz 3.76 cc/s N/cm² (0.158 cis/psi)	1.65 Hz 0.324 cc/s N/cm² (0.0136 cis/psi)	1.0 Hz 3.24 cc/s N/cm² (0.136 cis/psi)	DIFFICULTY IN OBTAINING CONSISTENT RESULTS CAN INTRODUCE AS MUCH AS 15% ERROR IN THESE READINGS.	1.0 Hz 3.24 cc/s N/cm² (0.136 cis/psi)

failure in a nonredundant actuator would result in loss of control and compromise or abort the flight mission. Figures 7, 8, and 9 are typical performance curves obtained during this testing.

therefore, it can be concluded that adequate DPF action is maintained with one failed DPF network. In a nonredundant configuration, complete load damping would have been lost.
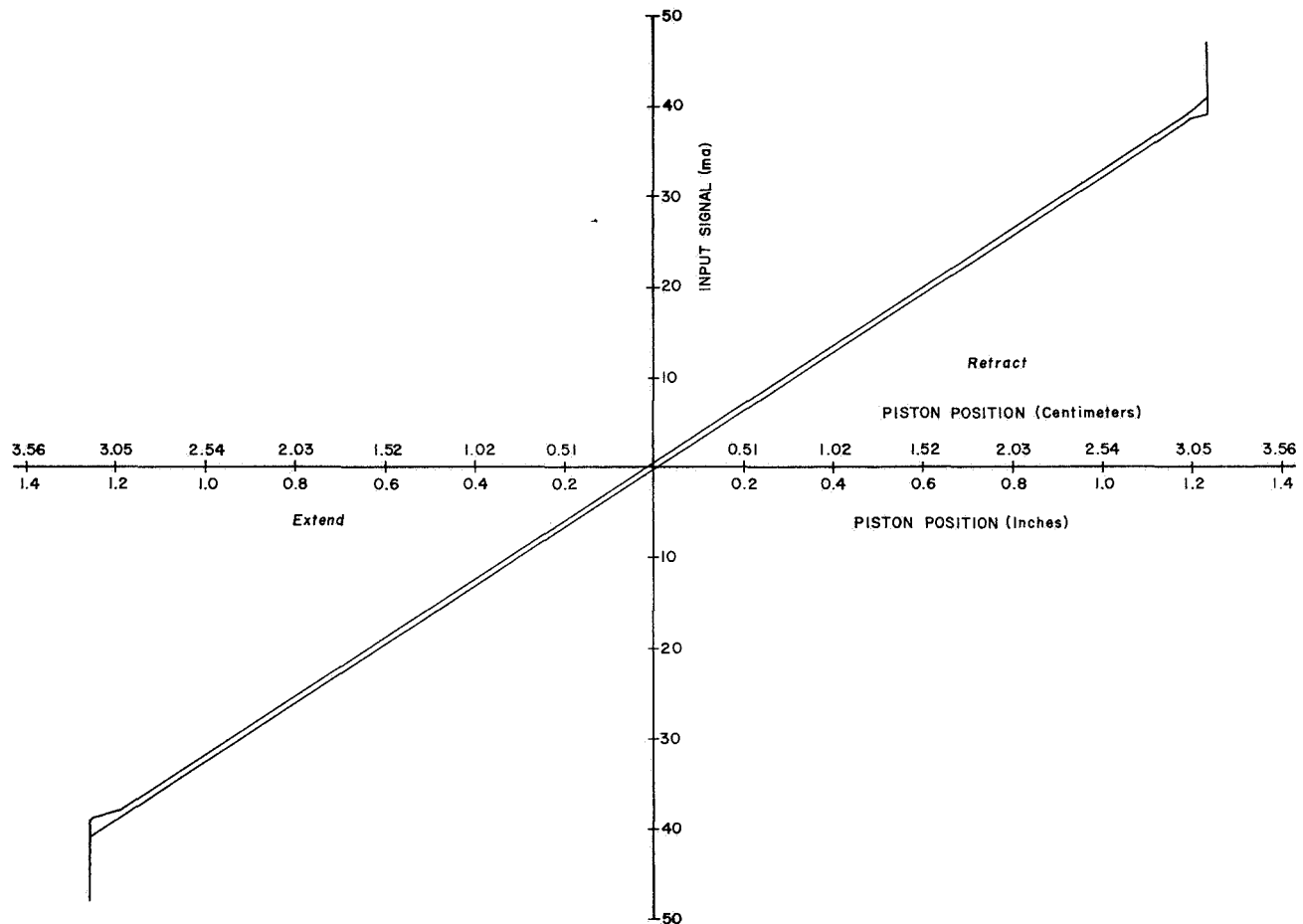

FIGURE 7. PERFORMANCE DATA - ALL TORQUE MOTORS ACTIVE

A failure in the load compensating, or DPF, network was also simulated. The worst case failure in the DPF section was simulated by removing a piston cap seal and "O" ring from one of the DPF pistons. A constant cylinder differential pressure of ±276 N/cm^2 (±400 psid) was maintained for this test. The break frequency of the DPF network increased from 0.8 Hz to 2.0 Hz, which would alter the load damping characteristics of the actuator. However, a reduction of this magnitude is too small to affect the control system. Other failures in the DPF network would not have any more influence over overall performance than that of a seal failure;

Additional test data were obtained primarily to insure overall hydraulic system compatibility of the majority voting actuator configuration in the S-IVB stage. Various system pressures were tested, and attempts were made to optimize the overall system with a minimum number of actual hardware changes. System thermal characteristics were studied for compatibility with the existing stage design.

The conclusion reached from this extensive test program was that the majority voting actuator could be used on the S-IVB stage without extensive
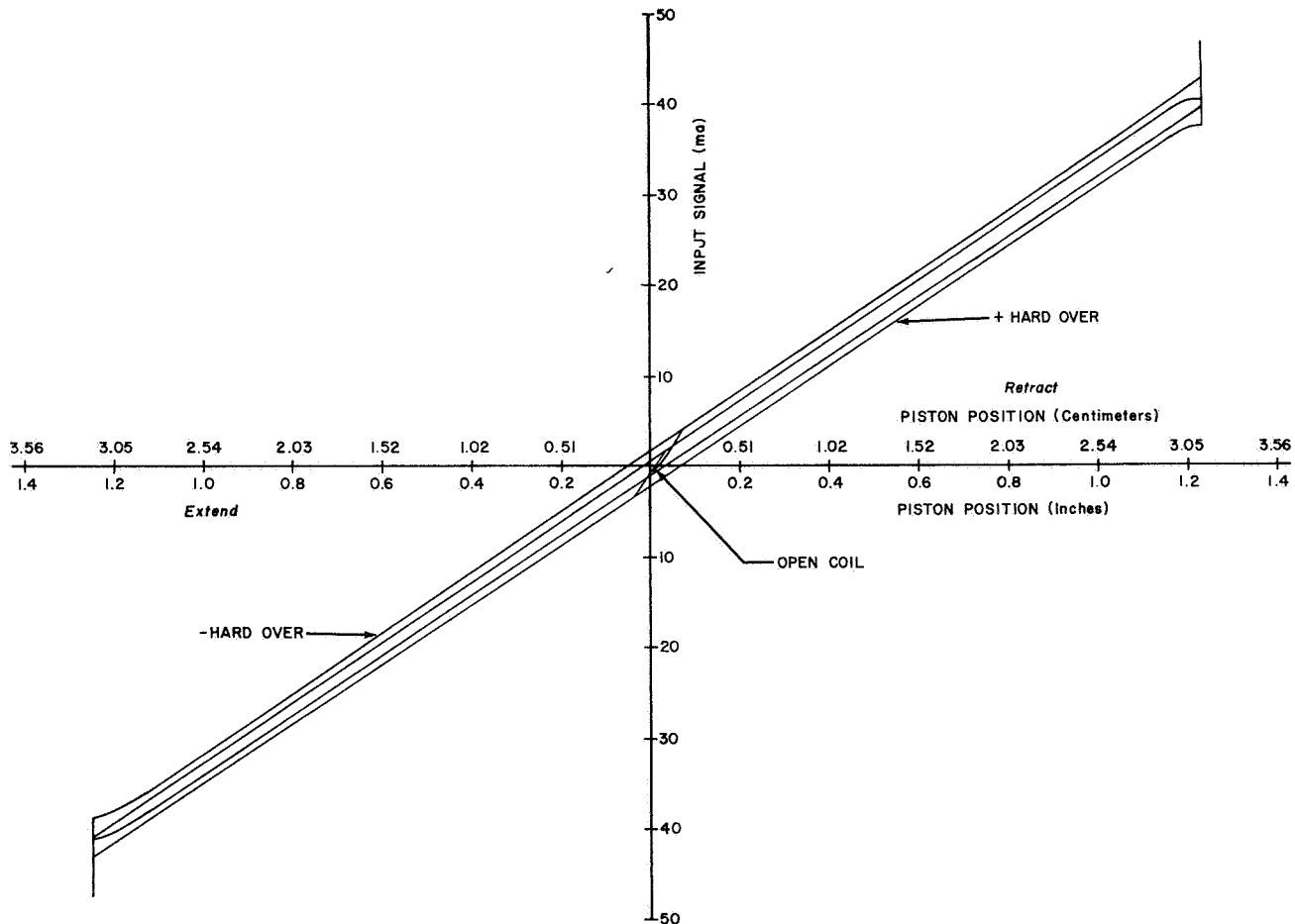
FIGURE 8. PERFORMANCE DATA - SIMULATED FAILURE MODES

redesign of the flight stage or existing ground support equipment. In a normal no failure mode the actuator was adequate for the control forces required. In a single failure mode of any of the critical servovalve components, actuator performance was compromised slightly, but proper vehicle attitude control could be adequately maintained to successfully complete a flight mission.

REQUIRED DESIGN CHANGES

Concurrent with the majority voting servoactuator program, the complete stage hydraulic system was analyzed to determine those parameters which might be changed to gain in overall reliability and to interface with the majority voting actuator. Various minor design changes in lines, brackets, etc., were made to facilitate incorporation of the new actuator configuration. All changes made to the stage or to the

actuator resulted in improvements to the control system performance and/or reliability. Table II is a summary comparing the conventional (non-redundant) actuator with the majority voting actuator design. The significant design changes are discussed briefly below.

CONTROL COMPUTER CHANGES

Since the control electronics were already triple redundant, the only changes to the control computer were to remove the comparator and switching circuits, which sensed an amplifier failure and provided switching to a good channel. This change was necessary since the selection, or voting, is now done by the actuator. This configuration effectively reduces the complexity of the S-IVB control electronics.

STAGE HYDRAULIC SYSTEM PRESSURE

The S-IVB stage hydraulic system was originally designed for an operating pressure of 2517 N/cm^2
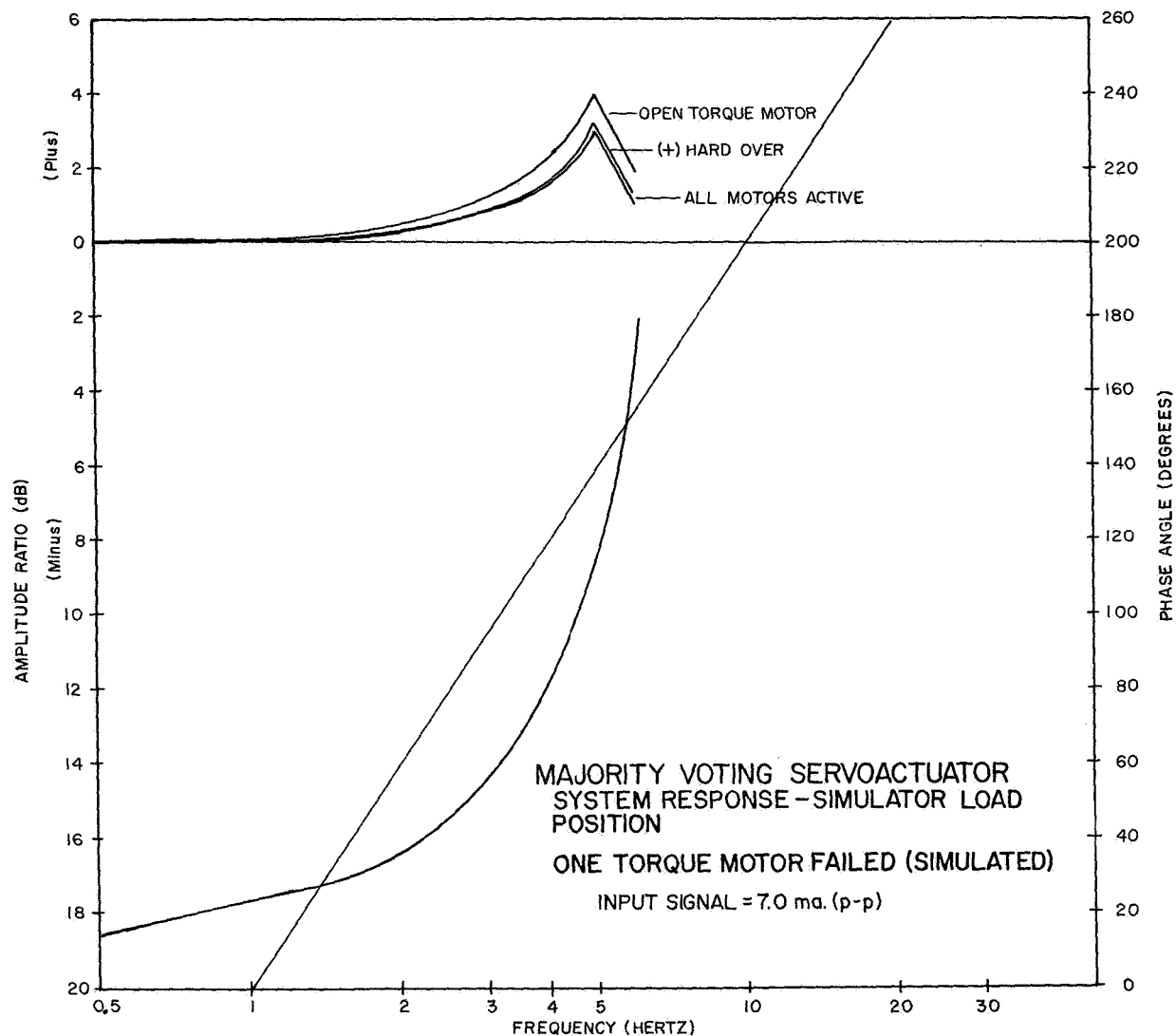
39

FIGURE 9. PERFORMANCE DATA - SIMULATOR PERFORMANCE

(3650 psi) and the thrust vector control actuator was sized accordingly. With experience gained through flight testing, it became evident that the in-flight loads and therefore the demands on the actuator were considerably less than the actuator design capability. When all aspects of the hydraulic system were considered, it was decided that the system operating pressure could be reduced to 1827 N/cm² (2650 psi). The effect of this system pressure reduction would be a reduction in actuator internal leakage, a reduction in the overall stresses on the various hydraulic system components, and a lower probability of external leakage of joints and fittings. The actuator is still capable of providing the required

control forces with this reduced system pressure and with no increase in actuator piston area.

SERVOACTUATOR STROKE

The prototype majority voting actuator was limited to a ±6 degree stroke, in comparison to a ±7 degree stroke in the original nonredundant actuator. This stroke reduction in the prototype actuator was necessary to conform to the stage mounting dimensions. In determining the final production configuration, repackaging of the three torque motors and some internal dimensional changes resulted in restoring the ±7 degree gimbal angle. Although the

40

TABLE II. SERVOACTUATOR COMPARISON SUMMARY			
SERVOACTUATOR PARAMETER	CONVENTIONAL ACTUATOR	MAJORITY VOTING PROTOTYPE	MAJORITY VOTING PRODUCTION
PISTON AREA	75.98 cm^2	75.98 cm^2	75.98 cm^2
STROKE	7.34 cm ($\pm$7 deg)	6.35 cm ($\pm$6 deg)	7.34 cm ($\pm$7 deg)
SUPPLY PRESSURE	2513 N/cm^2	2513 N/cm^2	1826 N/cm^2
POSITION GAIN	0.079 cm/ma	0.079 cm/ma	TO BE DETERMINED
RATED VELOCITY	8.6 cm/s	8.6 cm/s	TO BE DETERMINED
RATED INPUT SIGNAL	$\pm$50 ma	$\pm$50 ma	$\pm$50 ma
COIL RESISTANCE	100 ohms	100 ohms (3 ea)	100 ohms (3 ea)
MASS	18 kg	21 kg	21 kg
NOMINAL C. TO C. LENGTH	58.5 cm	58.5 cm	58.5 cm
ACTUATOR FEEDBACK	CONICAL CAM MFB	CONICAL CAM MFB	CONICAL CAM MFB
POSITION TELEMETRY TRANSDUCER	DUAL 2K POT	DUAL STRAIN GAGE	DUAL STRAIN GAGE
TAILSTOCK MATERIAL	6AL4V TITANIUM	6AL4V TITANIUM	6AL4V TITANIUM
BODY MATERIAL	AL 2014-T6	AL 2024-T4	AL 7075-T73
CAM FOLLOWER SPRING MATERIAL	15-7 STEEL	15-7 STEEL	INCONEL 718

$\pm$6 degree stroke would have been adequate for control purposes, the additional stroke is an added safety margin.

INTERNAL LEAKAGE

A three torque motor servovalve with three hydraulic amplifiers has a higher leakage rate than an actuator with a single first stage. Changes were made in the onboard auxiliary hydraulic system to provide the increased flow capability needed for proper auxiliary hydraulic system operation.

RELIABILITY IMPROVEMENT ASSESSMENT

Historically, most servovalve/servoactuator failures ($\approx$80 percent) result from a failure in the first stage of a servovalve because of its highly critical requirements. By incorporating redundancy in this first stage, it is evident that certain gains in reliability are achieved. Since there are, as yet, no inflight data on the majority voting servoactuator and no production quantities on which to base an analysis, the reliability assessments made thus far are based on experience with similar actuator and hydraulic system designs. The comparative numbers derived are based on the probability of known failures, their cause, and their end result. By considering not only the redesigned actuator but all other resultant system changes as well, the overall criticality improvement is approximately 20 to 1. The majority voting actuator itself is approximately 16 times less susceptible to functional failure than the original actuator design.

Table III is a comparison chart showing the improvement resulting from incorporation of the majority voting servoactuator. This table illustrates

TABLE III. CRITICALITY COMPARISON SUMMARY
(PRESENT vs. MAJORITY VOTING SYSTEM)

COMPONENT/ASSEMBLY	PRESENT SYSTEM	MAJORITY VOTING ACTUATOR SYSTEM	CRITICALITY IMPROVEMENT RATIO
ACTUATOR ASSEMBLY	2,224	111	20.0
AUXILIARY PUMP	740	410	1.8
THERMAL SWITCH	150	150	1.0
ACCUMULATOR	110	61	1.8
PLUMBING	4	2	2.0
TOTAL CRITICALITY EXCLUDING ACTUATOR ASSEMBLY	1,385	834	1.65
TOTAL CRITICALITY INCLUDING ACTUATOR ASSEMBLY	3,609	945	3.8

that the most significant improvement was in the servoactuator itself, and this combined with the other system changes significantly decreased system criticality. In no instance is a component less reliable than the original design.

CONCLUSION

To increase the overall thrust vectoring system reliability of the S-IVB stage, a study program was initiated to select the optimum improvement method. In accordance with existing requirements of the operational flight stage and the need to implement any changes with minimum impact on existing flight schedules, a majority voting actuator concept was

chosen. This concept provides redundancy in the critical first stage area of a servovalve, yet holds to a minimum the size, weight, and power consumption. Majority voting requires no failure detection devices or switching arrangements; therefore, overall system complexity for a redundant system is minimized.

A detailed study program was conducted to demonstrate the feasibility of a majority voting actuator, the overall design suitability, and the resultant gains in system reliability. Results to date indicate that the overall system reliability will be significantly improved by the majority voting actuator. The development is complete and only final formal qualification testing on the flight configuration system remains to be done.

BIBLIOGRAPHY

1. A Study of the Majority Voting Actuation System for the Saturn S-IVB Stage. General Test Plan Item M-41, Technical Memorandum No. 180, McDonnell Douglas Corporation, June 1967.

2. Evaluation Program of Majority Voting Mechanical Feedback Servoactuator for the Saturn S-IVB Stage. NASA Contract NAS8-11998, Report No. 1080, Moog, Inc., East Aurora, New York.

3. Garnjost, K. D.; and Thayer, W. J.: New Servovalves for Redundant Electrohydraulic Control. Presented at the Second Congress of the International Federation of Automatic Control, Basel, Switzerland, September 1963.

4. Hamilton, M. J.: Hydraulic Gimbaling in Space. Hydraulics and Pneumatics, November 1966.

5. Kalange, M. A.; and Neiland, V. R.: Saturn I Engine Gimbal Thrust Vector Control Systems. Presented to the National Conference on Industrial Hydraulics, October 17-18, 1963.

6. Kalange, M. A.; and Alcott, R. J.: Saturn V, S-IC Engine Gimbal Actuation System. Presented to the SAE Aerospace Fluid Power System and Equipment Conference, May 18-19, 1965.

7. Moore, F. B.; and White, J. B.: Application of Redundancy in the Saturn V Guidance and Control System. AIAA paper 67-553, presented at the AIAA Guidance, Control, and Flight Dynamics Conference, Huntsville, Alabama, August 14-16, 1967.

8. Optimization of Hydraulic Thrust Vector Control Systems for Launch Vehicles. Contract NAS8-11415, Report No. CR-65-5, Martin-Marietta Corporation, January 1965.

INDIVIDUAL ANGULAR MOMENTUM VECTOR DISTRIBUTION AND ROTATION LAWS FOR THREE DOUBLE-GIMBALED CONTROL MOMENT GYROS

By
Hans F. Kennel

SUMMARY

A distribution law and a rotation law for the individual angular momentum vectors of the three control moment gyros of the Apollo Telescope Mount are developed. The attitude control law controls the magnitude and the direction of the total angular momentum vector, using only three of the available six degrees of freedom. Without a distribution law, a highly undesirable distribution can develop where two of the three individual angular momentum vectors are parallel and the third is antiparallel, reducing the total angular momentum available by two thirds. The total is always fully available with the desirable distribution as provided by the distribution law, unless gimbal stops interfere. The desirable distribution has the following advantages: (1) antiparallel distribution is avoided, (2) the gain available for the attitude control law is maximized, and (3) the cross coupling is minimized. The rotation law minimizes the inner gimbal angles with the result that hitting the inner gimbal stops is avoided as much as possible. Operation of the distribution and rotation laws in case one of the CMG's fails is also discussed.

DEFINITION OF SYMBOLS

i, j, k	cyclic permuted subscripts (1, 2, 3, or 2, 3, 1 or 3, 1, 2)
m, n	general subscripts (range 1, 2, 3; all possible combinations)
—	a bar below a letter indicates a vector quantity
	a dot above a letter indicates a time derivative
A_i	a 2 × 3 matrix (equation 9)
B_i	a 3 × 2 matrix (equations 11 and 11a)
c	$\equiv \cos$
$\underline{e}_i$	a unit vector in direction of the ith CMG's angular momentum
e_{mn}	direction cosines of $\underline{e}_i$ (i = m) with respect to the vehicle axis n
e_{ik}'	$\equiv \sqrt{1/(1 - e_{ik}{}^2)}$
$\underline{e}_T$	$\equiv \underline{e}_1 + \underline{e}_2 + \underline{e}_3$. Normalized total angular momentum of the CMG cluster (maximum value: 3)
e_T	$\equiv |\underline{e}_T|$
e_{Ti}	components of $\underline{e}_T$ in vehicle space
E_i	intermediate quantity used in the digital program
$\tilde{e}$	$\equiv \begin{bmatrix} 0 & -e_3 & +e_2 \\ +e_3 & 0 & -e_1 \\ -e_2 & +e_1 & 0 \end{bmatrix}$
$\underline{h}_i$	see equation (5)
h_{mn}	components of $\underline{h}_i$ (i = m) in vehicle space
K_D	gain of the isogonal distribution [1/s]
K_D'	maximum of $|K_D|$, [1/s]
K_R	rotation gain ($K_R > 0$), [1/s]
q	determinant (see equation 13)
r_{mn}	intermediate quantities used in the digital program

s	$\equiv \sin$
t	$\equiv \tan$
$\underline{u}_i$	unit vector along the ith vehicle axis
x_V, y_V, z_V	vehicle axes
α_i β_i	angles used in conjunction with the rotation law, defined in Figure 4
$\delta_{1(i)}$	inner gimbal angle of ith CMG
$\delta_{3(i)}$	outer gimbal angle of ith CMG
$\underline{\delta}_i$	$\equiv \begin{bmatrix} \delta_{1(i)} \\ \delta_{3(i)} \end{bmatrix}$
ϵ_i	error of the isogonal distribution, [1/s]
ϵ_R	rotation error, [1/s]
ϵ_{Ri}	part of ϵ_R stemming from the ith CMG, [1/s]
ϵ_{Ri}	$= e_T^2 \, \epsilon_{Ri}/K_R$
λ_D	gain modifier for isogonal distribution
$\underline{\omega}_i$	actual angular velocity of $\underline{e}_i$, [1/s]
$\underline{\Omega}$	angular velocity command for rotation [1/s]

INTRODUCTION

The Apollo Telescope Mount (ATM) carries three double-gimbaled control moment gyros (CMG) [1,2]. The magnitude of the angular momentum of each CMG is fixed, and the arrangement has six degrees of freedom. The attitude control law will command the magnitude and the direction of the total angular momentum; therefore, it utilizes only three degrees of freedom. The distribution of the individual angular momenta is not controlled. This freedom can lead to highly undesirable distributions, such as the anti-parallel situation in which two vectors are parallel and the third is antiparallel. To avoid undesirable

distributions, a distribution law is developed. The desirable distribution is such that, after equilibrium is achieved, the individual angular momentum vectors have equal components along the total. Other results are equal angles between the individual vectors and equal angles between the individual vectors and the total. Because of these equal angles, the desired distribution is called the "isogonal distribution" (Fig. 1). The isogonal distribution has the following advantages: (1) antiparallel distribution is avoided, (2) the gain available for the attitude control law is maximized, and (3) the cross coupling is minimized. The distribution law uses two degrees of freedom; rotation about the total angular momentum vector still remains free. Therefore, a rotation law is added to minimize the inner gimbal angles with the result that hitting the inner gimbal stops is avoided as much as possible.
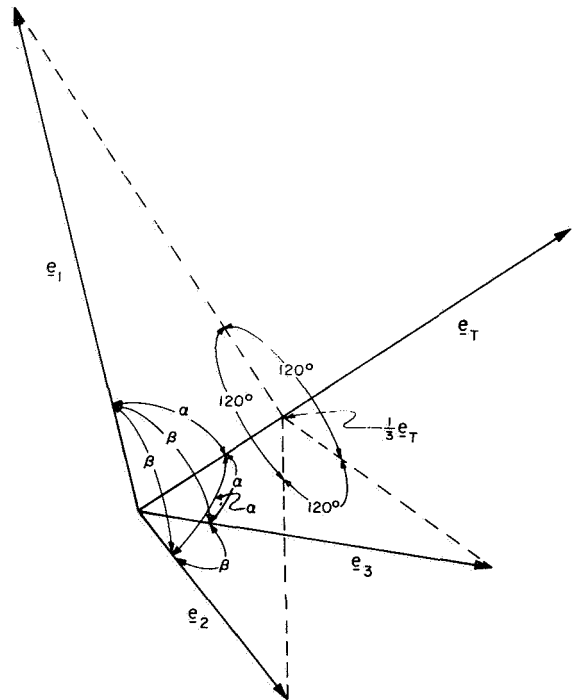

FIGURE 1. ISOGONAL DISTRIBUTION

The existing gimbal angles are the inputs to the distribution and rotation (D& R) laws and the gimbal angle rate commands are the outputs. These rate commands are in addition to those from the attitude control law. To develop the D& R laws it is assumed that the angular velocity of the vehicle is negligibly small and that the contribution of the gimbal rates

caused by the D&R laws to the total angular momentum is negligible. For simplicity, unit vectors along the individual angular momentum vectors are used and are called $\underline{e}_i$ ($i = 1, 2, 3$); their sum is $\underline{e}_T$ ($0 \leqq |\underline{e}_T| \leqq 3$). To avoid interference of the D&R laws with the attitude control law, it is necessary that these laws do not result in any change of the total angular momentum vector of the CMG cluster (i.e. , no acceleration on the vehicle).

The ratio of the angular velocity command to an angular error function may be called the gain for the D&R laws. In addition to a selectable constant, there is an inherent gain which varies with the gimbal angles. This is acceptable if the loop is stable with the highest inherent gain.

DISTRIBUTION LAW

For the sake of argument we can assume that two of the $\underline{e}_i$ vectors are summed first and then the third is added to form $\underline{e}_T$. If we desire to redistribute the first two without disturbing the total ($\underline{\dot{e}}_T = 0$), we can only rotate the first two about their sum. The angular rate $\underline{\dot{e}}_i$ about this sum is made proportional to the scalar function ϵ_i which, for $\underline{e}_1$ and $\underline{e}_2$, is given by $K_D (\underline{e}_1 \cdot \underline{e}_T - \underline{e}_2 \cdot \underline{e}_T)$. This scalar function provides a signal proportional to the deviation from the desired orientation. To assure rotation about the sum of the first two vectors, $\underline{\dot{e}}_i$ is also made proportional to their cross product. Pairing $\underline{e}_1$ and $\underline{e}_2$, for example, we have (Fig. 2)

$$\underline{\dot{e}}_1 = \epsilon_3 (\underline{e}_2 \times \underline{e}_1) \tag{1}$$

$$\underline{\dot{e}}_2 = \epsilon_3 (\underline{e}_1 \times \underline{e}_2) \tag{2}$$

with $\epsilon_3 = K_D (\underline{e}_1 \cdot \underline{e}_T - \underline{e}_2 \cdot \underline{e}_T)$

$$= K_D (\underline{e}_1 \cdot \underline{e}_3 - \underline{e}_2 \cdot \underline{e}_3) . \tag{3}$$

By cyclic permutation the equivalent equations for the other two pairs can be developed. The constant K_D can be chosen from other considerations (see discussion at the end of this section). The
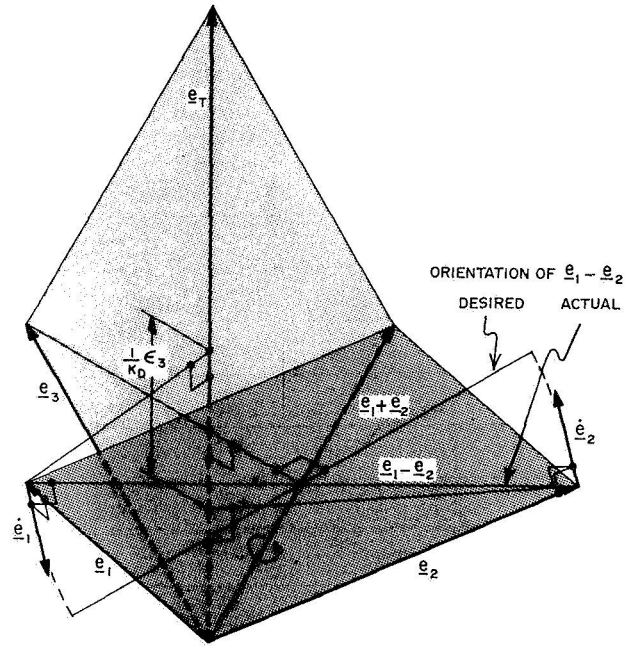

FIGURE 2. DEVELOPMENT OF DISTRIBUTION LAW

cyclic permutation allows us to use index notation with the understanding that we have the following three sets of values for i, j, and k:

i	j	k
1	2	3
2	3	1
3	1	2

The vector pairing can be assumed to be simultaneous and the resulting velocities vectorially added to form:

$$\underline{\dot{e}}_i = \underline{h}_i \times \underline{e}_i \tag{4}$$

with $\underline{h}_i = \epsilon_k \underline{e}_j + \epsilon_j \underline{e}_k$. $\tag{5}$

It can be seen (after expansion of equations 4 and 5) that no matter what value is chosen for K_D, the sum of the $\underline{\dot{e}}_i$'s (or $\underline{\dot{e}}_T$) is zero (Appendix A).

To develop the equations for the gimbal velocity commands, we must consider the following built-in relationship (Fig. 3):
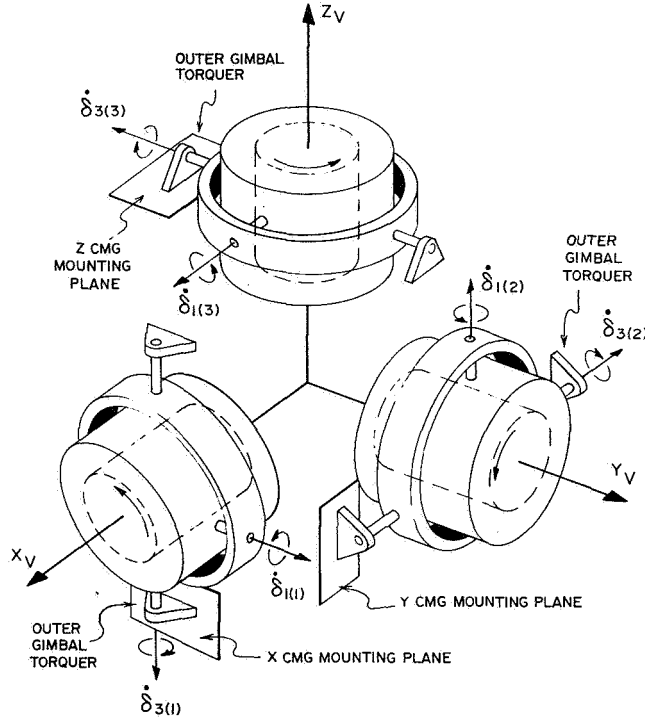
FIGURE 3. CONTROL MOMENT
GYRO ORIENTATIONS

$$\underline{e}_i = \begin{bmatrix} e_{ii} \\ e_{ij} \\ e_{ik} \end{bmatrix} = c\delta_{1(i)}\, c\delta_{3(i)}\, \underline{u}_i - c\delta_{1(i)}\, s\delta_{3(i)}\, \underline{u}_j - s\delta_{1(i)}\, \underline{u}_k \tag{6}$$

where the $\underline{u}_i$'s are unit vectors along the vehicle axes with the indices permuted as previously shown, and the δ's are gimbal angles defined in Figure 3. The second index on the components of $\underline{e}_i$ refers to the vehicle axes; for example, e_{ij} is the direction cosine of $\underline{e}_i$ with respect to vehicle axis j. Therefore we can also write:

$$\begin{bmatrix} \underline{e}_1 \\ \underline{e}_2 \\ \underline{e}_3 \end{bmatrix} = \begin{bmatrix} e_{11} & e_{12} & e_{13} \\ e_{21} & e_{22} & e_{23} \\ e_{31} & e_{32} & e_{33} \end{bmatrix} \begin{bmatrix} \underline{u}_1 \\ \underline{u}_2 \\ \underline{u}_3 \end{bmatrix} \tag{7}$$

The generally nonorthogonal direction cosine matrix in equation (7) will be needed later. The e_{ij}'s are given in terms of gimbal angles in Appendix B.

For an existing gimbal velocity we have

$$\dot{\underline{e}}_i = A_i\, \dot{\underline{\delta}}_{(i)} \tag{8}$$

with

$$\dot{\underline{e}}_i = \begin{bmatrix} \dot{e}_{ii} \\ \dot{e}_{ij} \\ \dot{e}_{ik} \end{bmatrix} \quad \text{and} \quad \dot{\underline{\delta}}_{(i)} = \begin{bmatrix} \dot{\delta}_{1(i)} \\ \dot{\delta}_{3(i)} \end{bmatrix}$$

$$A_i = \begin{bmatrix} -s\delta_{1(i)}\, c\delta_{3(i)} & -c\delta_{1(i)}\, s\delta_{3(i)} \\ +s\delta_{1(i)}\, s\delta_{3(i)} & -c\delta_{1(i)}\, c\delta_{3(i)} \\ -c\delta_{1(i)} & 0 \end{bmatrix} \tag{9}$$

As $\dot{\underline{\delta}}_i$-command law we need (see Appendix C and proof below):

$$\dot{\underline{\delta}}_{(i)} = B_i\, \underline{h}_i \tag{10}$$

with

$$B_i = \begin{bmatrix} +s\delta_{3(i)} & +c\delta_{3(i)} & 0 \\ -t\delta_{1(i)}\, c\delta_{3(i)} & +t\delta_{1(i)}\, s\delta_{3(i)} & -1 \end{bmatrix} \tag{11}$$

or in terms of direction cosines (with $e_{ik}' = \sqrt{1/(1 - e_{ik}^2)}$):

$$B_i = \begin{bmatrix} - e_{ik}'\, e_{ij} & e_{ik}'\, e_{ii} & 0 \\ e_{ik}(e_{ik}')^2\, e_{ii} & - e_{ik}(e_{ik}')^2\, e_{ij} & -1 \end{bmatrix} \tag{11a}$$

The existing hardware implementation through resolvers on the gimbals provides the direction cosines of equation (7) whereas the gimbal angles are not available explicitly. Thus, B_i is expressed in terms of the direction cosines (see Appendix B).

By multiplying, it can be shown that

$$\dot{\underline{e}}_i = A_i B_i\, \underline{h}_i = -\underline{e}_i \times \underline{h}_i = \underline{h}_i \times \underline{e}_i$$

if it is assumed that the actual and the commanded gimbal rates are identical. Equation (10) is, therefore, the proper solution for the gimbal velocity commands to solve equation (4).'

A discussion on the freely selectable isogonal distribution gain K_D (equation 3) is in order. When this gain is positive, we get a right-handed configuration (right-handed means that when we look down $\underline{e}_T$ and identify the individual vectors counterclockwise, we find the sequence 1 - 2 - 3); for a negative K_D, we get a left-handed configuration. Both configurations are stable. Since neither sign has a basic preference, we can dynamically (during operation of the CMG's) select the sign of the gain K_D so that the vectors are driven toward the closer solution. This action implies a knowledge of whether the instantaneous distribution is right- or left-handed. The following determinant affords this knowledge:

$$q = \begin{vmatrix} e_{11} & e_{12} & e_{13} \\ e_{21} & e_{22} & e_{23} \\ e_{31} & e_{32} & e_{33} \end{vmatrix} .$$

It can be recognized that this is the determinant of the direction cosines for the angular momentum vectors. If these vectors are mutually perpendicular, we have an orthogonal coordinate system, and it is well known that the value of the determinant q is +1 for a right-handed system and -1 for a left-handed one. For a continuously deformable system as the one at hand, the determinant can be anywhere between these limits and the sign of the determinant can be used as the sign for the distribution gain K_D. A value of zero for q indicates that the three vectors are in a plane. A change in sign for q occurs under certain conditions. Gimbal stops may disallow the isogonal distribution and deform the distribution so much that q changes sign. The distribution gain is much lower than the attitude control gain (as discussed later), and maneuver commands can cause a relatively fast change in the distribution which could result in a sign change of q. Finally, whenever $\underline{e}_T$ passes through zero, q changes sign.

Regardless of the reason for the sign change, it is always beneficial for the system behavior. A further improvement in system behavior can be made through the introduction of a multiplier λ_D so that the isogonal distribution gain becomes

$$K_D = \lambda_D K_D' \, \text{sgn} \, q$$

where

$$K_D' = |K_D|_{max}$$

and

$$0 \leqq \lambda_D \leqq +1 .$$

The multiplier λ_D is a function of $e_T = |\underline{e}_T|$. For small e_T we desire $\lambda_D = 0$, thus avoiding the possibility for large angular redistributions when $\underline{e}_T$ passes close to zero. When e_T is in the vicinity of unity (i.e., without a distribution law, antiparallel is a problem), the multiplier λ_D should be at its maximum. For large e_T, a small λ_D is sufficient. The exact function of $\lambda_D(e_T)$ is not critical, and straight line segments may be used (Appendix B). The maximum distribution gain K_D' should be large enough to avoid antiparallel, but not larger than necessary because gimbal stops sometimes disallow the isogonal distribution and the attitude control gain must be higher than the distribution gain so that the attitude control takes over in case of conflict. During normal operation there is no conflict because the distribution and rotation laws do not result in an acceleration of the vehicle.

Temporary deviations from the isogonal distribution can be tolerated to a large extent. For example, for the antiparallel case, $e_T = 1$. This case is depicted in Figure 1. The dot product between any of the isogonally distributed vectors and the antiparallel direction is -1/3, or there is an angle of almost 110 degrees between the desired individual vector direction as demanded by the isogonal distribution law and the antiparallel direction. This indicates that even a deviation of 40 or 50 degrees from the desired direction can be temporarily accepted.

ROTATION LAW

The isogonal distribution law concerns itself only with the relative distribution between the individual and the total angular momentum vectors. A rotation about the total leaves the distribution unaffected. The rotational freedom can therefore be used for some benefit. To reach some desired

orientation about $\underline{e}_T$, an angular velocity $\underline{\Omega}$ of the following form must be commanded:

$$\underline{\Omega} = \epsilon_R \, \underline{e}_T \qquad (14)$$

where ϵ_R will be developed later. For the individual angular momentum vectors, the relation exists

$$\underline{\dot{e}}_i = \underline{\Omega} \times \underline{e}_i \qquad (15)$$

Equation (15) is identical in form to equation (4); only $\underline{\Omega}$ is substituted for $\underline{h}_i$. Therefore we get analogous to equation (10)

$$\underline{\dot{\delta}}_{(i)} = B_i \, \underline{\Omega} \quad . \qquad (16)$$

No unique law exists for the rotation contrary to the unique isogonal distribution law. In the application of the three CMG system to ATM, the most benefit can be derived from a rotation law if the inner gimbal angles are minimized. Even under this assumption, minimizing must be first defined, since no unique definition exists. Avoidance of hitting the inner gimbal stops, which are at ±80 degrees, was given priority. It was also desirable to have a continuous function rather than a switching function for the rotation law. Because the three vectors rotate as a unit about $\underline{e}_T$, none of the inner gimbal angles will generally be at an absolute minimum, but a compromise will be reached for all three. The following form was selected for ϵ_R:

$$\epsilon_R = \sum_{i=1}^{3} \epsilon_{Ri} \qquad (17)$$

with

$$\epsilon_{Ri} = \frac{K_R}{e_T} \, t\delta_{1(i)} \, s\alpha_i \, c\beta_i \quad . \qquad (18)$$

Because ϵ_R will become zero at equilibrium and K_R is a freely selectable positive constant, no additional constants are necessary in equation (17).

The reasons for the various quantities in the error function ϵ_{Ri} are given. To make $\underline{\Omega}$ independent of the magnitude of $\underline{e}_T$, we have to divide by

e_T. The tangent of the inner gimbal angle (rather than the angle itself) is chosen for two reasons: (1) to give the larger angles more weight and (2) to make use of trigonometric functions which are readily available in the form of the direction cosines (equation 7). Figure 4 defines the two other angles used for $i = 1$. Consider, for the sake of the explanation, that the plane for which $\delta_{1(i)} = 0$ is the equatorial plane. Then the angle α_i indicates the separation of the meridian plane containing $\underline{e}_i$ and the one containing $\underline{e}_T$. The combination of $t\delta_{1(i)} \, s\alpha_i$ will select the proper sign for the angular velocity and go to zero when the desired conditions are reached. The multiplier $c\beta_i$ takes the effectiveness of a rotation in reducing $\delta_{1(i)}$ into account, eliminating the ϵ_{Ri}-contribution to ϵ_R completely when $\beta_i = \frac{\pi}{2}$ where a rotation does not change $\delta_{1(i)}$.
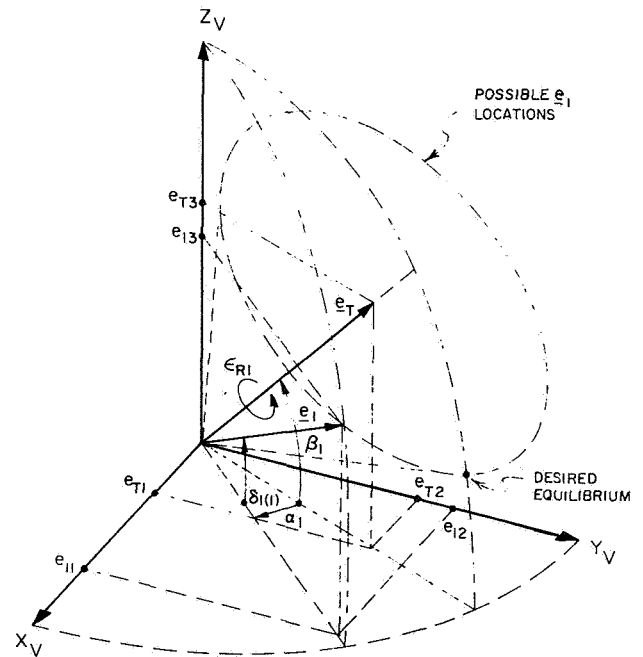

FIGURE 4. ANGLE DEFINITIONS
FOR ROTATION LAW

We can identify several cases; Figure 5 shows an opaque unit sphere, the equator of which indicates $\delta_{1(i)} = 0$. The vertical line is a longitude onto
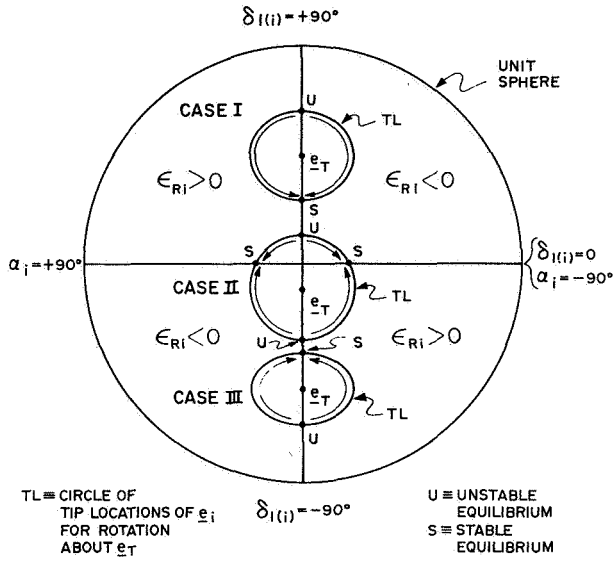
FIGURE 5. EQUILIBRIUM CASES
FOR ROTATION

which, for convenience, all intersects for the direction of $\underline{e}_T$ have been placed. Usually $\underline{e}_T$ will not terminate on the unit sphere.

CASE I. — The circle of possible tip locations for $\underline{e}_i$ (assuming a rotation about $\underline{e}_T$) does not intersect the equator, and the inner gimbal angle $\delta_{1(i)}$ is positive. We find two equilibrium conditions: one stable and one unstable.

CASE II. — The circle of tip locations intersects the equator. We find four equilibria: two are intersections and are stable, and two are unstable.

CASE III. — This case is equivalent to case I; only the sign on $\delta_{1(i)}$ is reversed.

Determination of equation (18) in terms of the readily available direction cosines and the components of the total angular momentum vector leads to (i=1):

$$t\delta_{1(1)} = -e_{13}e_{13}' \quad \text{with} \quad e_{13}' = \frac{1}{\sqrt{1 - e_{13}^2}}$$

$$c\beta_1 = \sqrt{1 - \left(\frac{e_{T3}}{e_T}\right)^2} = \frac{1}{e_T}\sqrt{e_T^2 - e_{T3}^2}$$

$$= \frac{1}{e_T}\sqrt{e_{T1}^2 + e_{T2}^2}$$

$$s\alpha_1 = \frac{e_{11}e_{T2} - e_{12}e_{T1}}{\sqrt{(e_{11}^2 + e_{12}^2)(e_{T1}^2 + e_{T2}^2)}}$$

$$= \frac{e_{11}e_{T2} - e_{12}e_{T1}}{\sqrt{(1 - e_{13}^2)(e_{T1}^2 + e_{T2}^2)}}$$

$$\epsilon_{R1} = \frac{1}{e_T^2}\left\{-e_{13}(e_{13}')^2(e_{11}e_{T2} - e_{12}e_{T1})\right\}. \tag{19}$$

Cyclic permutation of the indices leads to ϵ_{R2} and ϵ_{R3}:

$$\epsilon_{R2} = \frac{1}{e_T^2}\left\{-e_{21}(e_{21}')^2(e_{22}e_{T3} - e_{23}e_{T2})\right\} \tag{20}$$

$$\epsilon_{R3} = \frac{1}{e_T^2}\left\{-e_{32}(e_{32}')^2(e_{33}e_{T1} - e_{31}e_{T3})\right\} \tag{21}$$

DISTRIBUTION AND ROTATION LAW COMBINATION

Since the desired gimbal velocity commands from the distribution law and from the rotation law are independent of each other, they can be combined into

$$\dot{\underline{\delta}}_{(i)} = B_i(\underline{h}_i + \epsilon_R \underline{e}_T) \tag{22}$$

These gimbal velocity commands should be added to the commands from the attitude control law.

The distribution is unaffected by the rotation as already indicated during the development of the rotation law; i.e., the ϵ_i's of the distribution law are not affected. On the other hand, ϵ_R is affected by a change in the distribution, and it is advisable that K_R (contained in ϵ_R) is made smaller than K_D' (contained in $\underline{h}_i$ through ϵ_i). A ratio of $K_R/K_D' = 0.1$ was found to be acceptable, but it is not critical either way.

OPERATION WITH TWO CMG'S

A system with three CMG's has the capability to lose one and still be able to control the vehicle, even if the performance is degraded. Two CMG's have only four degrees of freedom, and three are being used for attitude control. There is no need for a distribution law since the two remaining angular momentum vectors have inherently the proper distribution, but the rotation law still can minimize the inner gimbal angles of the operative CMG's. To convert from the three to the two CMG operation, it is only necessary to set all the direction cosines of the inoperative CMG to zero. (Gimbal angle velocity commands issued by the computer to the inoperative CMG should be disregarded.) No distribution command will appear for the operative CMG's. But, as desired, the rotation law is working as usual, having now only two error sources, rather than three (equation 17).

CONCLUSIONS

The isogonal distribution law and the rotation law were implemented in a hybrid simulation, and the behavior was studied with the aid of a three-dimensional display.* Both laws performed as expected. It was also noted that, if gimbal stops disallowed the isogonal distribution, the distribution approximated the desired distribution as close as possible under the imposed restrictions. Analysis of the dynamic performance of the attitude control law showed a marked improvement in response of the desired channel and a strong reduction of the cross coupling into the other channels.

---

* The three-dimensional display shows the body axes, the three individual angular momentum vectors, their total, and the total commanded angular momentum vector simultaneously, identified by appropriate coding. This proved an invaluable tool for the investigation of the behavior of the system [3].

APPENDIX A

Sum of the $\dot{\underline{e}}$'s

Expansion and combination of equations (4) and (5) yield

$$\dot{\underline{e}}_1 = (\epsilon_3 \underline{e}_2 + \epsilon_2 \underline{e}_3) \times \underline{e}_1$$

$$\dot{\underline{e}}_2 = (\epsilon_1 \underline{e}_3 + \epsilon_3 \underline{e}_1) \times \underline{e}_2 \qquad (A-1)$$

$$\dot{\underline{e}}_3 = (\epsilon_2 \underline{e}_1 + \epsilon_1 \underline{e}_2) \times \underline{e}_3$$

For the sum of the $\dot{\underline{e}}_i$'s, we get

$$\dot{\underline{e}}_T = + (\underline{e}_2 \times \underline{e}_3 + \underline{e}_3 \times \underline{e}_2) \epsilon_1$$

$$+ (\underline{e}_3 \times \underline{e}_1 + \underline{e}_1 \times \underline{e}_3) \epsilon_2 \qquad (A-2)$$

$$+ (\underline{e}_1 \times \underline{e}_2 + \underline{e}_2 \times \underline{e}_1) \epsilon_3 .$$

Because the vectors in parentheses are all zero,

$\dot{\underline{e}}_T$ is zero and it is immaterial what is chosen for the ϵ_i's. The form chosen was (equation 3):

$$\epsilon_1 = K_D (\underline{e}_2 - \underline{e}_3) \cdot \underline{e}_1$$

$$\epsilon_2 = K_D (\underline{e}_3 - \underline{e}_1) \cdot \underline{e}_2$$

$$\epsilon_3 = K_D (\underline{e}_1 - \underline{e}_2) \cdot \underline{e}_3$$

Because the ϵ_i's are independent of each other, the K_D's could be different for each ϵ_i without affecting the condition that $\dot{\underline{e}}_T = 0$. This is not sensible though, because it would not treat the vector pairs alike, and there is no reason for that.

APPENDIX B

Suggested Digital Computer Implementation
(Sequence of Operations)

Inputs

$$e_{11} = +c\delta_{1(1)}c\delta_{3(1)}$$

$$K_D'$$

$$e_{12} = -c\delta_{1(1)}s\delta_{3(1)}$$

$$K_R$$

$$e_{13} = -s\delta_{1(1)}$$

$$e_{21} = -s\delta_{1(2)}$$

$$e_{22} = +c\delta_{1(2)}c\delta_{3(2)}$$

$$e_{23} = -c\delta_{1(2)}s\delta_{3(2)}$$

$$e_{31} = -c\delta_{1(3)}s\delta_{3(3)}$$

$$e_{32} = -s\delta_{1(3)}$$

$$e_{33} = +c\delta_{1(3)}c\delta_{3(3)}$$

The equivalences of the e_{mn}'s in terms of the gimbal angles are only given for completeness. The e_{mn}'s are provided by resolver chains in the existing hardware and constitute the actual inputs to the digital computer.

Sequence of Computations

$$(e_{13}')^2 = (1 - e_{13}^2)^{-1}$$

$$e_{13}' = [(e_{13}')^2]^{+\frac{1}{2}}$$

both quantities are needed in the following

$$(e_{21}')^2 = (1 - e_{21}^2)^{-1}$$

$$e_{21}' = [(e_{21}')^2]^{+\frac{1}{2}}$$

$$(e_{32}')^2 = (1 - e_{32}^2)^{-1}$$

$$e_{32}' = [(e_{32}')^2]^{+\frac{1}{2}}$$

$$e_{T1} = e_{11} + e_{21} + e_{31}$$

$$e_{T2} = e_{12} + e_{22} + e_{32}$$

$$e_{T3} = e_{13} + e_{23} + e_{33}$$

$$e_T^2 = e_{T1}^2 + e_{T2}^2 + e_{T3}^2$$

$$e_T = \sqrt{e_T^2}$$

$$q = e_{11}(e_{22}e_{33} - e_{32}e_{23}) + e_{21}(e_{32}e_{13} - e_{12}e_{33})$$
$$+ e_{31}(e_{12}e_{23} - e_{22}e_{17})$$

$$\text{sgn } q = +1 \quad \text{for } q \geq 0$$

$$\text{sgn } q = -1 \quad \text{for } q < 0$$

$$\lambda_D = 0 \qquad \text{for} \qquad e_T \leq 0.25$$

$$\lambda_D = 2e_T - 0.5 \qquad \text{for } 0.25 < e_T \leq 0.75$$

$$\lambda_D = +1 \qquad \text{for } 0.75 < e_T \leq 1.25$$

$$\lambda_D = +3.5 - 2e_T \qquad \text{for } 1.25 < e_T \leq 1.65$$

$$\lambda_D = +0.2 \qquad \text{for } 1.65 < e_T$$

$$K_D = K_D' \lambda_D \text{ sgn } q$$

$$E_1 = e_{21}e_{31} + e_{22}e_{32} + e_{23}e_{33}$$

$$E_2 = e_{11}e_{31} + e_{12}e_{32} + e_{13}e_{33}$$

$$E_3 = e_{11}e_{21} + e_{12}e_{22} + e_{13}e_{23}$$

$$\epsilon_{\lambda} = (E_3 - E_2)K_D$$

$$\epsilon_2 = (E_1 - E_3) K_D$$

$$\epsilon_3 = (E_2 - E_1) K_D$$

$$h_{11} = \epsilon_3 e_{21} + \epsilon_2 e_{31}$$

$$h_{12} = \epsilon_3 e_{22} + \epsilon_2 e_{32}$$

$$h_{13} = \epsilon_3 e_{23} + \epsilon_2 e_{33}$$

$$h_{21} = \epsilon_1 e_{31} + \epsilon_3 e_{11}$$

$$h_{22} = \epsilon_1 e_{32} + \epsilon_3 e_{12}$$

$$h_{23} = \epsilon_1 e_{33} + \epsilon_3 e_{13}$$

$$h_{31} = \epsilon_2 e_{11} + \epsilon_1 e_{21}$$

$$h_{32} = \epsilon_2 e_{12} + \epsilon_1 e_{22}$$

$$h_{33} = \epsilon_2 e_{13} + \epsilon_1 e_{23}$$

$$\epsilon_{R1}' = e_{13}(e_{13}')^2(e_{12}e_{T1} - e_{11}e_{T2})$$

$$\epsilon_{R2}' = e_{21}(e_{21}')^2(e_{23}e_{T2} - e_{22}e_{T3})$$

$$\epsilon_{R3}' = e_{32}(e_{32}')^2(e_{31}e_{T3} - e_{33}e_{T1})$$

$$\epsilon_R = \frac{K_R}{e_T^2} \left(\epsilon_{R1}' + \epsilon_{R2}' + \epsilon_{R3}' \right)$$

$$r_{11} = h_{11} + \epsilon_R e_{T1}$$

$$r_{12} = h_{12} + \epsilon_R e_{T2}$$

$$r_{13} = h_{13} + \epsilon_R e_{T3}$$

$$r_{21} = h_{21} + \epsilon_R e_{T1}$$

$$r_{22} = h_{22} + \epsilon_R e_{T2}$$

$$r_{23} = h_{23} + \epsilon_R e_{T3}$$

$$r_{31} = h_{31} + \epsilon_R e_{T1}$$

$$r_{32} = h_{32} + \epsilon_R e_{T2}$$

$$r_{33} = h_{33} + \epsilon_R e_{T3}$$

Outputs.

$$\dot{\delta}_{1(1)} = -e_{13}'(e_{12}r_{11} - e_{11}r_{12})$$

$$\dot{\delta}_{3(1)} = +(e_{13}')^2 e_{13}(e_{11}r_{11} + e_{12}r_{12}) - r_{13}$$

$$\dot{\delta}_{1(2)} = -e_{21}'(e_{23}r_{22} - e_{22}r_{23})$$

$$\dot{\delta}_{3(2)} = +(e_{21}')^2 e_{21}(e_{22}r_{22} + e_{23}r_{23}) - r_{21}$$

$$\dot{\delta}_{1(3)} = -e_{32}'(e_{31}r_{33} - e_{33}r_{31})$$

$$\dot{\delta}_{3(3)} = +(e_{32}')^2 e_{32}(e_{33}r_{33} + e_{31}r_{31}) - r_{32}$$

APPENDIX C

Development of Matrix B

We desire to get the gimbal velocities to solve equation (4), which is (subscripts dropped)

$$\underline{\dot{e}} = \underline{h} \times \underline{e} \quad . \tag{C-1}$$

The angular velocity of $\underline{e}$ can be defined as $\underline{\omega}$. Then,

$$\underline{\dot{e}} = \underline{\omega} \times \underline{e} \quad . \tag{C-2}$$

This leads to (equations C-1 and C-2)

$$(\underline{h} - \underline{\omega}) \times \underline{e} = 0 \tag{C-3}$$

and this equation can only be solved because $\underline{\omega}$ and $\underline{e}$ are known in terms of the gimbal angles and their velocities. With

$$\underline{e} = \begin{bmatrix} e_1 \\ e_2 \\ e_3 \end{bmatrix} = \begin{bmatrix} +c\delta_1 c\delta_3 \\ -c\delta_1 s\delta_3 \\ -s\delta_1 \end{bmatrix} \quad \text{and} \quad \underline{\omega} = \begin{bmatrix} +s\delta_3\dot{\delta}_1 \\ +c\delta_3\dot{\delta}_1 \\ -\dot{\delta}_3 \end{bmatrix}$$

we obtain for equation C-3

$$0 = \begin{bmatrix} 0 & -(h_3 + \dot{\delta}_3) & +(h_2 - c\delta_3\dot{\delta}_1) \\ +(h_3 + \dot{\delta}_3) & 0 & -(h_1 - s\delta_3\dot{\delta}_1) \\ -(h_2 - c\delta_3\dot{\delta}_1) & +(h_1 - s\delta_3\dot{\delta}_1) & 0 \end{bmatrix} \begin{bmatrix} +c\delta_1 c\delta_3 \\ -c\delta_1 s\delta_3 \\ -s\delta_1 \end{bmatrix} \tag{C-4}$$

The third equation in C-4 yields

$$\dot{\delta}_1 = + s\,\delta_3 h_1 + c\,\delta_3 h_2 \quad . \tag{C-5}$$

With equation C-5 the first or second equation of C-4 can be solved to get

$$\dot{\delta}_3 = + t\,\delta_1(s\,\delta_3 h_2 - c\,\delta_3 h_1) - h_3 \tag{C-6}$$

or

$$\begin{bmatrix} \dot{\delta}_1 \\ \dot{\delta}_3 \end{bmatrix} = \begin{bmatrix} +s\delta_3 & +c\delta_3 & 0 \\ -t\delta_1 c\delta_3 & +t\delta_1 s\delta_3 & -1 \end{bmatrix} \begin{bmatrix} h_1 \\ h_2 \\ h_3 \end{bmatrix}$$

i.e., $\quad \underline{\dot{\delta}} = B\,\underline{h} \quad .$

It might be interesting to note that the cross-product law is

$$(XPR) = BAB$$

and that

$$\tilde{e} = -AB$$

where $\tilde{e}$ is defined as

$$\tilde{e} = \begin{bmatrix} 0 & -e_3 & +e_2 \\ +e_3 & 0 & -e_1 \\ -e_2 & +e_1 & 0 \end{bmatrix}$$

REFERENCES

1.   Chubb, W. B.; Schultz, D. N. and Seltzer, S. M.: Attitude Control and Precision Pointing of the Apollo Telescope Mount. AIAA Guidance, Control, and Flight Dynamics Conference. Huntsville, Ala., Aug. 14-16, 1967, Paper 67-534.

2.   O'Conner, B. J. and Morine, L. A.: Description of the CMG and Its Application to Space Vehicle Control. AIAA Guidance, Control, and Flight Dynamics Conference. Huntsville, Ala., Aug. 14-16, 1967, Paper 67-550.

3.   Kennel, H F.: A Three-Dimensional Display. IN-R-ASTR-65-7, NASA/MSFC, Huntsville, Ala., March 12, 1965.

AN OPTIMALLY CONTROLLED MASS DISTRIBUTION GRAVITY GRADIENT SATELLITE CONTROL SCHEME

By

George B. Doane III

SUMMARY

This paper summarizes research done in exploring the potential of using gravity gradient phenomena to produce both damping and positioning torques on a satellite. The results demonstrate that, by properly controlling the inertia tensor of the satellite, the desired objectives may be achieved. The graphically displayed results show that asymptotically stable motion is achievable in attractively short lengths in time. The results were achieved by the use of iterative computational techniques.

INTRODUCTION

Present satellite technology tends to regard gravity-gradient-generated torque either as an unfortunate perturbative influence or as a strictly positioning torque. In the latter case, damping is typically achieved by such means as gas jets, control moment gyros, or structural losses. As satellites increase in both size and longevity, the need for other types of damping becomes apparent. Some investigators are working on such things as magnetic torquing of satellites. This investigation shows the potential of using gravity-gradient-based torquing as a means of achieving reasonably rapidly damped motion, and this torquing inherently does not require mass expulsion or an external field other than a gravitational one.

ANALYTICAL APPROACH

The approach taken was to write expressions, based on the angular definitions of Figure 1, for the torques applied to the vehicle, the inertial reaction torques of the vehicle, and the kinematics of rotation. These expressions are presented next.
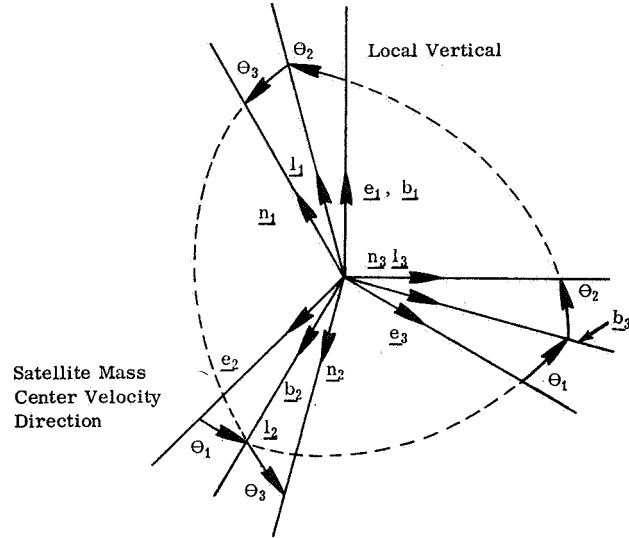
where e_i, b_i, l_i, n_i, denote base vectors

Θ_i denotes an Euler angle

FIGURE 1. EULER ANGLES DEFINED WITH RESPECT TO ORBITAL DIRECTIONS

The torque caused by gravity gradient is given by

$$T_{n1} = 3\omega_0^2 \{ (I_{22} - I_{33}) S_2 C_2 S_3 + C_2^2 C_3 S_3 I_{13}$$

$$+ [S_2^2 - C_2^2 S_3^2] I_{23} + C_2 C_3 S_2 I_{12} \} \qquad (1)$$

$$T_{n2} = 3\omega_0^2 \{ (I_{11} - I_{33}) S_2 C_2 C_3 + S_2 S_3 C_2 I_{12}$$

$$- C_2^2 C_3 S_3 I_{23} + [C_3^2 - S_2^2 (1 + C_3^2)] I_{13} \}$$

$$\qquad (2)$$

$$T_{n3} = 3\omega_0^2 \{ (I_{11} - I_{22}) S_3 C_3 C_2^2 - S_2 S_3 C_2 I_{13}$$

$$- S_2 C_2 C_3 I_{23} + C_2^2 [2C_3^2 - 1] I_{12} \}$$

$$\qquad (3)$$

where

I_{ij} $\begin{cases} \text{denotes moments of inertia when } i = j \\ \text{denotes products of inertia when } i \neq j \end{cases}$

S_i, C_i denote $\sin \Theta_i$ and $\cos \Theta_i$, respectively

T denotes the torque due to gravity gradient

ω_0 denotes the angular rate of a circular orbit

The torque caused by aerodynamics is given by

$$\underline{T}_{aero} = -\eta \left[S_1 C_2 \underline{n}_1 + (C_1 C_3 + S_1 S_2 C_3) \underline{n}_3 \right]$$

$$\eta = 3.162 \times 10^6 \text{ Nm} . \tag{4}$$

where

$\underline{T}_{aero}$ denotes aerodynamic torque

η denotes the numerical constant associated with the aerodynamic torque

The inertial reaction of the vehicle is given by

$$L_{n1} = I_{11} \dot{\omega}_1 + \omega_1 \dot{I}_{11} - I_{12} \dot{\omega}_2 - \omega_2 \dot{I}_{12} - I_{13} \dot{\omega}_3$$
$$- \omega_3 \dot{I}_{13} - I_{31} \omega_1 \omega_2 - I_{32} \omega_2^2 + I_{33} \omega_2 \omega_3$$
$$+ I_{21} \omega_1 \omega_3 - I_{22} \omega_2 \omega_3 + I_{23} \omega_3^2 \tag{5}$$

$$L_{n2} = - I_{21} \dot{\omega}_1 - \omega_1 \dot{I}_{21} + I_{22} \dot{\omega}_2 + \omega_2 \dot{I}_{22} - I_{23} \dot{\omega}_3$$
$$- \omega_3 \dot{I}_{23} + I_{31} \omega_1^2 + I_{32} \omega_1 \omega_2 - I_{33} \omega_1 \omega_3$$
$$+ I_{11} \omega_1 \omega_3 - I_{12} \omega_3 \omega_2 - I_{13} \omega_3^2 \tag{6}$$

$$L_{n3} = - I_{31} \dot{\omega}_1 - \omega_1 \dot{I}_{31} - I_{32} \dot{\omega}_2 - \omega_2 \dot{I}_{32} + I_{33} \dot{\omega}_3$$
$$+ \omega_3 \dot{I}_{33} - I_{21} \omega_1^2 + I_{22} \omega_1 \omega_2 - I_{23} \omega_1 \omega_3$$
$$- I_{11} \omega_1 \omega_2 + I_{12} \omega_2^2 + I_{13} \omega_2 \omega_3 \tag{7}$$

where

L_{ni} denotes the component of torque applied to the satellite by external sources about the i axis of the n coordinate triad

ω_i denotes an angular rate

and the various inertias in equations (5, 6, 7) are assumed to be time variable.

The kinematical equations are given by

$$
\begin{bmatrix} \omega_{n1} \\ \omega_{n2} \\ \omega_{n3} \end{bmatrix} = \omega_0 \begin{bmatrix} S_1 S_3 - C_1 S_2 C_3 \\ S_1 C_3 + C_1 S_2 S_3 \\ C_1 C_2 \end{bmatrix}
$$
$$
+ \begin{bmatrix} C_2 S_3 & S_3 & 0 \\ -C_2 S_3 & C_3 & 0 \\ S_2 & 0 & 1 \end{bmatrix} \begin{bmatrix} \dot{\Theta}_1 \\ \dot{\Theta}_2 \\ \dot{\Theta}_3 \end{bmatrix} . \tag{8}
$$

The problem was formulated for solution by the method of continuous dynamic programing by defining a cost function of the form

$$V = \sum_j \lambda_j [x_{iT} - x_i(T)]^2 + \int_0^T \left\{ \sum_k \lambda_k [x_{kT} - x_k(\sigma)]^2 \right.$$
$$\left. + \sum_l \lambda_l [x_{pT} - x_p(\sigma)]^2 + \sum_n \lambda_n [u_{mT} - u_m(\sigma)]^2 \right\} d\sigma$$

$$\begin{aligned} &i = 1, \ldots, 6 & &p = 1, 2, 3 \\ &j = a, b, c, 1, 2, 3 & &n = 7, \ldots, 12 \\ &k = 4, 5, 6 & &m = 1, \ldots, 6 \\ &l = d, e, f & & \end{aligned} \tag{9}$$

where

T (limit on the integral) denotes the end of solution period

T (subscript) denotes a variable's desired terminal value

u denotes a control vector element

V denotes the cost (i.e., a number)

σ denotes a dummy variable of integration

λ denotes the cost function weighting factor

In equation (9) the λ's are weighting factors by which the importance of one term relative to another is specified. Damping, and hence transition time, is controlled by the first two terms in the integrand.

The last term in the integrand guarantees that the control vector metric remains finite.

Numerical solutions were obtained by assuming an inertia element control law of the form

$$\tau \, \frac{d\,I(t)}{dt} = -I(t) + u(t) \qquad (10)$$

where

t   denotes time

τ denotes time constant in inertia element changing relationship

and writing all expressions in state notation as given in Table I. The state variable definitions as well as

TABLE I. SATELLITE STATE EQUATIONS

Dynamics:

$$\dot{x}_1 = \frac{E_1\,Tn_1}{D} + \frac{E_2\,Tn_2}{D} + \frac{E_3\,Tn_3}{D} + \frac{x_1}{\tau} - \frac{E_1\,E_7}{D\tau} - \frac{E_2\,E_8}{D\tau} - \frac{E_3\,E_9}{D\tau} - \frac{E_1\,E_{10}}{D} - \frac{E_2\,E_{11}}{D} - \frac{E_3\,E_{12}}{D}$$

$$\dot{x}_2 = \frac{E_2\,Tn_1}{D} + \frac{E_4\,Tn_2}{D} + \frac{E_5\,Tn_3}{D} + \frac{x_2}{\tau} - \frac{E_2\,E_7}{D\tau} - \frac{E_4\,E_8}{D\tau} - \frac{E_5\,E_9}{D\tau} - \frac{E_2\,E_{10}}{D} - \frac{E_4\,E_{11}}{D} - \frac{E_5\,E_{12}}{D}$$

$$\dot{x}_3 = \frac{E_3\,Tn_1}{D} + \frac{E_5\,Tn_2}{D} + \frac{E_6\,Tn_3}{D} + \frac{x_3}{\tau} - \frac{E_3\,E_7}{D\tau} - \frac{E_5\,E_8}{D\tau} - \frac{E_6\,E_9}{D\tau} - \frac{E_3\,E_{10}}{D} - \frac{E_5\,E_{11}}{D} - \frac{E_6\,E_{12}}{D}$$

Kinematics:

$$\dot{x}_4 = \frac{\cos x_6}{\cos x_5}x_1 - \frac{\sin x_6}{\cos x_5}x_2 + \frac{3\omega_0^2 \cos x_4 \sin x_5}{\cos x_5}$$

$$\dot{x}_5 = x_1 \sin x_6 + x_2 \cos x_6 + 3\omega_0^2 \sin x_4$$

$$\dot{x}_6 = \left(-\frac{\sin x_5 \cos x_6}{\cos x_5}\right)x_1 + \left(\frac{\sin x_5 \sin x_6}{\cos x_5}\right)x_2 + x_3 - \frac{3\omega_0^2 \cos x_4}{\cos x_5}$$

Inertia Control Law:

$$\dot{x}_7 = -\frac{x_7}{\tau} + \frac{1}{\tau}u_1$$

$$\dot{x}_8 = -\frac{x_8}{\tau} + \frac{1}{\tau}u_2$$

$$\dot{x}_9 = -\frac{x_9}{\tau} + \frac{1}{\tau}u_3$$

$$\dot{x}_{10} = -\frac{x_{10}}{\tau} + \frac{1}{\tau}u_4$$

$$\dot{x}_{11} = -\frac{x_{11}}{\tau} + \frac{1}{\tau}u_5$$

$$\dot{x}_{12} = -\frac{x_{12}}{\tau} + \frac{1}{\tau}u_6$$

Associated Definitions

$E_1 = x_8 x_9 - x_{12}^2$

$E_2 = x_9 x_{10} + x_{11} x_{12}$

$E_3 = x_{10} x_{12} + x_8 x_{11}$

$E_4 = x_7 x_9 - x_{11}^2$

$E_5 = x_7 x_{12} + x_{10} x_{11}$

$E_6 = x_7 x_8 - x_{10}^2$

$E_7 = u_1 x_1 - u_4 x_2 - u_5 x_3$

$E_8 = -u_4 x_1 + u_2 x_2 - u_6 x_3$

$E_9 = -u_5 x_1 - u_6 x_2 + u_3 x_3$

$E_{10} = x_9 x_2 x_3 + x_{10} x_1 x_3 + x_{12} x_3^2$

$\qquad - x_{11} x_1 x_2 - x_{12} x_2^2 - x_8 x_2 x_3$

$E_{11} = x_{11} x_1^2 + x_{12} x_1 x_2 + x_7 x_1 x_3$

$\qquad - x_9 x_1 x_3 - x_{10} x_2 x_3 - x_{11} x_3^2$

$E_{12} = x_8 x_1 x_2 + x_{10} x_2^2 + x_{11} x_2 x_3 - x_{10} x_1^2$

$\qquad - x_{12} x_1 x_3 - x_7 x_1 x_2$

$D = x_7 x_8 x_9 - 2x_{10} x_{11} x_{12} - x_8 x_{11}^2$

$\qquad - x_9 x_{10}^2 - x_7 x_{12}^2$

$x_1 = \omega_1 \qquad x_4 = \Theta_1 \qquad x_7 = I_{11} \qquad x_{10} = I_{12} = I_{21}$

$x_2 = \omega_2 \qquad x_5 = \Theta_2 \qquad x_8 = I_{22} \qquad x_{11} = I_{13} = I_{31}$

$x_3 = \omega_3 \qquad x_6 = \Theta_3 \qquad x_9 = I_{33} \qquad x_{12} = I_{23} = I_{32}$

ranges of suitable weighting factors are given in Table II.

TABLE II. WEIGHTING FACTOR SUMMARY

Problem Variable	State Variable	Acceptable Ranges	Nominal λ Values
ω_{1T}	x_{1T}	$10^3 < \lambda_a < 10^5$	1.0×10^4
ω_{2T}	x_{2T}	$10^3 < \lambda_b < 10^5$	1.0×10^4
ω_{3T}	x_{3T}	$10^3 < \lambda_c < 10^5$	1.0×10^4
Θ_{1T}	x_{4T}	$10^3 < \lambda_1 < 10^5$	1.0×10^4
Θ_{2T}	x_{5T}	$10^3 < \lambda_2 < 10^5$	1.0×10^4
Θ_{3T}	x_{6T}	$10^3 < \lambda_3 < 10^5$	1.0×10^4
$\Theta_1(t)$	$x_4(t)$	$10^6 < \lambda_4 < 10^8$	2.5×10^7
$\Theta_2(t)$	$x_5(t)$	$10^6 < \lambda_5 < 10^8$	2.5×10^7
$\Theta_3(t)$	$x_6(t)$	$10^6 < \lambda_6 < 10^8$	1.0×10^7
$\omega_1(t)$	$x_1(t)$	$10^6 < \lambda_d < 10^8$	2.5×10^7
$\omega_2(t)$	$x_2(t)$	$10^6 < \lambda_e < 10^8$	2.5×10^7
$\omega_3(t)$	$x_3(t)$	$10^6 < \lambda_f < 10^8$	1.0×10^7
$U_1(t)$	N/A	$10^{-11} < \lambda_7 < 10^{-9}$	2.5×10^{-10}
$U_2(t)$	N/A	$10^{-12} < \lambda_8 < 10^{-10}$	1.0×10^{-11}
$U_3(t)$	N/A	$10^{-12} < \lambda_9 < 10^{-10}$	1.0×10^{-11}
$U_4(t)$	N/A	$10^{-10} < \lambda_{10} < 10^{-8}$	2.5×10^{-9}
$U_5(t)$	N/A	$10^{-11} < \lambda_{11} < 10^{-9}$	1.0×10^{-10}
$U_6(t)$	N/A	$10^{-11} < \lambda_{12} < 10^{-9}$	1.0×10^{-10}

RESULTS

A number of computer runs were made to establish roughly workable ranges of the weighting factors. Although convergence was obtained for a wide range of initial conditions, a set of initial conditions corresponding to a 25-degree initial misalignment in all axes, with zero initial angular velocity was used as a general case to be investigated.

The first sets of runs were made with no constraint on the relationship between the inertia tensor element values other than insuring desirable initial and terminal values and also insuring that the moments of inertia remained positive. These runs allowed freedom in exploring the computational

aspects of the problem and were typified by the satellite's angular rate and displacement excursions shown in Figures 2 and 3.
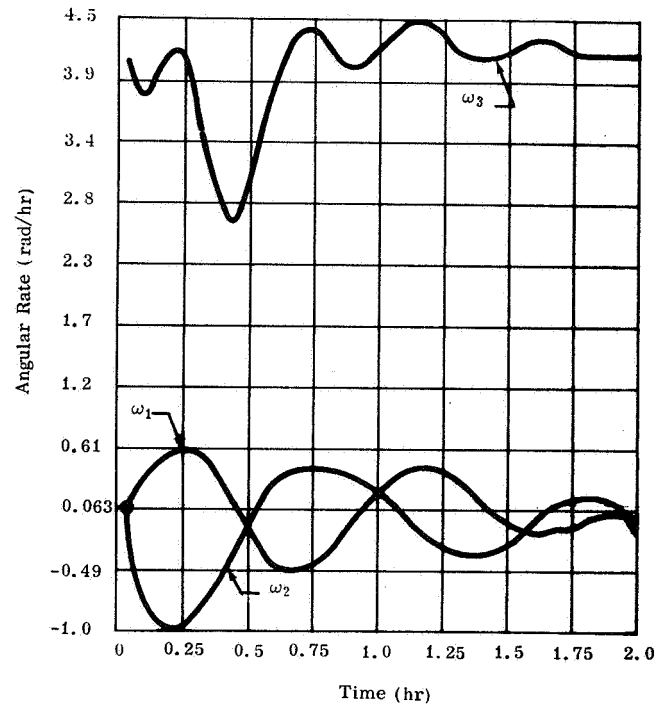

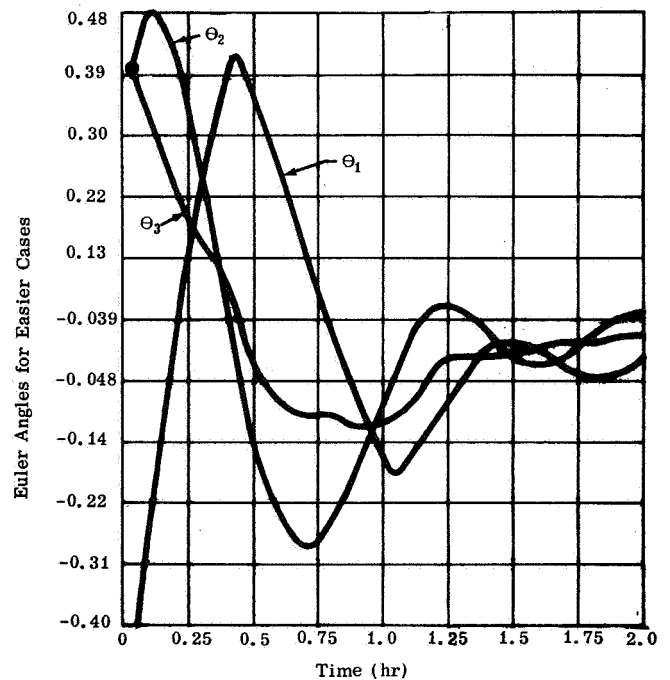FIGURE 2. ANGULAR RATES FOR EASIER CASES

FIGURE 3. EULER ANGLES FOR EASIER CASES

Runs were then made placing the constraint on the system that the sum of any two eigenvalues of the inertia tensor must always exceed, or at most equal, the third eigenvalue. Typical results obtained are shown in Figures 4 and 5.

As would be expected, the motion was not damped as rapidly in Figures 4 and 5 as that in Figures 2 and 3 because the inertia tensor element changes were not as large in Figures 4 and 5 as those in Figures 2 and 3.

Using the initial results as a yardstick by which to judge the results of the more constrained problem, it was decided to see if more rapid damping could be achieved in the constrained case. The method chosen to do this was to time program the λ weighting factors in the cost function (they previously were assumed to be constant). After some experimentation it was found that by reducing the six weighting factors of the inertia tensor elements to 20 percent of their initial values at 0.8 of one hour (out of a two-hour solution period), measurable improvement occurred. Typical results are given in Figures 6 and 7.

Clearly, additional improvement could be achieved by further tuning of the weighting factors.

CONCLUSIONS

The results achieved to date demonstrate the feasibility of the inertia changing scheme in achieving damped satellite motion. The major unresolved problem area, from an analytical viewpoint, is that of achieving closed loop control. The results achieved so far were obtained from an iterative process so that, in the classical sense, only open loop control was achieved. Some research on this problem has been accomplished but no definitive results have been obtained.
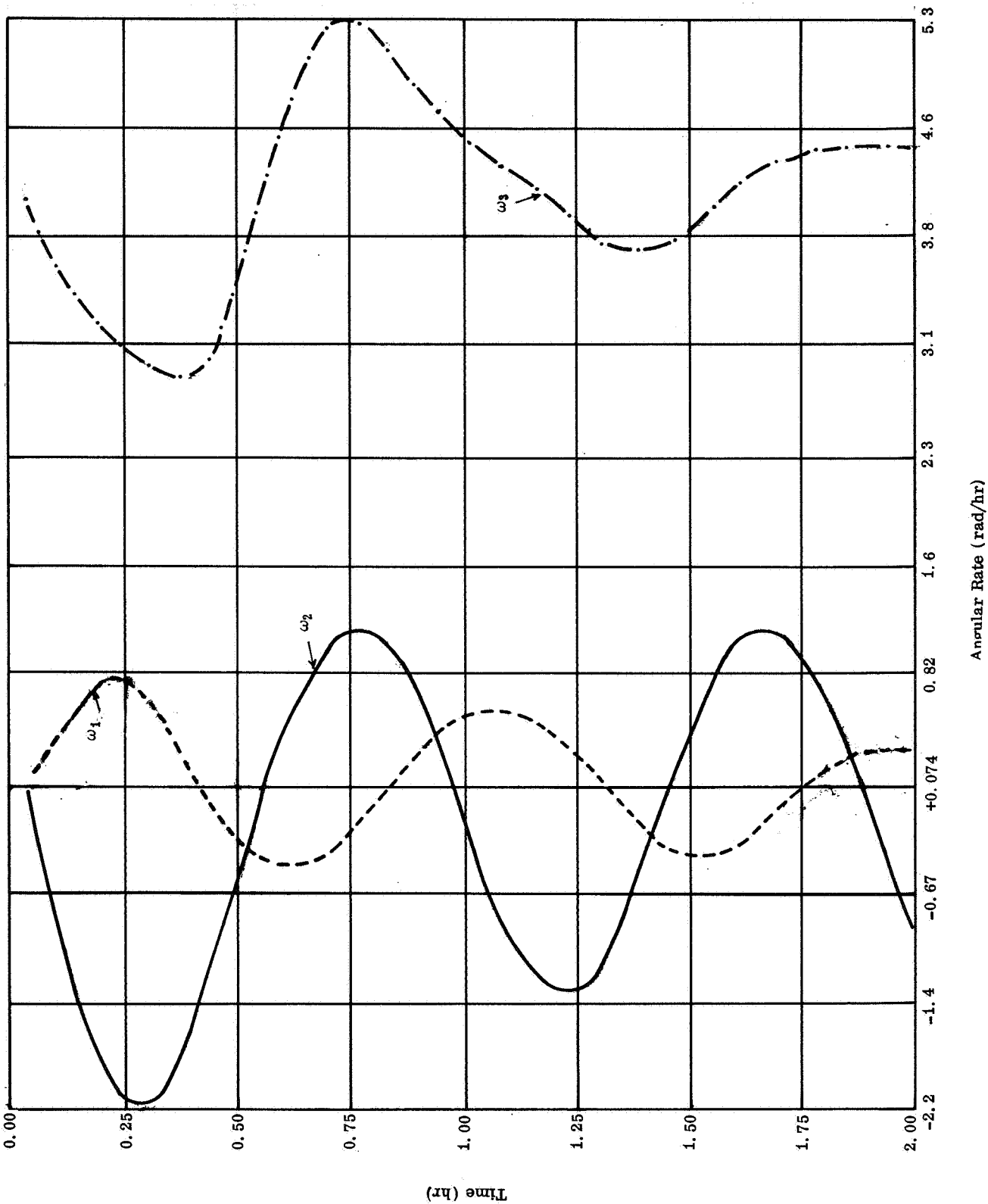
FIGURE 4. ANGULAR RATES FOR THE CONSTRAINED INERTIA CASE WITH CONSTANT COST WEIGHTING FACTORS
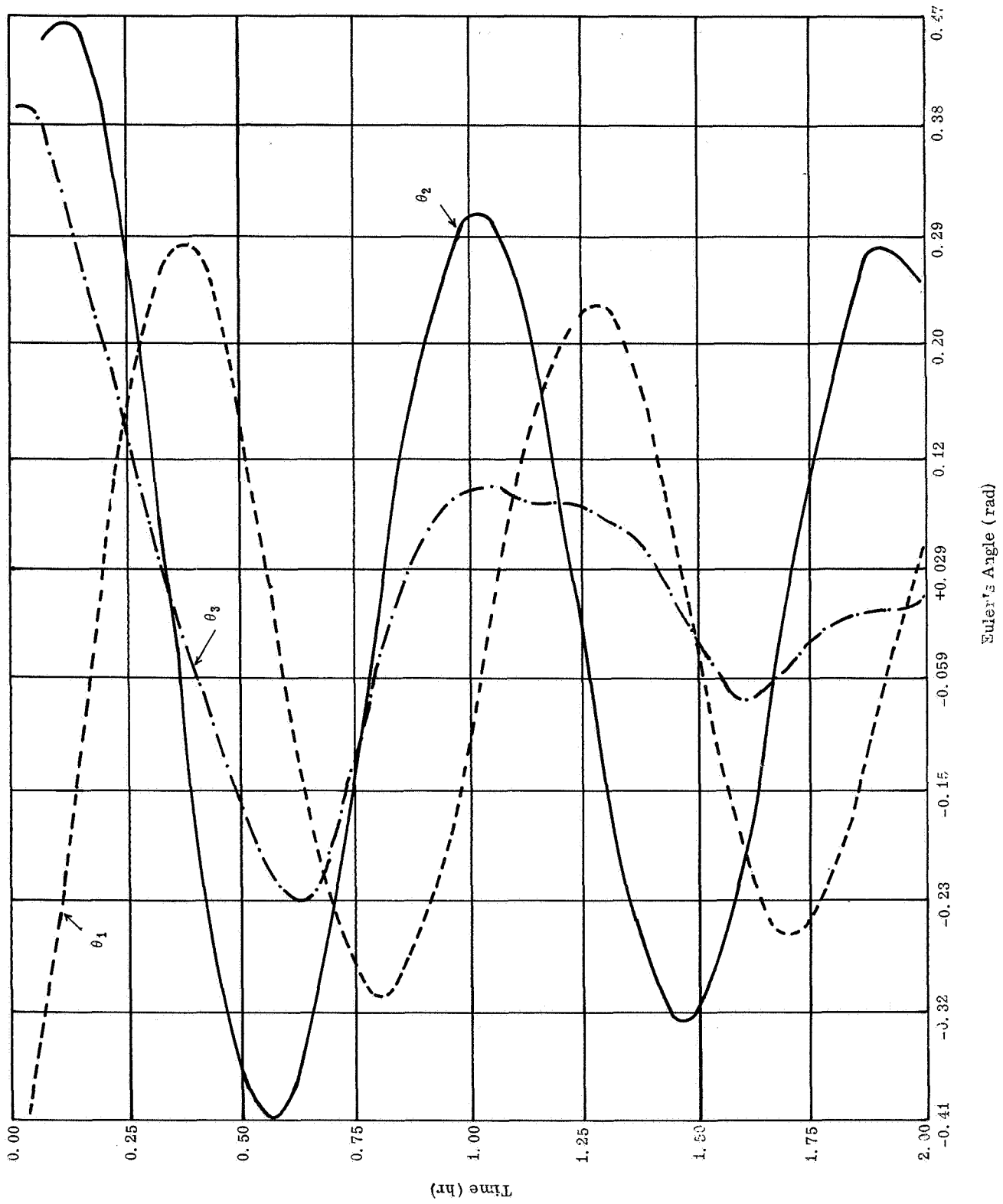
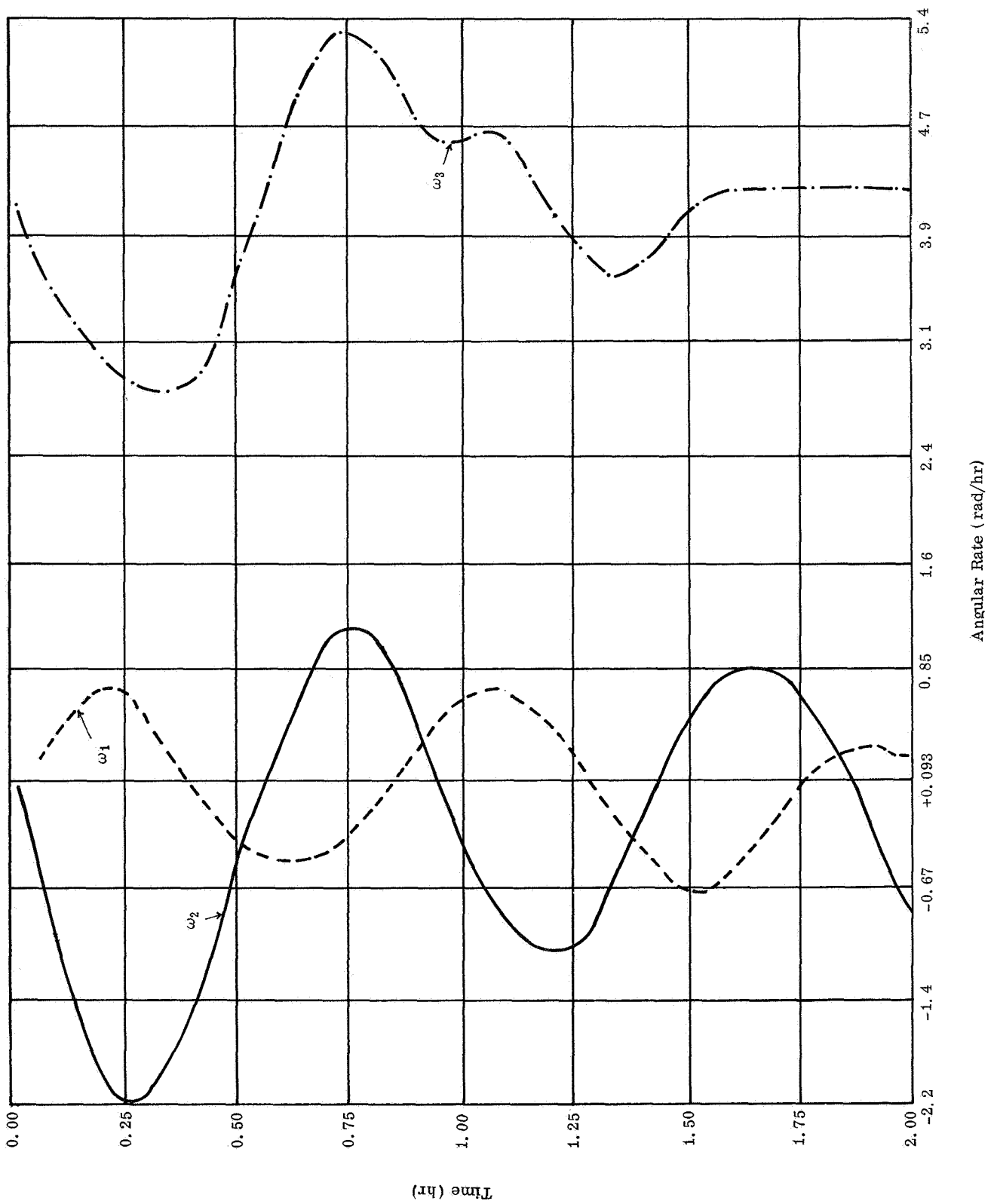FIGURE 5. EULER ANGLES FOR THE CONSTRAINED INERTIA CASE WITH CONSTANT COST WEIGHTING FACTORS

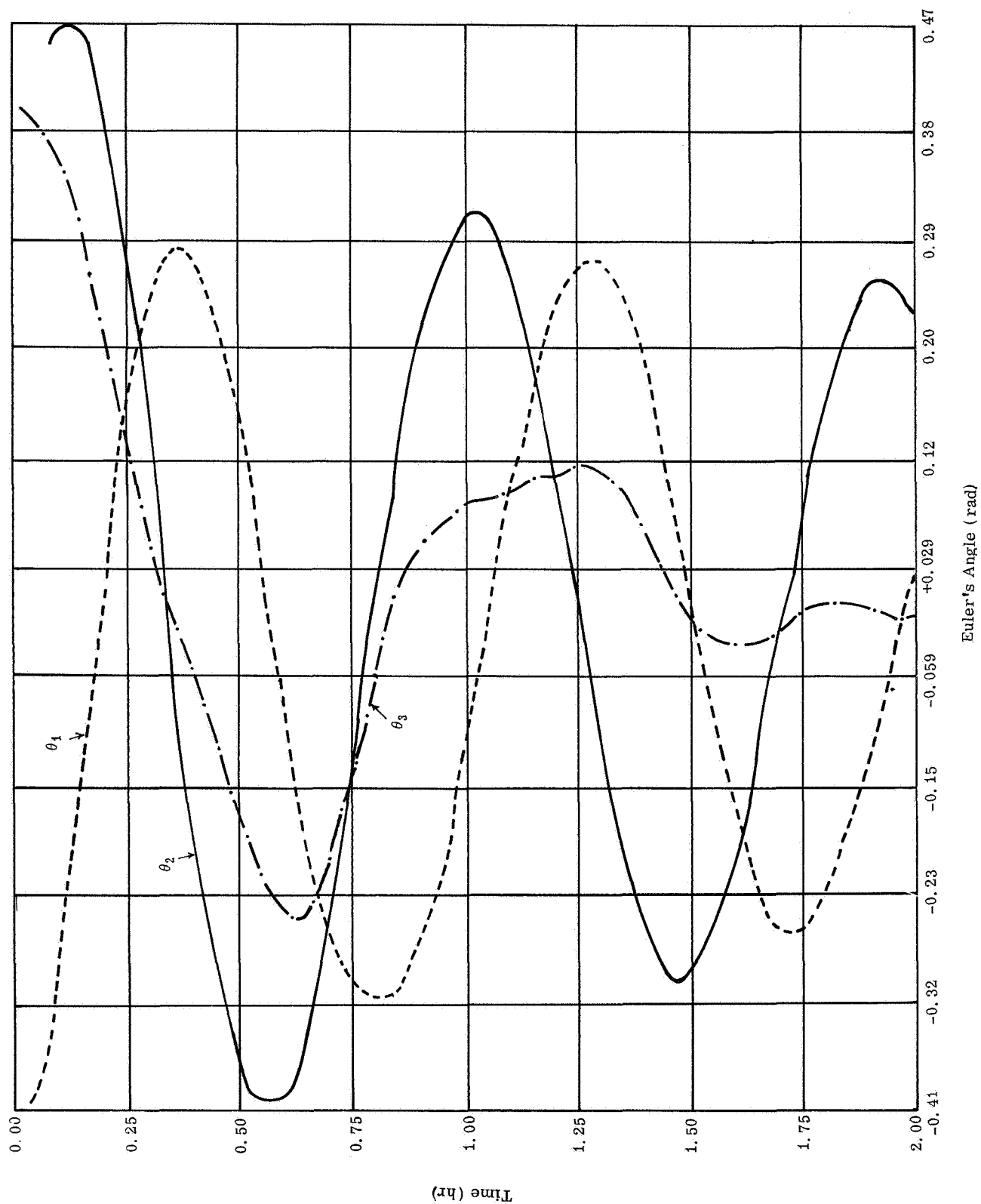FIGURE 6.   ANGULAR RATES FOR THE CONSTRAINED INERTIA CASE WITH TIME PROGRAMED COST WEIGHTING FACTORS

FIGURE 7. EULER ANGLES FOR THE CONSTRAINED INERTIA CASE WITH TIME PROGRAMED COST WEIGHTING FACTORS
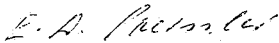
BIBLIOGRAPHY

1. De Bra, D. B.: The Large Attitude Motions and Stability, Due to Gravity, of a Satellite with Passive Damping in an Orbit of Arbitrary Eccentricity about an Oblate Body. Ph.D. dissertation, Stanford University, Stanford, California, 1962.

2. De Bra, D. B.; and Delp, R. H.: Rigid Body Attitude Stability and Natural Frequencies in a Circular Orbit. The Journal of the Astronautical Sciences, VIII, no. 1, Spring 1960.

3. Doane, George B. III: A Semipassive Gravity Gradient Satellite Control Scheme Using Optically Controlled (Variable) Mass Distribution. Ph.D. dissertation, Auburn University, Auburn, Alabama, August 22, 1968.

4. Dyer, P.: The Application of Variational Methods to Aircraft Control (Appendixes 1 and 2). Ph.D. dissertation, University of Nottingham, England, October 1966.

5. Meirovitch, L.; and Wallace, F. B.: On the Effect of Aerodynamic and Gravitational Torques on the Attitude Stability of Satellites. American Institute of Aeronautics and Astronautics Journal, IV, no. 12, 1966.

6. Nidey, R. A.: Gravitational Torque on a Satellite of Arbitrary Shape. ARS Journal, XXX, no. 2, February 1960, pp. 203-204.

7. Noton, A. R. M.; Dyer, P.; and Markland, C. A.: Numerical Computation of Optimal Control. IEEE Transactions, Automatic Control, AC XII, no. 1, February 1967, pp. 59-66.

8. Roberson, R. E.; and Likins, P. W.: Attitude Stability of Space Vehicles. Notes for a two-week short course at the University of California, Los Angeles, April 1966.

9. Schiehlen, Werner: Über Die Lagestabilisierung Künstlicher Satelliten Auf Elliptischen Bahnen. Von der Technischen Hochschule Stuttgart zur Erlangung der Würde eines Doktor-Ingenieurs genehmigte Abhandlung, 1966.

10. Weygandt, P., and Moyer, R.: Attitude Control for the Gravity Gradient Test Satellite. Paper presented at the JACC/AIAA Guidance and Control Conference, American Institute of Aeronautics and Astronautics, New York, August 15-16, 1966, pp. 238-248.

APPROVAL

RESEARCH ACHIEVEMENTS REVIEW
VOLUME III   REPORT NO. 3

The information in these reports has been reviewed for security classification. Review of any information concerning Department of Defense or Atomic Energy Commission programs has been made by the MSFC Security Classification Officer. These reports, in their entirety, have been determined to be unclassified.

These reports have also been reviewed and approved for technical accuracy.

E. D. GEISSLER
Director, Aero-Astrodynamics Laboratory

W. HAEUSSERMANN
Director, Astrionics Laboratory

UNITS OF MEASURE

In a prepared statement presented on August 5, 1965, to the U. S. House of Representatives Science and Astronautics Committee (chaired by George P. Miller of California), the position of the National Aeronautics and Space Administration on Units of Measure was stated by Dr. Alfred J. Eggers, Deputy Associate Administrator, Office of Advanced Research and Technology:

"In January of this year NASA directed that the international system of units should be considered the preferred system of units, and should be employed by the research centers as the primary system in all reports and publications of a technical nature, except where such use would reduce the usefulness of the report to the primary recipients. During the conversion period the use of customary units in parentheses following the SI units is permissible, but the parenthetical usage of conventional units will be discontinued as soon as it is judged that the normal users of the reports would not be particularly inconvenienced by the exclusive use of SI units."

The International System of Units (SI Units) has been adopted by the U. S. National Bureau of Standards (see NBS Technical News Bulletin, Vol. 48, No. 4, April 1964).

The International System of Units is defined in NASA SP-7012, "The International System of Units, Physical Constants, and Conversion Factors," which is available from the U. S. Government Printing Office, Washington, D. C. 20402.

SI Units are used preferentially in this series of research reports in accordance with NASA policy and following the practice of the National Bureau of Standards.

CALENDAR OF REVIEWS

FIRST SERIES (VOLUME I)

REVIEW	DATE	RESEARCH AREA	REVIEW	DATE	RESEARCH AREA
1	2/25/65	RADIATION PHYSICS	12	9/16/65	AERODYNAMICS
2	2/25/65	THERMOPHYSICS	13	9/30/65	INSTRUMENTATION
3	3/25/65	CRYOGENIC TECHNOLOGY	14	9/30/65	POWER SYSTEMS
4*	3/25/65	CHEMICAL PROPULSION	15	10/28/65	GUIDANCE CONCEPTS
			16	10/28/65	ASTRODYNAMICS
5	4/29/65	ELECTRONICS	17	1/27/66	ADVANCED TRACKING SYSTEMS
6	4/29/65	CONTROL SYSTEMS	18	1/27/66	COMMUNICATIONS SYSTEMS
7	5/27/65	MATERIALS			
8	5/27/65	MANUFACTURING	19	1/6/66	STRUCTURES
9	6/24/65	GROUND TESTING	20	1/6/66	MATHEMATICS AND COMPUTATION
10	6/24/65	QUALITY ASSURANCE AND CHECKOUT	21	2/24/66	ADVANCED PROPULSION
11	9/16/65	TERRESTRIAL AND SPACE ENVIRONMENT	22	2/24/66	LUNAR AND METEOROID PHYSICS

SECOND SERIES (VOLUME II)

REVIEW	DATE	RESEARCH AREA	REVIEW	DATE	RESEARCH AREA
1	3/31/66	RADIATION PHYSICS	7	3/30/67	CRYOGENIC TECHNOLOGY
2	3/31/66	THERMOPHYSICS	8**	5/25/67	COMPUTATION
3	5/26/66	ELECTRONICS	9	7/27/67	POWER SYSTEMS
4	7/28/66	MATERIALS	10	9/28/67	TERRESTRIAL AND SPACE ENVIRONMENT
5	9/29/66	QUALITY AND RELIABILITY ASSURANCE	11	11/30/67	MANUFACTURING
6	1/26/67	CHEMICAL PROPULSION	12	1/25/68	INSTRUMENTATION RESEARCH FOR GROUND TESTING

THIRD SERIES (VOLUME III)

REVIEW	DATE	RESEARCH AREA	REVIEW	DATE	RESEARCH AREA
1	3/28/68	AIRBORNE INSTRUMENTATION AND DATA TRANSMISSION	3	7/25/68	CONTROL SYSTEMS
2	5/22/68	ASTRODYNAMICS, GUIDANCE AND OPTIMIZATION	4	9/26/68	AEROPHYSICS

*Classified. Proceedings not published.

**Proceedings summarized only.

Correspondence concerning the Research Achievements Review Series should be addressed to:
Chief, Research Program Office, R-EO-R, Marshall Space Flight Center, Alabama   35812